Appendix 2B-2: Modeling Mercury Cycling and Bioaccumulation in Everglades Marshes with the Everglades Mercury Cycling Model (E-MCM)

Tom Atkeson, Don Axelrad and Larry Fink

Modeling Mercury Cycling and Bioaccumulation in Everglades Marshes with the Everglades Mercury Cycling Model (E-MCM)

Final Draft Report

Prepared for

Tom Atkeson and Don Axelrad
Florida Department of Environmental Protection

and

Larry Fink
South Florida Water Management District

Submitted by

Reed Harris, Don Beals, David Hutchinson, and Curt Pollman
Tetra Tech Inc.
Lafayette, CA

June 2003

Table of Contents

1 Background and Objectives 1-1

1.1 Review of previous model application to WCA 3A-15 1-2

2 Overview of study sites 2-1

3 Study Technical Approach 3-1

3.1 Overview of model calibration approach and data sources 3-1
3.1.1 Calibrating E-MCM to a new site 3-2
3.1.2 Calibrating E-MCM to a trophic gradient 3-5
3.1.3 Overview of datasets used for model calibrations. 3-5
3.1.4 Assigning model cell dimensions 3-6

4 Model Modifications 4-1

4.1 Overview of the deterministic, single cell version of E-MCM 4-1

4.2 Version of E-MCM with Linked Cells 4-2

4.3 Sulfur Module 4-2

4.4 Bottom-up Food Web Module 4-12

4.5 E-MCM Monte Carlo Capability and Model Input Dependencies 4-15

4.6 Linking E-MCM with External models 4-16

5 E-MCM applications to individual sites 5-1

5.1 Application of E-MCM to ENR 5-1
5.1.1 ENR Site Description 5-1
5.1.2 Deterministic E-MCM simulations for ENR 5-3
5.1.2.1 Single Cell Deterministic Simulation of ENR 5-3
5.1.2.2 ENR Simulation with Two Linked Cells. 5-13
5.1.2.3 Discussion of deterministic ENR simulations (Single Cell and Two-Cell Scenarios) 5-15
5.1.3 Monte Carlo ENR simulation 5-16

5.2 Updated calibration of E-MCM to WCA 2A sites F1 and U3 5-23
5.2.1 F1 and U3 Site Descriptions 5-23
5.2.2 Calibration Approach for F1 and U3 during Phase III 5-26
5.2.3 Model Results for F1 and U3 5-28
5.2.4 WCA-2A Discussion 5-37

5.3 Model calibration at STA-2 5-38

6 Management Scenarios 6-1

6.1 Background *6-1*

6.2 Description of Management Scenarios for Phase III *6-2*

6.3 Trophic State Considerations *6-4*
6.3.1 Fractions of marsh areas with open water, sawgrass, and cattails 6-5
6.3.2 Estimation of macrophyte and periphyton particle pools and the supply of detrital matter 6-8
6.3.3 Estimation of sedimentation (peat accretion) rates 6-8
6.3.4 Estimation of decomposition rates 6-9

6.4 Development of relationships between total phosphorus and methylation rate constants for management scenarios *6-11*

6.5 Results of Management Scenario Simulations *6-15*
6.5.1 F1 Management Scenario Results 6-15
6.5.2 U3 Management Scenario Results 6-16

6.6 Discussion of Management Scenario Simulations *6-24*

7 Future Directions **7-1**

8 Conclusions **8-1**

9 References **9-1**

Appendix A Detailed list of data sources for ENR simulations
Appendix B Probabalistic input distributions assigned for sample ENR Monte Carlo simulation
Appendix C Dependencies used for ENR Monte Carlo simulations
Appendix D Detailed list of data sources for WCA 2A (F1 and U3) simulations
Appendix E Summary of data sources for STA-2 simulations
Appendix F Model inputs for simulations of WCA 3A-15 from earlier studies

List of Figures

Figure 2-1. Map showing study sites ENR, F1, U3 and WCA 3A-15. 2-1
Figure 2-2. Observed mean concentrations of total mercury in surface waters at four sites. 2-3
Figure 2-4. Observed methylmercury concentrations in surface waters at four sites 2-3
Figure 4-1. Overview of Hg cycling in E-MCM 4-1
Figure 4-2. Schematic diagram of conceptual sulfate-sulfide cycling sub-model for E-MCM ... 4-9
Figure 4-3. Comparison of modeled steady state relationship between water column SO42- and porewater S2- with observed values along NZ transect in WCA-2A 4-11
Figure 4-4, Comparison of porewater sulfate and surface water sulfate concentrations from samples collected along the "N and Z" transects in WCA-2A, October 1997 through November 2001. 4-11
Figure 5-1. Site map for the Everglades Nutrient Removal (ENR) project 5-2
Figure 5-2. Total mercury concentrations in surface waters for 3 ENR locations (Data source: SFWMD 2000a) 5-4
Figure 5-3. Surface water MeHg concentrations at 3 ENR locations. (Data source: SFWMD 2000a) 5-5
Figure 5-4. Observed and predicted total mercury concentrations in ENR surface waters. (Data source: SFWMD, 2000a) 5-7
Figure 5-5. Observed and predicted surface water methylmercury concentrations at ENR 5-8
Figure 5-6. Observed and predicted total mercury concentrations for surficial sediments (0-3 cm) at ENR. (Source of observations: Gilmour *et al.,* 1998a) 5-8
Figure 5-7. Observed and predicted methylmercury concentrations in sediment solids in surficial sediments (0-3 cm) at ENR. (Source of observations: Gilmour *et al.*, 1998a) 5-9
Figure 5-8. Observed and predicted mercury concentrations in ENR mosquitofish 5-10
Figure 5-9. Observed and predicted mercury concentrations in 2-3 year old sunfish at ENR .. 5-10
Figure 5-10. Observed and predicted mercury concentrations in largemouth bass (age 3-4 years) at ENR (Source of observations: Florida Fish and Wildlife Conservation Commission, 2000) 5-11
Figure 5-11. Predicted sources and sinks of inorganic Hg(II) for ENR at near-steady-state conditions 5-12
Figure 5-12. Predicted sources and sinks of methylmercury for ENR at near steady-state conditions 5-13
Figure 5-13. E-MCM sample input screen for Monte Carlo inputs 5-17
Figure 5-14. Methylation rate constants generated by E-MCM for sample ENR Monte Carlo simulation (n=100) 5-18
Figure 5-15. Predicted and observed concentrations of total mercury in ENR surface waters for sample Monte Carlo application. 5-21
Figure 5-16 Observed and predicted surface water MeHg concentrations at ENR. 5-21
Figure 5-17 Predicted vs observed cumulative frequency distribution for age 4+ largemouth bass at ENR - initial simulation with low biological variability 5-22
Figure 5-18. Predicted vs observed cumulative frequency distribution for age 4+ largemouth bass at ENR - initial simulation with high biological variability. 5-22
Figure 5-19. Range of predicted methylmercury concentrations in 4-5 year old largemouth bass at ENR (simulation with high biological variability) 5-23
Figure 5-20. Surface water inorganic Hg(II) concentration gradient observed across WCA-2A. 5-25
Figure 5-21. S10 flows and sampling dates for surface water Hg concentrations at S10, F1 and U3. 5-25
Figure 5-22 Observed and predicted total mercury concentrations in F1 surface waters 5-30
Figure 5-23 Observed and predicted methylmercury concentrations in surface waters at F1 5-30

Figure 5-24. Observed and predicted total mercury concentrations in F1 sediments. 5-31
Figure 5-25. Observed and predicted methylmercury concentrations in F1 sediments..... 5-31
Figure 5-26. Observed and predicted Hg concentrations in mosquitofish at F1. 5-32
Figure 5-27. Observed and predicted total mercury concentrations in surface waters at U3. ... 5-33
Figure 5-28. Observed and predicted methylmercury concentrations in surface waters at U3. . 5-33
Figure 5-29. Observed and predicted total mercury concentrations in U3 sediments..... 5-34
Figure 5-30. Observed and predicted methylmercury concentrations in U3 sediments. 5-34
Figure 5-31. Observed and predicted mercury concentrations in mosquitofish at U3 5-35
Figure 5-32. Observed and predicted mercury concentrations in age 2-3 largemouth bass at U3. 5-35
Figure 5-33. Observed and predicted mercury concentrations in age 3-4 largemouth bass at U3. 5-36
Figure 5-34. Predicted and observed surface water total mercury concentration gradient between F1 and U3. 5-36
Figure 5-35. Predicted and observed surface water MeHg concentration gradient between F1 and U3. 5-37
Figure 5-36. Site map and sampling stations for STA-2 5-38
Figure 5-37. Preliminary predicted MeHg concentrations in STA-2 Cell 1 surface waters with methylation in sediments. 5-39
Figure 5-38. Predicted and observed MeHg concentrations in STA-2 Cell 1 surface waters, with water column methylation assumed..... 5-40
Figure 5-39. Predicted and observed total mercury concentrations in STA-2 Cell 1 surface waters, with water column methylation assumed..... 5-40
Figure 5-40. Simulated average MeHg sources and sinks for STA-2 from July 2000 – March 2001 5-41
Figure 5-41. Simulated average Hg(II) sources and sinks for STA-2 from July 2000 through March 2001 5-42
Figure 5-42. Simulated MeHg in STA-2 surface waters with the addition of a periphyton bloom in December 2000..... 5-43
Figure 6-1. Estimated fractions of vegetated areas covered by cattails and sawgrass as a function of surface water total phosphorus concentration (mg L^{-1}). 6-7
Figure 6-2. Estimated fractions of total marsh area covered by cattails, sawgrass and open water as a function of surface water total phosphorus concentration (μg L^{-1})..... 6-8
Figure 6-3. Predicted supply of detrital matter as a function of phosphorus concentrations in surface waters 6-8
Figure 6-4. Predicted particle fluxes as a function of phosphorus concentrations in surface waters 6-10
Figure 6-5. Predicted particle burial rate as a function of total phosphorus concentration in surface waters..... 6-10
Figure 6-6. Alternative particle budget used to show sensitivity of model to particle fluxes ... 6-11
Figure 6-7. Estimated sediment gross methylation rates as a function of total phosphorus in surface waters at 4 Everglades sites - estimated by (1) E-MCM calibration and (2) ^{203}Hg incubations by Gilmour *et al.* (1998b)..... 6-13
Figure 6-8. Estimated relationship between total phosphorus in surface waters and sediment methylation rate constants for Phase III management scenarios 6-15
Figure 6-9. Predicted effects of management scenarios on surface water Hg(II) concentrations at F1. 6-18
Figure 6-10. Predicted relationship between porewater Hg(II) concentrations and total phosphorus in surface waters at F1..... 6-18
Figure 6-11. Predicted effects of total phosphorus concentrations on surface water methylmercury concentrations at F1..... 6-19

Figure 6-12. Predicted effects of surface water total phosphorus concentrations on largemouth bass Hg concentrations at F1 6-19
Figure 6-13. Predicted effects of management scenarios on surface water Hg(II) concentrations at U3 6-20
Figure 6-14. Predicted relationship between porewater Hg(II) concentration and surface water total phosphorus concentration at U3. 6-20
Figure 6-15. Predicted effects of surface water concentrations of total phosphorus on predicted concentrations of methylmercury in surface waters (ng/L unfiltered) at U3. 6-21
Figure 6-16. Predicted effects of total phosphorus concentrations in surface waters on mercury concentrations in largemouth bass at U3. 6-21
Figure 6-17. Predicted rates of gross methylation in sediments vs surface water total phosphorus concentrations at F1. 6-22
Figure 6-18. Predicted gross methylation rates in sediments vs surface water total phosphorus concentrations at U3. 6-22
Figure 6-19. Comparison of effects of management scenarios on predicted Hg levels in age 3-4 largemouth bass at F1 for two different particle budgets. 6-23
Figure 6-20. Comparison of effects of management scenarios on predicted Hg levels in age 3-4 largemouth bass at U3, for two different particle budgets. 6-23

List of Tables

Table 2-1. General characteristics of four marsh sites in the Florida Everglades 2-2
Table 3-1. Differences in E-MCM calibration values used between four marsh sites. 3-3
Table 4-1. Model equations for E-MCM sulfur module. 4-7
Table 4-2. Example production matrix from bottom-up food web module 4-13
Table 5-1. Mean observed Hg concentrations in ENR from August 1994 to August 1997 5-3
Table 5-2. Predicted and observed means for selected parameters 5-7
Table 5-3. Predicted and observed inorganic Hg(II) concentrations in surface waters and sediments for ENR simulation using 2 linked cells, initial Hg partitioning and sedimentation based on feldspar data 5-14
Table 5-4. Minimum and maximum observed weight by age for largemouth bass at ENR (1995 to 1999) (Source: Florida Fish and Wildlife Conservation Commission. (2000)). 5-19
Table 5-5. Water quality gradients across WCA-2A. 5-24
Table 5-6. Comparison of observed and predicted mercury concentrations and apparent partitioning at F1 and U3 5-28
Table 6-1 . Phase III management scenarios. 6-3
Table 6-2. Surface water phosphorus concentrations applied to F1, Middle, and U3 cells in model scenarios (Source SFWMD 2000g) 6-4
Table 6-3. Estimated fraction of vegetated marsh area covered with sawgrass, and associated F transect sites and total phosphorus concentrations in surface waters. 6-6
Table 6-4. Comparison of sediment methylation rate estimates using (1) E-MCM calibrations and (2) sediment core incubations with 203 Hg (derived from Gilmour *et al.* (1998b)). 6-13

1 Background and Objectives

Tetra Tech Inc. was retained by the Florida Department of the Environment (FDEP) and South Florida Water Management District (SFWMD) to enhance and apply a mechanistic model of mercury cycling in Everglades marshes. This study is one component of a broad series of studies investigating mercury in the Florida Everglades that have been ongoing since the early 1990's. Such studies include Phase I and II of the ACME studies 1995 – present (e.g., Krabbenhoft *et al.* 1998, Gilmour *et al.*, 1998a and b, Hurley *et al.,*1998, Cleckner *et al.* 1998), the Florida Atmospheric Mercury Study (FAMS) (Guentzel *et al.*, 2001 and 1995; Gill *et al.,* 1999), the USEPA Regional Environmental Monitoring and Assessment (REMAP) project in south Florida (1994 – 1999; Stober *et al*., 2001) with extensive spatial synoptic data on water, soil, vegetation and fish from randomly selected sites in both Everglades marshes and canals; a long-term database on mercury in largemouth bass and other fishes, developed by Lange *et al.* of the Florida Fish and Wildlife Conservation Commission, and an extensive program investigating mercury cycling in the Everglades Nutrient Removal Project (ENR) (SFWMD (1995, 1996, 1997, 1998, 1999a, 1999b), Miles and Frank 1998, Fink and Rawlik 2000, Fink 2000a, Fink 2001).

Through a contract with the USEPA, Tetra Tech previously adapted a dynamic model of mercury cycling in lakes (D-MCM) (Tetra Tech 1999a, Hudson *et al*. 1994) for conditions in Everglades marshes, resulting in the Everglades Mercury Cycling Model (E-MCM) (Tetra Tech 1999b). Prior to the development of E-MCM, a screening level model of mercury cycling in the Everglades was developed (Tsiros and Ambrose 1998, Ambrose *et al.* 1997). Original E-MCM model development was carried out using Water Conservation Area 3A-15 as the first calibration site. E-MCM was also applied to WCA 3A-15 to predict the response of fish mercury concentrations to changes in atmospheric Hg deposition, as part of a pilot mercury TMDL study for the USEPA (Tetra Tech 2001).

Under the current contract with FDEP and the SFWMD, a three-phase study has been carried out to enhance E-MCM and apply it to a broader set of conditions. This document is an integrated report discussing the overall study, and follows an earlier interim report describing Phase I and II studies (Tetra Tech, 2002). During this study the model was applied to four new sites, including the Everglades Nutrient Removal (ENR) project, two sites in Water Conservation Area 2A (F1 and U3), and STA-2. Some simulations were done with the deterministic version of the model designed for single wetland marsh cells. Other simulations were done with versions of the models that featured enhancements added during the study, including a version of E-MCM that runs a series of linked cells simultaneously, and a version which includes a probabilistic Monte Carlo capability.

A mass balance model describing a simplified sulfur cycle in the Everglades was also developed for inclusion in E-MCM. The objective of this simplified model is to give E-MCM the ability to simulate sulfur mass balance dynamics including fundamental sulfur biogeochemical processes. In addition, E-MCM was modified to accommodate a bottom-up approach to simulating bioenergetics and interactions across trophic levels in the cycling and transfer of mercury through aquatic biota. Finally, a set of management scenarios provided by Larry Fink of the South Florida Water Management District (SFWMD) was simulated for Water Conservation Area 2A between the F1 and U3 sites. Empirical relationships between total phosphorus concentrations in

surface waters and system primary productivity and particle budgets were developed and embedded in the model simulations.

This document describes the technical approach to the study, describes model modifications and enhancements, deterministic model calibrations to individual sites (ENR, F1, U3, STA-2), a Monte Carlo application to the ENR, a deterministic simulation representing ENR as two linked cells (buffer cell, downstream cells) and a series of management scenarios requested by the SFWMD. Finally, key findings are discussed and recommendations are provided for future research directions that would benefit the state of knowledge of mercury cycling and the development of the E-MCM model.

1.1 Review of previous model application to WCA 3A-15

Initially, Tetra Tech worked on the development of E-MCM using data from WCA 3A-15 as a test location. WCA 3A-15 was an attractive site for simulating Hg dynamics because it had high fish mercury concentrations. As a result it was also selected as a location for a US EPA pilot mercury TMDL (Tetra Tech, 2001, FDEP, 2002). Key results of the 3A-15 simulations are summarized as follows:

- Hg cycling is very rapid at 3A-15 relative to most lakes modeled with the Dynamic Mercury Cycling Model (D-MCM), due to a combination of large fluxes of particulate material, shallow waters, elevated temperatures, and conditions likely conducive to methylation.
- The dominant predicted methylmercury source was *in situ* production (7.6 $\mu g\ m^{-2}\ yr^{-1}$, 87% of total MeHg load to the marsh). This is consistent with the hypothesis that local site factors play an important role in determining "hot spots" observed for methylmercury across the Everglades.
- The relative importance of upstream versus *in situ* supply of total mercury and methylmercury is significantly influenced by the size, shape and flow velocity assumed for the modeled marsh.
- Based on model results, a load reduction of 77% is needed for predicted long-term average mercury concentrations in age 3 largemouth bass to drop from 1.80 to 0.5 $\mu g\ g^{-1}$ wet muscle.
- Regardless of the magnitude of the load reduction, fish mercury concentrations at WCA 3A-15 were predicted to change by 50% of the ultimate response within 8-9 years, and 90% within 25-30 years. The site response time was strongly influenced by the rate of peat accretion. It also should be noted that these simulations were done assuming methylation occurred primarily in sediments and that the active sediment layer is on the order of 3-4 cm thick. Field studies carried out recently in Everglades mesocosms by D. Krabbenhoft, C. Gilmour *et al*. and elsewhere (e.g., the METAALICUS project (R. Harris unpublished data)) indicate the potential for more rapid responses.

2 Overview of study sites

Following the calibration of E-MCM to WCA 3A-15 in earlier studies, E-MCM was applied to four sites during this study: (1) the Everglades Nutrient Removal Project (ENR), (2) F1, a highly eutrophic site in Water Conservation Area 2A, (3) U3, a less impacted, lower productivity site also in Water Conservation Area 2A, and (4) STA-2, an artificial wetland constructed to remove phosphorus from runoff.

Figure 2-1 shows the locations of these 4 sites, as well as Water Conservation Area 3A-15. Table 2-1 provides general characteristics of the study sites, as well as WCA 3A-15. More detailed descriptions of the sites are provided in later sections.

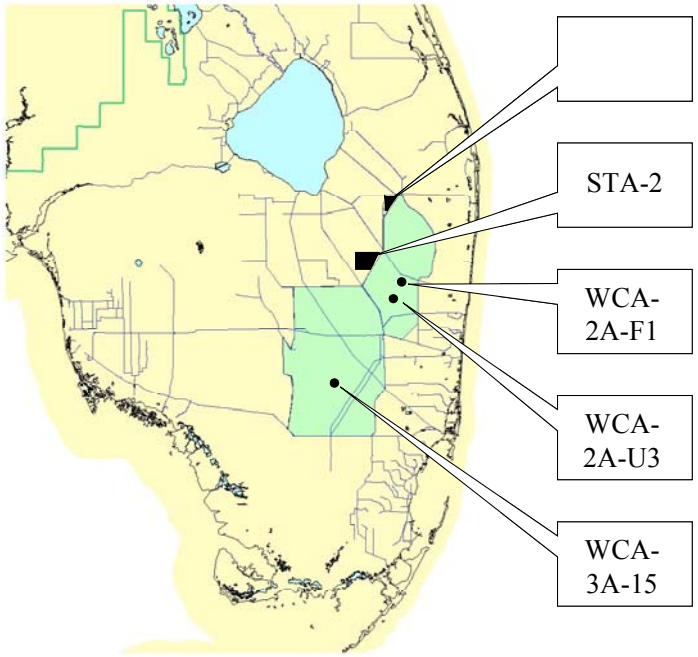

Figure 2-1. Map showing study sites ENR, F1, U3 and WCA 3A-15.

(Source: L. Fink)

Parameter	Units	Values by Site				
		ENR	**F1**	**U3**	**WCA 3A-15**	**STA-2 Cell 1**
Area modeled	km^2	15.4	3.6	3.6	1.0	8.05
Air Temperatures (monthly means)	Celsius	12 to 30 C	12 to 30 C	12 to 30 C	12 to 30 C	12-30 C
Productivity		High	High	Low (oligotrophic)	Low (oligotrophic)	High
Total phosphorus in surface waters	ug L^{-1}	~50	~140	~10	~14	~41
Flow pattern		Surface flow and groundwater	Surface flow	Surface flow	Surface flow	Surface Flow
Estimated mean hydraulic residence time	days	23	11	8.5	48	12
Anoxia		Yes	Yes	Yes	Yes	Likely (min 0.5 mg/L observed at outlet)
Dissolved organic carbon	mg L^{-1}	~ 30	44	~39	~ 16	~37
Surface water pH		~ 7.2	~7.3	~7.5	~ 7.2	7.5
Surface water chloride	mg L^{-1}	~ 100	155	136	~ 28	180
Surface water sulfate	μeq L^{-1}	1400	1045	1043	100	769
Estimated annual sedimentation rate at 3 cm depth	cm yr^{-1} bulk	1.1	0.75	0.3	0.28	0.35
Macrophytes		Cattails, other macrophytes and a small amount of sawgrass	Dominated by cattails	Dominated by sawgrass	Sawgrass (dominant), cattails, water lilies	Sawgrass, cattails, water lilies
Percent of marsh surface with open water	Percent	29	4	15	<50%	50%
Periphyton density		Moderate	Low	Dense	Dense	Dense
Top predator fish		Largemouth bass	NA	Largemouth bass	Largemouth bass	NA

Table 2-1. General characteristics of four marsh sites in the Florida Everglades

Figure 2-2 and Figure 2-3 show mean observed concentrations of total and methylmercury in surface waters at the five sites modeled with E-MCM to-date. Observed concentrations of total and methylmercury were lowest at ENR. Methylmercury concentrations were higher at the less productive sites (3A-15 and U3). Interestingly, F1, the most eutrophic site along the WCA-2A gradient that we simulated, had significantly higher MeHg concentrations in surface waters than ENR. Samples were not always collected on the same dates nor by the same agency. ENR data were collected by the SFWMD from March 1995 through March 1999. F1 and U3 data were collected by the USGS 1995 to 2000. WCA 3A-15 data were collected by the USGS on 11

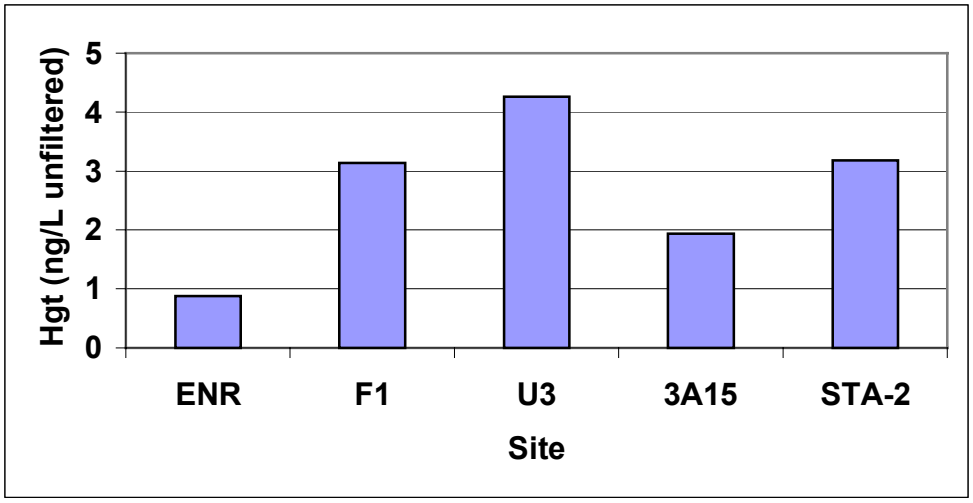

occasions from December 1995 to July 2000 (USGS, 2001). STA-2 data were from Fink (2002e).

Figure 2-2. Observed mean concentrations of total mercury in surface waters at four sites. (Source: ENR data: SFWMD 2000a; F1, U3, and 3A-15 data: USGS, 2001; Fink 2002e).

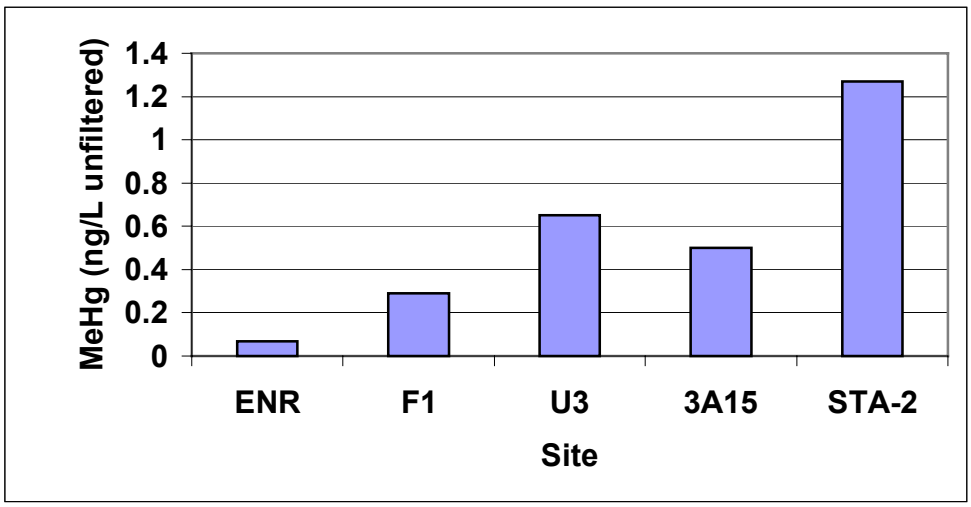

Figure 2-3. Observed methylmercury concentrations in surface waters at four sites

(Source: SFWMD 2000a; F1 and U3 data and 3A-15 data: USGS, 2001, Fink 2002e).

3 Study Technical Approach

Overall, the basic approach taken during this study was to:

1. Carry out E-MCM simulations at ENR and STA-2 using the deterministic (as opposed to probabilistic) version of the model. These applications help to improve the knowledge of Hg cycling as a result of testing the model under a variety of conditions. In these cases, the model was tuned to site-specific conditions to attempt to reflect as much of the observed site data as possible (e.g., mercury concentrations in different compartments, mercury fluxes and pools).
2. Modify E-MCM so that series of linked cells could be run simultaneously. This was needed in situations where the assumption of similar conditions longitudinally could not be made, for example the gradient of site conditions and mercury concentrations across Water Conservation Area 2A precluded a simulation representing the entire area with one cell.
3. Apply the "linked cell" version of E-MCM to a calibration of WCA 2A from the F1 site to U3. To the extent possible, the same model calibration rate constants were used across the gradient of site conditions modeled. A similar linked cell application was undertaken at ENR, to accomodate conditions varying at different locations in ENR, particularly the initial buffer cell.
4. Enhance E-MCM with additional features to help apply the model to a range of conditions and account for uncertainty regarding model estimates. This included the addition of a module with simplified sulfur cycling, the addition of a module to link food web dynamics to total phosphorus levels, and the addition of a probabilistic Monte Carlo capability to the model.
5. Link E-MCM to external models providing estimates of the effects of changing total phosphorus concentrations on site conditions, specifically particle budgets and water quality. During the course of the study, no suitable model was found to link to E-MCM for this purpose. In lieu of such information, Tetra Tech developed an initial set of empirical relationships to estimate particle budgets and water quality at sites as a function of total phosphorus concentrations in surface waters.
6. Apply E-MCM to a series of management scenarios provided by L. Fink of the South Florida Water Management district.
7. Identify gaps and future research needs to provide E-MCM with a stronger predictive capability

3.1 Overview of model calibration approach and data sources

This section outlines the sequence of steps involved when calibrating E-MCM to (1) a single site, or (2) calibrating the model during a simulation spanning conditions across a nutrient gradient. There are some unique considerations when calibrating Everglades marshes, due to the lack of clearly defined boundaries for the area to model. This topic is also briefly discussed.

3.1.1 Calibrating E-MCM to a new site

With the exception of the first Everglades site simulated (3A-15), a previous scenario was cloned and used as a starting point for a new site. Inputs associated with site conditions (particle budgets, hydrology, water chemistry, food web structure, fish diets, etc) and external mercury loading were then modified to reflect conditions at the new location. The model was then run and results compared to field data. Ideally the model would generate reasonable predictions at this point, without changing any model constants related to reactions or partitioning. Currently however, the model predictive strength is not fully developed. The calibration procedure is thus an iterative process that follows the sequence itemized below and summarized as follows: First calibrate some model components related to site conditions (not Hg), then calibrate Hg(II) in water and sediments, followed by MeHg in water and sediments, and finally, MeHg in the food web (lower food web first, then fish). The reason for this sequence is that there is no point adjusting inputs affecting just MeHg in fish, until MeHg concentrations in their dietary items are reasonably predicted. Similarly there is no point in calibrating MeHg production and levels in the system until Hg(II) levels are reasonably predicted, since in-situ Hg(II) levels affects methylation rates in the model. Thus calibrations of mercury cycling start with Hg(II) and work systematically towards MeHg in fish.

During this study, it was not possible to generate satisfactory model results using one set of model constants for all sites. Table 3-1 shows model constants that had to be varied for at least one of the study sites. Although the model fit to observations could also have been improved in some cases by altering inputs for site conditions where uncertainty existed (*e.g.,* missing information on sediment accretion rates), this was not done. Only selected inputs related to reaction rate constants or mercury partitioning constants were altered, with the exception of the particle decomposition rates in sediments and at the sediment-water interface (Table 3-1). In particular, biological methylation and demethylation rates were effectively tuned at each site to generate good results for methylmercury concentrations. Thus the application of E-MCM at these sites to-date represents a calibration exercise, not a true predictive exercise. As will be discussed further in the document, the effects of sulfides and bacterial activity are not sufficiently established in the literature or the model to robustly predict methylation and demethylation rates at a given site.

Input Description	3A-15	ENR (Single cell)	ENR (Two cell)	F1	U3	STA-2
MeHg partitioning constant for periphyton	0.77	0.35	0.35	0.365	0.365	0.77
MeHg partitioning constant for detritus	0.77	0.07	0.07	0.77	0.77	0.77
MeHg partitioning constant for suspended solids	0.77	0.77	10	0.77	0.77	0.77
Hg(II) partitioning constant for detritus	2.07E+10	5.15E+10	5.15E+10	4.07E+10	4.07E+10	2.07E+10
MeHg partitioning constant for surficial sediment solids	0.29	0.07	0.07	0.29	0.29	0.29
Hg(II) partitioning constant for settling solids (not detritus)	5.035E+12	1.035E+10	8.535E+12	1.035E+10	1.035E+10*	1.035E+10
Sediment biological demethylation rate constant	0.018	0	0	0	0.018	0.018
Sediment biological methylation rate constant	0.01715	0	0	0	0.01715	0.001715
Water column biological methylation rate constant	0	0	0	0.001	0	0.2
Fraction of settling particles decomposed at sediment-water interface	0.1	0.1	0.08 *	0.75 *	0.55 *	0.001-0.95
Fraction of settling detritus decomposed at sediment-water interface	0.1	0.1	0.24*	0.75 *	0.55 *	0.001-0.95
MeHg photodegradation rate constant at water surface	0.0006	0.0006	0.0006	0.000624	0.000624	0.000624
HgII photoreduction rate constant at water surface	0.004	0.004	0.0027	0.002	0.002	0.002

* calculated from empirical relationship based on total phosphate

Table 3-1. Differences in E-MCM calibration values used between four marsh sites.

Occasionally it was found that, regardless of how a calibration is adjusted within reason, good results could not be attained. Examples include the initial ENR and F1 runs. At ENR, it was not plausible to get reasonable total mercury levels in surface waters unless some of the inflowing total mercury in the buffer cell was removed via settling. The model was suggesting that the assumption of treating all of ENR as a single entity was flawed. At F1, initial simulations assumed methylation was in sediments, but results improved if methylation occurred in the water column, which was subsequently invoked.

Calibration of selected site conditions

1. Typically the first component of the model calibrated are the **water budget and water levels**. The existing model has the shortcoming that it does not do an internal mass balance for water[1] (although the Hg in water is mass balanced), but inflows, outflows, and water levels are compared to see if the numbers are consistent. A proper water budget for the water column is recommended as a future improvement.

[1] The model currently relies upon an external hydrologic mass balance, and it is incumbent on the user to ensure that hydrologic mass balance is maintained for each time step.

2. Next the **particle budget** (excluding Hg at this stage) is typically calibrated to match observed bulk sedimentation rates. For the water column, inputs are entered that dictate the supply of litter to the water column and sediment interface from macrophytes and periphyton. This is designated as a detrital pool of particles. A second term is input called settling solids to accommodate suspended particles of other origin (autochthonous, algal production, etc.). This term is typically closer to measured values of total suspended solids (TSS) in the water column, while the detrital material is assumed to settle out but still be connected to the water column in terms of mercury pools. Some of the settling TSS and detritus is then assumed to decompose before it ever actually works into the sediment matrix. The remainder is the source of particles to sediments. Some of the sediment particles may either decompose or resuspend, and the rest is buried into the next layer. A mass balance is used for sediment particles to solve for burial at the bottom of each sediment compartment. The above calibration of the particle budget is used when the user has data on parameters such as macrophyte coverage and sedimentation rates. An alternative approach was also set up during Phase III that estimated various particle fluxes on the basis of total phosphorus concentrations in surface waters at the site. This approach was used for the final Phase III model calibrations at F1 and U3, and is discussed in detail in Section 6.3.

3. If data are available for **fish growth rates, weight vs length relationships, and fish diets**, these parameters are calibrated for relevant fish species. **Fish population sizes** are adjusted to match the observed productivity if data are available.

Calibration of the Hg(II) component of the model

4. Following an initial simulation, selected model constants may be adjusted related to **partitioning of Hg(II) and methylmercury concentrations** between dissolved and particulate phases, in both sediments and the water column. The objective is to match apparent partitioning between field-estimated concentrations in the dissolved and particulate phases.

5. If needed, a few model parameters may be adjusted so **Hg(II) concentrations in water** (unfiltered) **and sediments** (on solids) better agree with observations. This might involve additional adjusting partitioning of Hg(II) onto solids and in some cases modifying rate constants for reactions such as Hg(II) reduction.

Calibration of the methylmercury component of the model

6. Once Hg(II) levels in the system are reasonably calibrated, attention is focused on methylmercury. Adjustments may be made to selected model parameters such that **methylmercury concentrations in water** (unfiltered) **and sediments** (on solids) better agree with observations. This might involve adjusting partitioning of MeHg onto solids and, if needed, modifying rate constants for reactions such as methylation and demethylation.

7. Adjusting model parameters, if necessary, so that **methyl mercury concentrations in the lower food web** agree with observations. Partitioning of MeHg into benthos and zooplankton can be adjusted.

8. Examining fish mercury levels. **Fish diet** and, in rare instances, species-specific bioenergetic parameters can be re-examined to improve agreement between the model and observed fish mercury levels.

In terms of the criteria used for calibrations, the approach to-date has typically been to simply examine whether predictions for a particular parameter improve or worsen following a change to an input (e.g., predicted Hg(II) concentrations in water, MeHg concentration in fish), based on mean predicted and observed values. Once mean predicted and observed values are similar visual comparisons of predicted versus observed time-series graphs were used to compare the data.

3.1.2 Calibrating E-MCM to a trophic gradient

As described in later sections, it is now possible to run a series of linked cells simultaneously with E-MCM, for example spanning the nutrient gradient across WCA 2A. While site conditions will vary between cells that are linked, the model constants for reaction rates and Hg partitioning should be the same for all cells if the model is operating well mechanistically. The objective is to obtain the best overall fit for a given parameter, considering all cells simulated. The goodness of fit assessment could be done with a least sum of squares approach for any given parameter. E-MCM is moving in this direction but has not yet reached that level of mechanistic robustness, and some adjustments to rate constants between cells are still needed.

3.1.3 Overview of datasets used for model calibrations.

Site conditions were assigned based on the best available data. Data sources for inputs for ENR, WCA 2A (F1 and U3) and STA-2 are documented in Appendices A, D, and E respectively. When calibrating the model, simulations were run for the periods of record for Hg data (*e.g.,* 1995-1999). There were water quality and hydrologic data available for the same time periods as the Hg monitoring data. For example, a water budget was developed for STA-2 Cell 1 by L. Fink (2002e) and this budget was used in the simulation. ENR had the most comprehensive dataset available of the 4 sites simulated, although substantial datasets also existed for F1 and U3. Data for STA-2 were somewhat limited.

Data related to particle budgets

Macrophyte densities and turnover rates and accompanying detrital loads for the deterministic single cell ENR simulation were estimated as a function of total phosphorus using regression equations from Ambrose *et al.* (1997). Sediment accretion rates were tuned to field measurements by tuning the model using detrital loading and decay rates to arrive at the appropriate amount of sediment accretion. At ENR, sediment accretion rates for the deterministic single cell simulation were based on feldspar markers applied to the sediments (data reference: S8). For the two-cell ENR simulation, done at a later date, empirical equations derived from Walker and Kadlec (1996) were used to estimate particle budgets and sedimentation rates. These mass sedimentation rates were lower than in the earlier single cell ENR simulation. At F1 and U3, sediment accretion rates were tuned to observed rates from Vaithiyanathan *et al*. (1996). For STA-2 Cell 1, sediment accretion rates were not tuned as estimated rates were unavailable. Suspended solids and detritus levels were assigned but no further adjustments were made to these estimates.

Estimation of wet and dry atmospheric Hg(II) deposition

At ENR, field measurements for wet Hg(II) and methylmercury deposition from March 1995 to February 1999 from the SFWMD (2000a) were used in simulations. At F1 and U3 annual mercury wet deposition rates developed for WCA 3A-15 (See Appendix F and Tetra Tech, 2001) were used. At STA-2, wet deposition was estimated from total Hg concentrations in wet deposition samples obtained from the MDN site at the ENR Project (Fink, 2002e).

RGM deposition rates for inorganic Hg(II) at the ENR, F1,U3 and STA-2 were based the rates developed for WCA 3A-15 by Keeler *et al*. (2001), but adjusted for site conditions regarding macrophyte coverage to account for the effects of leaf areas. Dry particle Hg(II) deposition at ENR, F1 and U3 were based Keeler *et al*. (2001), again adjusted for site conditions regarding macrophyte coverage. Dry particle deposition of inorganic Hg(II) at STA-2 was derived from Fink (2002e).

MeHg wet and dry deposition fluxes were assumed to be 0.5% of the corresponding total Hg fluxes (Fink, 2002e).

Estimating flowrates and inflow mercury concentrations

Compared to most lakes, water throughput rates for the sites modeled in this study are quite rapid (see hydraulic residence times, Table 2-1). This increases the importance of inflows as a source of mercury to the modeled marshes. At ENR, inflow rates and Hg concentrations were well documented. At F1 and U3, it was necessary to estimate both the flowrates and the inflowing concentrations. As described below, a simple three-compartment linked wetland approach was used to simulate mercury concentrations along the WCA gradient from S10 to U3.

3.1.4 Assigning model cell dimensions

ENR and STA-2 are constructed wetlands with defined boundaries. F1 and U3 however are sampling stations in the midst of expansive marsh areas without discrete boundaries. For modeling purposes we had to assign cell dimensions for F1 and U3. For F1 and U3, initially a 1 km^2 square cell size was chosen, as was assigned to WCA 3A-15. Due to difficulties estimating inflow concentrations at the upstream boundaries of the these 1 km^2 cells, plus the importance of these inflow fluxes to predicted Hg levels, a simple 3 compartment (F1, middle cell, U3) linked wetland approach was used with rectangular compartments 1 kilometer wide and several kilometers long to simulate mercury concentrations along the WCA gradient from S10 to U3. Additional details are provided in later sections.

There are implications associated with the choice of cell dimensions. A basic consideration is that mercury concentrations and the site conditions affecting mercury within a given cell must be relatively homogeneous horizontally for a single cell (continuously stirred tank reactor) model to perform reasonably. If site conditions and mercury concentrations show a gradient across a cell (e.g. along the flow path), then it is not possible to represent the modeled area as a single cell and it is appropriate to set up a simulation as a series of 2 or more linked cells, or if needed, treat the waterbody as a river where concentrations are solved as a function of distance along the flowpath. E-MCM is not immediately amenable to conversion to a riverine model, and the mercury gradients across Water Conservation area 2A were modeled using a series of linked cells. Similarly, some ENR simulations used 2 linked cells.

One of the basic questions for mercury cycling in the Everglades is whether most of the inorganic mercury loaded to a given area or the overall system is from inflows or from direct atmospheric deposition. If a model framework is set up with many linked cells, individual cell sizes get smaller. As individual cells get smaller in area but not in depth, the relative importance of inflow to each cell increases relative to atmospheric Hg deposition. For example, if one examined the Everglades as a whole, it could be that direct atmospheric mercury deposition rates exceed the mercury loads from inflows. However if one chose to represent the Everglades as a series of linked 1m x 1m cells (extreme example), it is very likely that inflows would load more mercury into any given cell than the load from the atmosphere. This appears to present the problem that the choice of cell size affects the relative importance of mercury loaded from direct deposition versus inflows. The appropriate measure however is to add up the fluxes associated with all cells representing the entire Everglades. Every cell would contribute atmospheric depostion to this total, but only the most upstream cell would load mercury to the overall modeled area. Flows between cells would not represent external loading. This would increase the importance of atmospheric deposition relative to inflows, because the entire Everglades was being considered. The same situation applies when comparing inflowing methylmercury loads to in-situ methylation, if the latter is an area-based process. Inflows may appear to be the dominant source to a very small area, but if the methylation rates for all cells in the modeled area are added up, in-situ methylation would increase to a level more appropriate when considering the entire Everglades.

4 Model Modifications

This study involved several enhancements to the structure of E-MCM. These included the creation of a version of the model that runs with linked cells, the addition of a module simulating simplified sulfur cycling, the addition of an option to set up the food web using a "bottom-up" approach dictated by nutrient levels (specifically total phosphorus).

4.1 Overview of the deterministic, single cell version of E-MCM

E-MCM is designed to accommodate unique features of Everglades marshes, including shallow waters, a warm subtropical climate, intense sun exposure, neutral to alkaline pH, high concentrations of dissolved organic carbon, managed water levels, large biomasses of aquatic macrophytes and periphyton, and a wide range of nutrient levels and primary productivity.

The model representation of mercury cycling in an Everglades marsh is shown in Figure 4-1. There are three primary mercury forms in E-MCM: methylmercury, inorganic Hg(II) and elemental mercury. Inorganic Hg(II) is defined here as all mercury which is neither methylmercury nor elemental mercury. FDEP and the SFWMD are familiar with E-MCM and only a brief description is provided here. A detailed description of model processes and equations in E-MCM is available in the user's guide (Tetra Tech 1999b). This "core" version of the model is deterministic (not probabilistic) and is appropriate where conditions are assumed to be relatively homogeneous horizontally across the marsh.

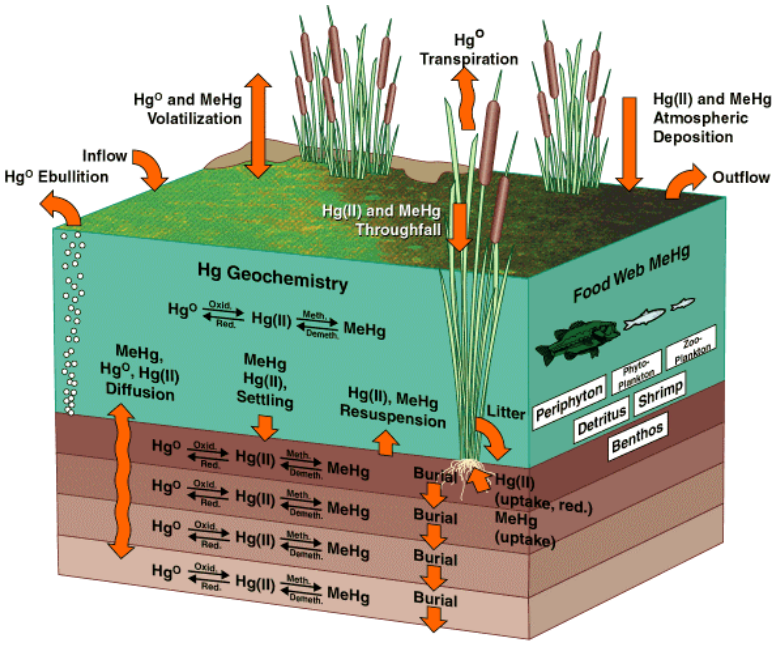

Figure 4-1. Overview of Hg cycling in E-MCM

4.2 Version of E-MCM with Linked Cells

E-MCM was modified to allow multiple cell scenarios to be linked in series and the behaviour of the collection of linked cells to be examined in a single simulation run. The linked cell approach provides the ability to more easily model an area where the site conditions change along a downstream gradient.

Description of the linked cell model

E-MCM was reorganized so that a collection of wetland cells could be specified as a linked cell run. Flow through the linked wetland cells is one-dimensional and unidirectional. An individual cell is directly linked to adjacent cells immediately upstream and downstream. Mercury concentrations in surface waters flowing into a particular cell are taken to be those in the surface waters of the cell immediately upstream. The model solution is run simultaneously for all of the scenarios in a linked cell simulation. Consequently, the model provides calculated mercury inflow concentrations for all but the furthermost upstream cell during a simulation. Inflowing Hg concentrations must be specified for the user in the case of the first cell.

The mercury flux associated with surface water flow into a linked cell is calculated as the surface water inflow rate multiplied by the unfiltered mercury concentration in the upstream cell. Flowrates for all cells are model inputs, as was the case for the single cell model. This provides the ability to consider the case where only part of the outflow from an upstream cell flows into the cell immediately downstream cell. However, it is important to note that the mercury mass balance for the entire system will not be maintained unless the water flowrate out of an upstream cell is set to be equal to the water inflow rate into the next cell. Where water outflow exceeds inflow into the next cell, for example, some mercury will be lost to the system as a whole.

In addition to simulating linked cells, the linked cell version of E-MCM can be run in single wetland mode or in multiple wetlands mode. The single wetland mode is identical to the original E-MCM where the simulation is run for a single scenario. The multiple wetlands mode allows the user to simultaneously run more than one independent (unlinked) scenario.

4.3 Sulfur Module

Sulfur dynamics have been linked to the aquatic mercury cycle through several different pathways. First, because sulfate-reducing bacteria are linked with methylation in freshwater sediments (Gilmour *et al*. 1991), addition of sulfate in systems with relatively low sulfate concentrations can stimulate methyl Hg production (Gilmour et al., 1991 and 1995; Branfireun et al., 1999). At higher ambient water column sulfate concentrations, sulfide produced by sulfate reducing bacteria may seriously limit methylation by sequestering labile Hg(II), which is the critical substrate for the production of MeHg. Recently, Benoit et al. (1999a, 1999b and 2001) have suggested that Hg methylation occurs most rapidly when conditions favor the formation of neutral dissolved Hg-S species. Higher sulfide concentrations may promote the formation of charged Hg-S complexes, and the fraction of inorganic Hg available for methylation could be reduced.

Within the Everglades, there is a marked gradient in surface water sulfate concentrations from north to south that reflects surface water source and flow patterns (Stober et al., 2001). Analysis of the isotopic composition of sulfate indicates that sulfur originating from the Everglades

Agricultural Area (EAA) is the source of excess sulfate in the northern Everglades (Bates et al., in review). This excess sulfate in turn has been linked to sulfide production with possible implications for the aquatic mercury cycle in the Everglades.

Because of these reasons, one element of this project was to introduce into E-MCM the ability to predict sulfur cycling in a simplified manner to provide some key sulfur-related inputs into E-MCM simulations. Initially, the project contemplated incorporating the sulfur cycling module from Tetra Tech's Integrated Lake Watershed Acidification Study model (ILWAS). ILWAS was originally developed in part to predict the effects of sulfate loading and losses to the sediments through dissimilatory sulfate reduction on major ion chemistry and acid neutralizing capacity (ANC) (Gherini et al., 1985). The advantages to using the ILWAS sulfur cycling module were principally two-fold: (a) ILWAS has a well-documented and tested pedigree for predicting changing sulfate dynamics in a variety of lacustrine environments; and (2) the conceptual model used to predict sulfate dynamics was comparatively simple.

As both this study and the state-of-the-art regarding the possible role of sulfate in the Everglades progressed, it became readily apparent that the conceptual model for ILWAS was not capable of capturing all the major features of the sulfur cycle that are believed to critically influence Hg cycling in the Everglades. More specifically, ILWAS maintained a mass balance for sulfate in the water column only and, although sulfate losses to the sediment were used to infer ANC production through dissimilatory sulfate reduction, the development of porewater sulfide concentrations was not explicitly simulated.

We have thus developed a somewhat more complete sulfur cycling conceptual model to incorporate into E-MCM that is designed to predict not only changes in surface water sulfate concentrations as a function of loading rates, hydrology, and biological uptake, but the development of porewater sulfide concentrations as well (Figure 4-2). This conceptual model assumes that porewater sulfide derives from the mineralization of organic S (e.g., ester sulfate compounds) sedimenting from the water column, as well as from diffusive exchange across the sediment-water interface of sulfate, followed by sulfate reduction (cf. Cook and Kelly, 1992). Sulfate reduction in the sediments is simulated as a first-order reaction dependent upon sulfate concentrations that develop in porewater.

Key features or assumptions of the model include:

- Deposition of SO_4^{2-} to sediments occurs via two processes: (a) formation of organic S in water column, followed by sedimentation and subsequent decomposition; and (2) diffusion of SO_4^{2-} across the sediment-water interface in response to developing gradients between the water column and porewater.
- Assume S^{2-} flux into water column is dependent on porewater concentration and mass transfer coefficient.
- Assume all S^{2-} fluxing upward into the oxic water column is instantaneously oxidized to SO_4^{2-}.
- Assume all dry deposited SO_2 is instantaneously converted to SO_4^{2-}.
- The model predicts total dissolved reduced S concentrations in the porewater. Speciation as a function of pH and the formation of complexes with Hg(II) and CH_3Hg^+ are subsequently computed using the existing thermodynamic routines and equilibrium constants built into E-MCM.
- All sediment species (dissolved and solid phase) are removed from the surficial sediment layer as a function of the rate of net sediment accumulation.

The model was first developed as a separate model outside E-MCM using the model simulation package STELLA™. Table 4-1 shows the governing equations subsequently used to code the sulfur module into E-MCM.

Sulfur Module Parameterization

Limited data are available to currently parameterize the sulfur sub-model for E-MCM. Compared to such biogeochemically active contaminants as Hg or phosphorus, sulfate is nearly conservative within the "unit wetland" spatial dimensions for which E-MCM has been applied as part of this study. As a result, a calibration to the characteristic unit wetland for sulfate concentrations may very easily do a poor job of predicting water column sulfate concentrations much further downstream. Ideally, model calibration thus would extend to including larger scale units or systems of units such as WCA-2A; developing the requisite hydrologic and mass balance information, however, was beyond the scope of this study.

The mass balance dynamics of sulfate in the water column have been developed for Lake Barco, an oligotrophic seepage lake in northcentral Florida (Pollman *et al*., 1991 and Pollman, unpublished data). This mass balance can be used to help parameterize the model as a "first-order" exercise to predict the relationship between changing sulfate and hydrologic loads, and resultant water column sulfate concentrations. It should be noted that sulfate uptake by primary producers is essentially a zero-order process – in other words, sulfate is rarely nutritionally limiting. Thus a change in primary production induced by changes in total phosphorus concentrations (*e.g*., a change from 5 to 10 $\mu g\ L^{-1}$) should result in a concomitant change in sulfate uptake due to organic S formation in the water column. The model currently assumes that organic S formation is a first order process. Since, similar to phosphorus, sulfate loads to the upper Everglades largely derive from export from the EAA, changes in sulfate loads likely correlate with phosphorus as well, and the first order representation is probably a reasonable approximation in lieu of tying uptake directly to primary production rates[2].

Limited data from the so-called "N and Z" transects in WCA-2A are available for both water column sulfate and porewater sulfide concentrations (L. Fink, personal communication, 2002). Data for the two parameters included a total of 37 observations for porewater sulfide between October 1997 and November 2001, and 108 observations for surface water sulfate between October 1997 and January 2002. Both data sets included data from the same nine stations, and were merged by station, year and month to produce an integrated data set of 37 observations for comparing porewater sulfide and surface water sulfate concentrations. The model was then calibrated to yield to produce both the water column concentration relationship with load and hydrologic conditions consistent with the Lake Barco mass balance, and the relationship between porewater sulfide and surface water sulfate consistent with the "N and Z" transect data.

This latter relationship is shown in Figure 4-3. The predicted sulfide concentrations generally lie within the range of observed values as a function of surface water sulfate concentrations, although the curvilinear nature of the relationship is not well captured by the model. The observational data suggest that, until surface water sulfate concentrations exceed 30 to 40 mg/L,

[2] Sulfate losses to the sediments because of the diffusional gradient imposed by sulfate reduction in the porewater, however, is a first order process – both because of how diffusion is treated by the model, and because the model simulates sulfate reduction in the porewater as a first order process dependent upon porewater sulfate concentrations. Thus increasing sulfate loadings will lead to increased sulfate reduction regardless of how organic uptake of sulfate in the water column is treated.

porewater sulfide concentrations remain below 1 mg/L and are essentially independent of surface water sulfate. Above 30 to 40 mg/L sulfate, porewater concentrations then increase linearly with sulfate. This behavior may reflect differing redox conditions. In other words, the redox environment of the surficial sediments may be too weakly reducing to support strong rates of sulfate reduction because of presumably lower TP loading rates. Conversely, high sulfate concentrations should reflect high TP loading rates, and this would translate to more organic matter loading to the sediments, and a more aggressive (reducing conditions) environment for sulfate reduction.

Such a conceptual model should be reflected in the porewater sulfate concentrations. If sulfate reduction is not occurring, then a comparison of porewater and surface water sulfate concentrations should show both variables corresponding on a 1:1 basis. If sulfate reduction is occurring, then porewater sulfate concentrations should be depleted relative to surface water concentrations. Figure 4-4, which shows this comparison for the "N and Z" transects, supports this conceptual view. Below 40 mg/L, there is variability about the 1:1 correspondence line, which likely reflects both analytical and sampling uncertainty (the porewater samples are time-integrated samples while the surface water samples simply reflect principally a single grab sample during the same month the porewater samples were retrieved). Above 40 mg/L, all the observations lie below the 1:1 correspondence line, indicating consistently sulfate reducing conditions.

Conclusions and Recommendations for the Sulfur Module

By necessity, the current version of the S module is a highly simplified conceptualization of a very complicated biogeochemical cycle. It is designed as an aggregated model that tries to capture the minimum, essential features of the S cycle relevant to predicting the effects of changing sulfate loading on the Hg cycle in the Everglades. A more sophisticated model can be developed, but it should be noted that even the current version is not sufficiently well-parameterized and calibrated. Thus, investing further effort in improving the conceptualization of the model without a concomitant effort to develop the requisite rate constants and storages of sulfur in different compartments (*e.g.*, porewater and solid phase concentrations) from field observations and experiments is risky. Some improvements nonetheless can be recommended for consideration for future work. Currently, the S module assumes that biota uptake of sulfate in the water column and its incorporation into biota is a first order process. As stated earlier, sulfate in all likelihood is not nutritionally limiting for reactions other than dissimilatory sulfate reduction, and direct uptake in the water column is not expected to change following changes in sulfate concentrations (except under conditions where sulfate is reduced to very small concentrations on the order of ambient phosphorus levels) unless other factors produce changes in productivity rates. Future changes in the model should, however, link organic S fluxes to primary production rates so that the effect of changing sulfate and phosphorus loads on the S and Hg cycles can be independently evaluated.

The sulfur module has been coded as an independent module within the E-MCM model framework, and can be run from the main E-MCM model interface. However, the model exists as a prototype and a broad scale calibration of the S module to the Everglades has not been conducted, nor can it be conducted until a spatially distributed E-MCM model has been applied across the Everglades. Tetra Tech is currently under contract with USEPA to apply E-MCM in such a manner, and a "proof-of-concept" version that links E-MCM to the hydrologic and TP concentration outputs from Tetra Tech's Everglades Phosphorus and Hydrology Model (EPH) has been completed for WCA-2A. Such a calibration exercise for the S module for E-MCM, will

require both surface water sulfate, and porewater sulfide data, as well as net sedimentation rates for organic S. Data sets for the latter two parameters for the Everglades, however, are limited.

Table 4-1. Model equations for E-MCM sulfur module.

See also Figure 4-2.

```
Mass_Org_S(t)      = Mass_Org_S(t - dt) + (Org_S_Prod - Org_S_Dep - Surface_Export_Org_S) * dt
INIT Mass_Org_S  = 0

INFLOWS:
Org_S_Prod         = Kso4:orgS*Conc_SO4*Volume

OUTFLOWS:
Org_S_Dep                = Area*vdep_Org_S*Conc_Org_S
Surface_Export_Org_S  = Conc_Org_S*Qout
Mass_SO4(t)              = Mass_SO4(t - dt) + (Surface_Inputs + SO4_Atm_Dep +
S2_SO4_Oxidation_Flux + SO4_Diff_Flux - Surface_Export_SO4  - Org_S_Prod) * dt
INIT Mass_SO4          = 0

INFLOWS:
Surface_Inputs           = Qin*Sulfate_In
SO4_Atm_Dep              = Area*Rain_Depth*SO4_Rain
S2_SO4_Oxidation_Flux = Kf_oxid_S2_SO4*Water_Column_S2_Mass
SO4_Diff_Flux            = (SO4_Pore_Conc-Conc_SO4)*Diff_Piston_Velocity*Porosity*Area

OUTFLOWS:
Surface_Export_SO4       = Conc_SO4*Qout
Org_S_Prod               = Kso4:orgS*Conc_SO4*Volume
Org_S_Sediment_Mass(t) = Org_S_Sediment_Mass(t - dt) + (Org_S_Dep - Org_S_Burial -
Org_SO4_Decomp) * dt
INIT Org_S_Sediment_Mass = Initial_Org_S_Sediment*Mass_Sediment_Particles

INFLOWS:
Org_S_Dep          = Area*vdep_Org_S*Conc_Org_S

OUTFLOWS:
Org_S_Burial             = Area*Org_S_Bulk_Sed_Conc*V_burial/100
Org_SO4_Decomp         = K_org_S*Org_S_Sediment_Mass
SO4_Porewater_Mass(t) = SO4_Porewater_Mass(t - dt) + (Org_SO4_Decomp - SO4_Porewater_Burial
          - SO4__S2_Pore_Conversion_Flux - SO4_Diff_Flux) * dt
INIT SO4_Porewater_Mass = Initial_SO4_Porewater*Vol_Sed_H2O

INFLOWS:

Org_SO4_Decomp       = K_org_S*Org_S_Sediment_Mass

OUTFLOWS:
```

Table 4-1. Model equations for E-MCM sulfur module.

See also Figure 4-2.

SO4_Porewater_Burial = Area*SO4_Pore_Bulk_Conc*V_burial/100
SO4__S2_Pore_Conversion_Flux = SO4_Porewater_Mass*Kf_Pore_SO4_S2-
Sulfide_Porewater_Mass*Kb_Pore_SO4S2
SO4_Diff_Flux = (SO4_Pore_Conc-Conc_SO4)*Diff_Piston_Velocity*Porosity*Area
Sulfide_Porewater_Mass(t) = Sulfide_Porewater_Mass(t - dt) + SO4__S2_Pore_Conversion_Flux
- S2_Porewater_Burial - S2_Diff_Flux) * dt
INIT Sulfide_Porewater_Mass = Initial_S2_Porewater*Vol_Sed_H2O

INFLOWS:
SO4__S2_Pore_Conversion_Flux = SO4_Porewater_Mass*Kf_Pore_SO4_S2-
Sulfide_Porewater_Mass*Kb_Pore_SO4S2
OUTFLOWS:
S2_Porewater_Burial = S2_Pore_Bulk_Conc*V_burial*Area/100
S2_Diff_Flux = Area*(S2_Pore__Conc-Water_Column_S2_Conc)*Diff_Piston_Velocity*Porosity
Water_Column_S2_Mass(t) = Water_Column_S2_Mass(t - dt) + (S2_Diff_Flux - S2_SO4_Oxidation_Flux
- Surface_Water_Export_S2) * dt
INIT Water_Column_S2_Mass = 0

INFLOWS:
S2_Diff_Flux = Area*(S2_Pore__Conc-Water_Column_S2_Conc)*Diff_Piston_Velocity*Porosity
OUTFLOWS:
S2_SO4_Oxidation_Flux = Kf_oxid_S2_SO4*Water_Column_S2_Mass
Surface_Water_Export_S2 = Qout*Water_Column_S2_Conc

Conc_Org_S = Mass_Org_S/Volume
Conc_SO4 = Mass_SO4/Volume
Conc_SO4_ueq_L = Conc_SO4*1000/16
Diff_Piston_Velocity = 2
Org_S_Bulk_Sed_Conc = Org_S_Sediment_Mass/Vol_Sed
Org_S_Sed_Conc = Org_S_Sediment_Mass/Mass_Sediment_Particles
Porosity = Sed_H2O_Content/(Sed_H2O_Content+(100-Sed_H2O_Content)/rho_sed)
S2_Pore_Bulk_Conc = Sulfide_Porewater_Mass/Vol_Sed
S2_Pore__Conc = Sulfide_Porewater_Mass/Vol_Sed_H2O
SO4_Pore_Bulk_Conc = SO4_Porewater_Mass/Vol_Sed
SO4_Pore_Conc = SO4_Porewater_Mass/Vol_Sed_H2O
Volume = Area*Mean_Depth
Vol_Sed = Area*Z_sed/100
Vol_Sed_H2O = Z_sed/100*Area*Porosity
Water_Column_S2_Conc = Water_Column_S2_Mass/Volume

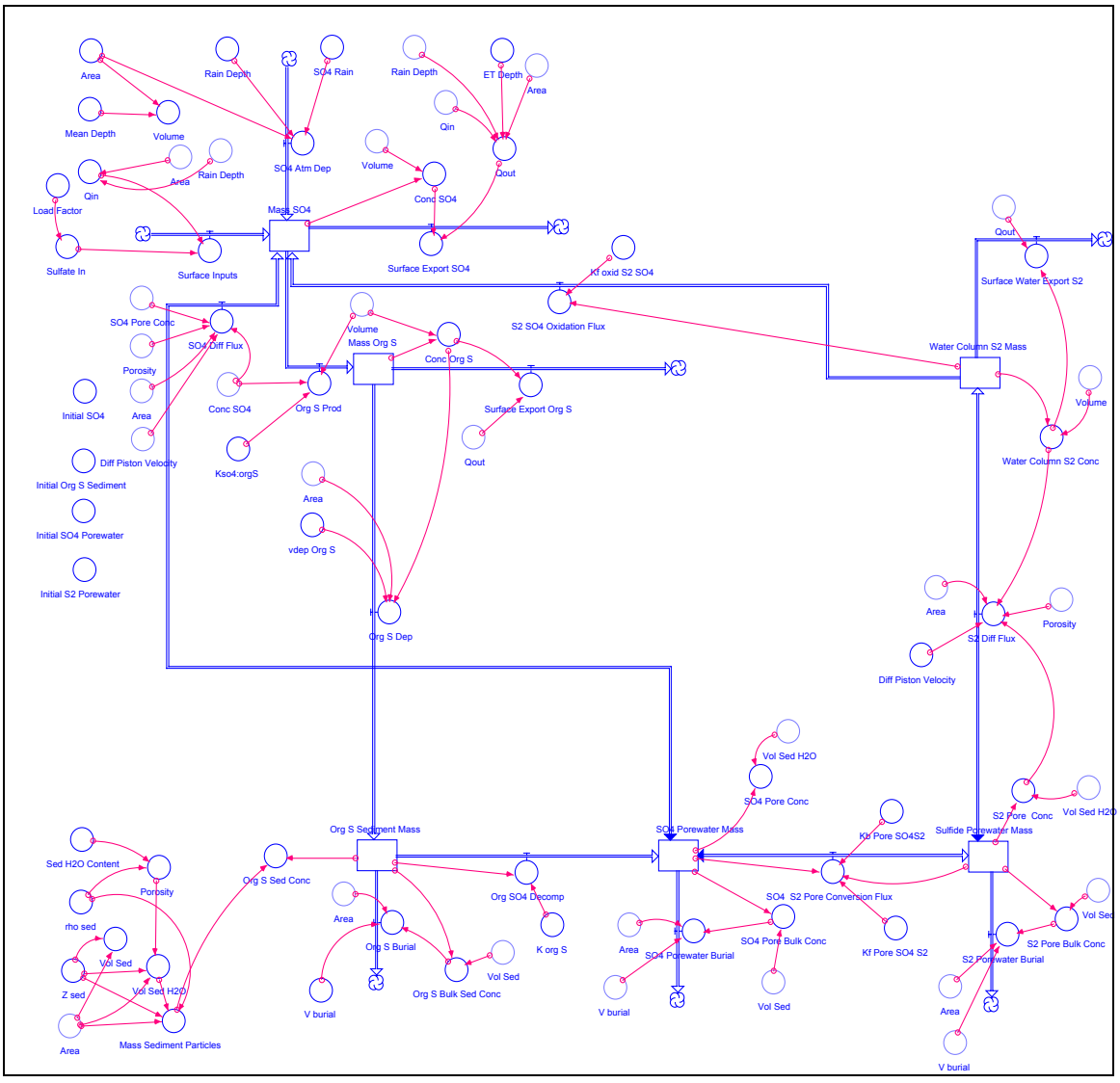

Figure 4-2. Schematic diagram of conceptual sulfate-sulfide cycling sub-model for E-MCM

See Table 4-1 for model equations specific to each interaction depicted.

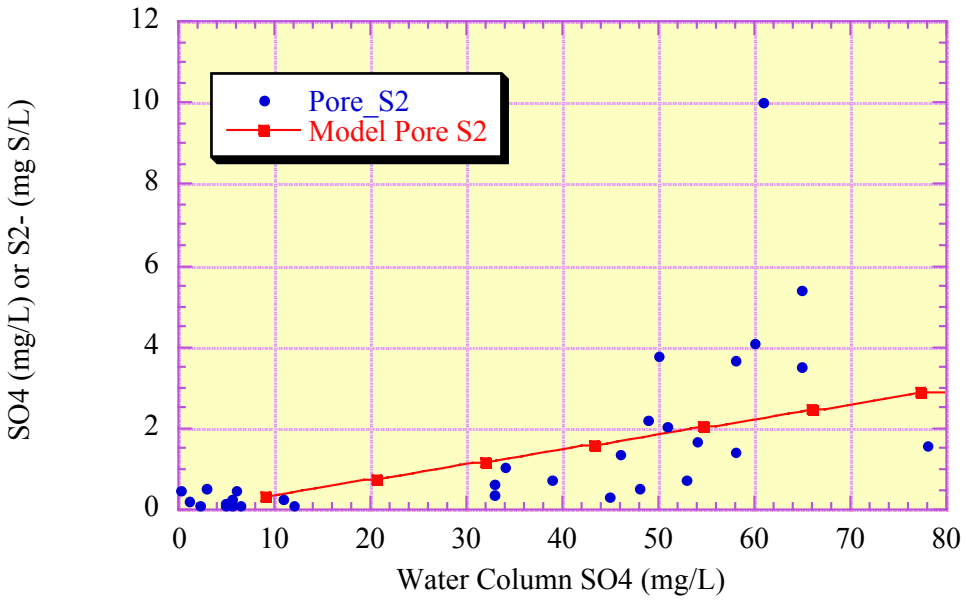

Figure 4-3. Comparison of modeled steady state relationship between water column SO42- and porewater S2- with observed values along NZ transect in WCA-2A

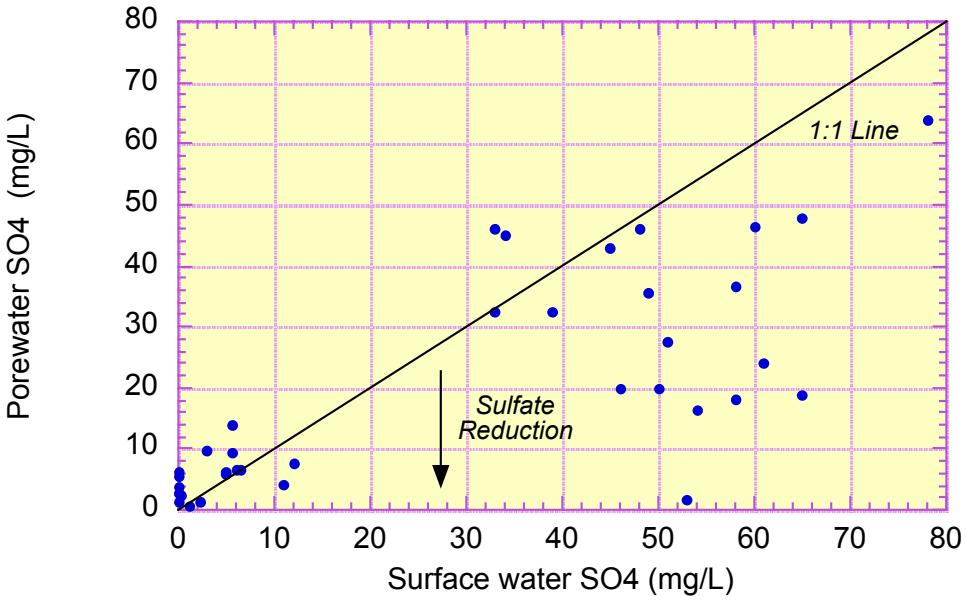

Figure 4-4, Comparison of porewater sulfate and surface water sulfate concentrations from samples collected along the "N and Z" transects in WCA-2A, October 1997 through November 2001.

4.4 Bottom-up Food Web Module

One of the intended applications of E-MCM is to examine the response of mercury cycling to changes in nutrient conditions. This includes changes to conditions such as plant species and particle budgets, but could also include changes in the structure of the food web. E-MCM has to-date used a "top-down" approach to assign the biomasses of fish populations, with the user specifying the initial biomass of the predatory fish species. The model then determines the biomasses and production of two underlying fish populations to support the predators. Lower food web biomasses (plankton, benthos, etc.) are simply input directly by the model user, as are fish growth rates and dietary preferences. This top-down approach requires the user to assign inputs reflecting the trophic status of a site. The South Florida Water Management District and Florida Department of Environmental Protection expressed an interest in establishing a "bottom-up" approach in which the model would start with primary productivity and move up the food web. Each higher level in the food web would have its biomass and production affected by the ability of the underlying system to support it. This section of the report describes the bottom-up approach developed and set up as a prototype for testing within E-MCM. Note that the model interface is designed so the user can use the original (top-down) or (bottom-up) new approach to represent the food web.

Biomass, turnover and aerial coverage equations from Fink (2002a) were used to yield production of cattails, sawgrass, lilies and periphyton as functions of total phosphorus concentrations in surface waters. These four plants, plus detritus production from these plants comprise primary production. The secondary level of the food web is composed of zooplankton, shrimp, and benthos. The third level is comprised of fish populations.

To set up initial conditions, a predator level is allowed to consume a specified amount of production from lower levels of the food web. For zooplankton, shrimp, and benthos, a "growth efficiency" term from the literature (Jorgensen 1991, Christian 1999) coupled with the "consumed productivity" from lower levels allows the growth or production of that predator level to be calculated. The production/biomass ratio for the predator (Jorgensen 1991, Christian 1999) allows the predator biomass to be calculated. Stated in quasi-mathematical terms:

> *Predator Production = (sum of prey production consumed by predator) x (predator growth efficiency)*
>
> *Predator Biomass = (predator production) / (predator production/biomass ratio)*

In the model, this translates into the following: "FracAvail", shown in Table 4-2, is the total fraction of production of a particular prey item that is available to all predators. Each column represents predators and each row represents prey. The fractions under the predators in each column represent the fraction of prey production consumed by that particular predator. For example, the fraction at the intersection of zooplankton column and the periphyton row represents the fraction of periphyton production consumed by zooplankton. The sum of the fractions in each row can be less than or equal to 1 since production can be "left over" to satisfy demand from other predators. Macrophytes that consist of cattails, sawgrass and "other macrophytes" are assumed to be available as the ratio of their individual biomass to the total macrophyte biomass.

Predator consumption of a prey item is calculated as:

Predator consumption of prey item = (prey production) x (prey FracAvail) x (fraction of prey production consumed by predator)

As predators consume the prey the available biomass of a prey item is adjusted downward. The sum of predator consumption over all prey items is the total prey consumption by that predator. The product of predator growth efficiency and total prey consumption available equals predator growth or production. Predator biomass is then calculated from the productivity/biomass ratio ratio (Jorgensen 1991, Christian 1999).

Row Name	FracAvail	Peri	Cattail	Sawgrass	Other macro	Detritus	Zooplankton	Shrimp	Benthos	Non-pred fish	Omni fish	Pred Fish
Periphyton	0.3	0	0	0	0	0	0.3	0.2	0.1	0.05	0	0
Cattails	0.02	0	0	0	0	0	0.3	0.2	0.1	0.01	0	0
Sawgrass	0.01	0	0	0	0	0	0.3	0.2	0.1	0.01	0	0
OtherMacro	0.01	0	0	0	0	0	0	0	0	0.01	0	0
Detritus	0.01	0	0	0	0	0	0.3	0.2	0.1	0.01	0	0
Zooplankton	0.2	0	0	0	0	0	0	0.3	0.2	0.1	0.05	0.001
Shrimp	0.2	0	0	0	0	0	0	0	0.3	0.1	0.05	0.001
Benthos	0.2	0	0	0	0	0	0	0	0	0.05	0.05	0.01
NonPredFish	0.2	0	0	0	0	0	0	0	0	0	0.1	0.02
OmniFish	0.2	0	0	0	0	0	0	0	0	0	0	0.1
PredFish	0.2	0	0	0	0	0	0	0	0	0	0	0

Table 4-2. Example production matrix from bottom-up food web module

The next step is to move up the food web to the next level. The production of the previous lower level of the food web becomes available to that predator and the process is repeated. The above method is used for the determination of initial conditions for all food web levels.

During each time step of the model run after time zero, available primary productivity is assessed and compared to initial primary productivity. Fish spawning success is adjusted based on the ratio of current and initial primary productivity.

The primary and secondary producers are assumed to instantaneously change in biomass and productivity based on phosphorus levels using the method outlined above. Thus it is recommended that phosphorus levels be changed gradually (e.g., over at least a year or two) to allow the fish populations to "adjust" to changes in phosphorus levels.

In the dynamic simulation fish consumption is driven by the "who eats what" food preference matrices not the production matrix. The food preference matrices give a detailed cohort-by-cohort breakdown of fish consumption and are a necessary level of detail to track mercury consumption. The user should make sure that the initial conditions for fish in the production matrix and the food preference matrices have similar values.

Fish "search" for prey as follows: The top level predatory fish get the first "choice" for available food, followed by smaller fish. They first prey on other fish (including self-predation) based on

size preference and the specified fraction of fish in their diet. If insufficient biomass (limited by mortality rate) is available in preferred size categories they will the search for smaller fish. All fish-to-fish predation is limited by mortality rates. Any "left over" fish-to-fish consumption is transferred down to lower levels of the food web. Consumption of lower levels of the food chain by fish is limited by the fraction of a diet item that is available as indicated by the production matrix. If the fish reaches the bottom of the food chain (i.e. detritus) any remaining consumption is allocated to detritus. Excess consumption of detritus is limited by the total amount of detritus. A message will appear in the unlikely event that total amount of detritus is depleted.

At this juncture, the bottom-up module has been coded and has undergone some preliminary testing. The model has been parameterized within the limitations of available data and knowledge. The user selects the bottom-up or top-down approach with a switch on the model interface. It is not currently feasible, however, to proceed with the bottom-up module beyond the conceptualization stage into rigorous testing and validation. This is because a number of limitations emerged as the module was developed, including the following:

- One of the primary reasons for interest in a bottom-up food web is to have a framework to adjust trophic structure, biomasses, and hence pathways for methylmercury to move through the food web to fish, as a function of primary productivity (using total phosphorus as a governing factor). Unfortunately, little information was found in the literature describing energy flows through the lower food web for the Everglades, and no information was found describing how these pathways might change as a function of total phosphorus concentrations. For a bottom-up approach to function properly to help predict the effects of changes in system productivity on fish mercury concentrations, information is needed on trophic structure and energy flows in Everglades marshes under a range of productivity conditions. A set of governing relationships describing how the lower (below fish) trophic level structure changes as a function of system productivity is needed.

- Relationships estimating fish biomasses, growth rates and diets as functions of system productivity need to be developed.

- The effects of water level fluctuations and wet/dry cycles on habitat and fish behavior are not included, for fish staying within the modeled area.

- Fish leaving or returning to the system are not modeled. This is particularly relevant in situations with wet/dry cycles that might induce fish to leave marshes for periods of time. This problem is also relevant for the top-down approach, if fish spend significant periods of time outside the modeled domain.

Conceptually, the development and incorporation of the bottom-up food web module is a sound idea, and is consistent development of a model framework capable of examining the effects of various types of system perturbations on mercury cycling (e.g., mercury loading, hydrology, nutrients, and sulfate loading). Until the primary data and questions relating to trophic energy transfer, growth rates and diets can be gathered and resolved, however, the utility or this approach is constrained. Prior to further testing and validation of the bottom-up module, the following should occur:

- Relationships between food web structure and energy dynamics in Everglades marshes as functions of trophic status (e.g. total phosphorus) need to be established. In particular, shifts in the pathways that methylmercury follows from the "base" of the trophic system to top

predatory fish as a function of system productivity need to be clarified. This includes energy and methylmercury flows through the lower food web and through fish populations to the top predators. The effects of system productivity on lower food web and fish species dominance, growth rates and diets need to be quantified.

- With the above information in-hand, the current model approach to the bottom-up food web should be revisited; and

- The costs of pursuing those two research goals (coupled with the costs of more extensive testing and validation) should be examined in terms of the benefits of having a bottom-up approach vs. the relative inefficiencies and potential errors inherent with the manual manipulations of the top-down approach.

4.5 E-MCM Monte Carlo Capability and Model Input Dependencies

Background

The capability to conduct probabilistic (Monte Carlo) simulations was built into E-MCM during Phase I. A sample application of the Monte Carlo method was carried out for the Everglades Nutrient Removal Project (ENR), and is described in a later section (Section 5.1.3). This section describes the Monte Carlo approach and its implementation in the model.

The Monte Carlo approach allows a model to be run in a manner that systematically attempts to estimate the uncertainty in model predictions, based on uncertainty or natural variability in model inputs. This is fundamentally different to a deterministic simulation, for which inputs and outputs have no associated uncertainty.

Description of the Monte Carlo capability in E-MCM

The probabilistic version of E-MCM currently includes three types of probability distributions: normal, lognormal and rectangular. Algorithms from Knuth (1990) were used for the normal and lognormal distributions. The random number generator used was included with Visual Basic 5.0 Professional Edition. Knuth's shuffle algorithm was used shuffle the random number series to ensure randomness (Knuth 1990).

E-MCM is now set up so the user can select whether to run the model in deterministic or probabilistic mode. From the main menu, the user can select "View" then "User Options", and check or uncheck the probabilistic option. If the probabilistic option is chosen, input forms allow the user to enter distribution types and values for mean, minimum and maximum values for input variables. Specification of minima and maxima for variables truncates distributions so that unwanted extreme or negative values are avoided. The model interface screen for viewing outputs was modified so that histograms and summary statistics of desired outputs can be viewed. Note that a probabilistic scenario can also be run in deterministic mode. The model will simply use the mean values for input distributions, and does not make use of the standard deviations, minima or maxima. In the case of a lognormal distribution, the user should enter the geometric, not arithmetic, values for the means and standard deviations. If the model is then run deterministically, the model will simply use the geometric mean as the value for the simulation.

One of the key concerns surrounding the use of the Monte Carlo method for environmental simulations is that unrealistic combinations of inputs can emerge if all inputs are assumed to behave independently, when in fact some inputs are often related to others. To help reduce the potential for this situation to occur, E-MCM has been designed such that some inputs can be made to depend on other inputs for probabilistic simulations. Dependencies between selected inputs can be switched on or off, but the relationships between inputs are "hard-wired" and can not be modified by general model users.

A sample application of the Monte Carlo approach for an ENR simulation is described in Section 5.1.3

The Monte Carlo module has not been activated for the linked-cell version of E-MCM and, as mentioned previously, is only available for the unit wetland version of E-MCM. There are a number of difficulties involved in adding this capability to a linked model, and these relate principally to managing inputs in a meaningful and consistent manner. Difficulties arise when considering parameters such as DOC or mercury partitioning constants that are input by the user for each cell, and the statistical properties (type of distribution, minima, maxima, and standard deviation) that apply for that variable in one cell in the model may not be appropriate for another cell. The difficulties are principally related to coding the interface to properly control how parameter data are input to the Monte Carlo module and handled by the model to ensure self-consistent perturbations of a variable in a manner that does not violate any constraints within a given cell, and in essence treats each cell in the same manner. These difficulties can be overcome, but to resolve these so that the Monte Carlo module could be implemented in the linked-cell model at this time was considered beyond the scope of this project.

The benefits of extending Monte Carlo capabilities beyond the unit wetland model to the linked model inure principally when simulating portions of the Everglades where the Hg loading to the cells in question is dominated by surface water rather than atmospheric inputs. Otherwise, using the unit wetland model for sites dominated by atmospheric inputs (e.g., WCA 3A-15) and conducting Monte Carlo simulations should give a very good idea of the inherent uncertainty in the predicted results (this, of course, assumes that the uncertainty input by the user is well characterized).

4.6 Linking E-MCM with External models

E-MCM was modified to enable it to input directly (soft-linked) simulation output results from the SFWMD's General Ecosystems Model (GEM; Fitz et al. 1996). GEM forms the unit wetland module for the spatially distributed Everglades Landscape Model (ELM), which is used to predict various aspects of trophic state changes such as production rates, decomposition rates and the peat sediment formation rates resulting from changes in phosphorus loading to the system. Ultimately it is was not possible to use the current version of ELM supported by the District to provide inputs related to system productivity because modifications to ELM were required to output the full suite of hydrologic and trophic state variables needed for E-MCM. As described in later sections, Tetra Tech Inc. subsequently developed a set of empirical relationships to predict particle budgets and sedimentation rates as a function of total phosphorus concentrations in surface waters.

5 E-MCM applications to individual sites

5.1 Application of E-MCM to ENR

5.1.1 ENR Site Description

The Everglades Nutrient Removal Project (ENR) is a 1,535-hectare engineered wetland created by flooding former farm land. It is designed to remove excess phosphorus from about one-third of the runoff from the 283,280 ha Everglades Agricultural Area (SFWMD, 1999b). General characteristics of the ENR are shown in Table 2-1.

There are two parallel treatment areas in the ENR. Each consists of an upper flow way and a lower treatment cell (see Figure 5-1). Initially water is pumped from a supply canal into a 55 hectare buffer cell at the northern end of the area. Water exits the buffer cell into the 515 hectare Cell 1 and the 405 hectare Cell 2 with a 40/60 percent split in the flows respectively. Water exits cell 1 into cell 3 (414 hectares) and from cell 2 into cell 4 (158 hectares). The combined outflow from cells 3 and 4 is discharged through the outflow station (SFWMD, 1999b).

Cells 1,2 and 3 are vegetated mainly with cattails while cell 4 is maintained as open water through herbicide spraying. Open water areas in cells 1, 2 and 3 are covered with water lettuce, water hyacinth, coontail and dense mats of submerged and floating periphyton. Cell 4 open waters are principally covered with submerged macrophytes and periphyton (SFWMD, 1999b).

The target mean water depth and hydraulic retention time are 0.6 m and 28 days respectively (SFWMD, 1999b).

There was a concern that a newly flooded area would result in increased fish mercury concentrations (SFWMD 1999b) as has often been documented for new hydroelectric reservoirs. ENR began operations in 1994 and an extensive mercury monitoring program was established from March 1995 and continues through the present.

Unfiltered and filtered grab samples of inflow, interior culverts, and outflow were collected biweekly and two interior marsh sites in each cell every four weeks for total mercury and methylmercury analysis (L. Fink pers. comm.). Total mercury concentrations in precipitation were based on monthly integrated samples (L. Fink pers. comm.). Mosquitofish were collected from the same two interior sites in each cell quarterly, plants semi-annually and 10-cm sediment cores annually and analyzed for total mercury and methylmercury. This intensive sampling occurred from January 1995 through January 1999 when the first and last sediment samples were collected (L. Fink pers. comm.). In addition, an intensive study of Hg(0) production and evasion was carried out in 1995-1997 by Lindberg et al. (1999, 2000, 2002), an intensive study of fish concentrations was conducted in 1995-1998 by Lange *et al*. (1998), food web structure in June 1998 by Hurley *et al*. (1999), and an intensive study of methylation and demethylation rates was carried out in 1995-1998 by Gilmour *et al*., 1998a,b; 1999 and Marvin-DiPasquale and Oremland (1998) and Marvin-DiPasquale *et al*. (1999) and a follow-up intensive study in February 2000 (Marvin DiPasquale *et al*., 2001). Other programs monitored water quality in the ENR. Data

from all these sources were used as inputs and outputs for E-MCM (see Appendix A for data sources for E-MCM inputs for ENR simulations).

The monitoring program showed that contrary to the hypothesis that ENR would behave like a new reservoir and result in elevated fish Hg levels, concentrations of methylmercury in water, sediments, and fish were very low. This dataset provided an excellent opportunity to explore factors affecting fish mercury concentrations in Everglades marshes, and to calibrate and test the Everglades Mercury Cycling Model, previously applied to Water Conservation Area 3A-15 (Tetra Tech, 2001).

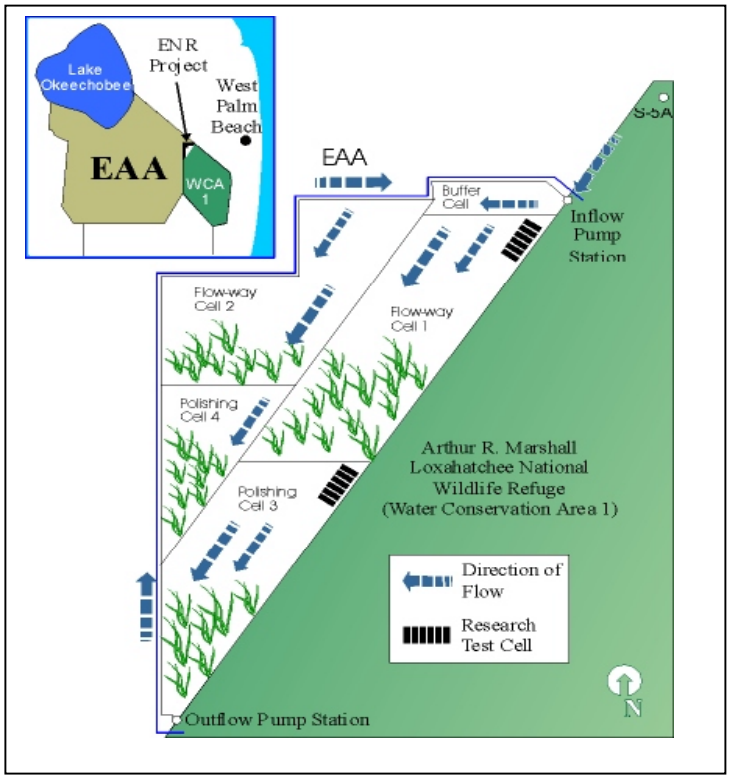

Figure 5-1. Site map for the Everglades Nutrient Removal (ENR) project

Source:(SFWMD)

Three distinct types of simulations were performed for ENR:

Deterministic application using a single cell approach to ENR
Deterministic application using a 2-cell approach to ENR
Monte Carlo application using a single cell approach to ENR*

* Note that it is not yet possible to carry out probabilistic simulations with a multi-cell scenario.

Each of these ENR model applications is described below. In all cases ENR calibration simulations were carried out for the period March 1995 when ENR began operations through March 1999. Initial conditions were based on observed ENR field conditions.

5.1.2 Deterministic E-MCM simulations for ENR

5.1.2.1 Single Cell Deterministic Simulation of ENR

Initial ENR calibration runs considered the entire ENR (Cells 1-4 and the buffer cell) as a single entity. Inflow mercury concentrations to the buffer cell were used as inputs to the ENR. Simulation results predicted high inorganic Hg(II) concentrations relative to field data. It was hypothesized that significant sediment borne mercury was settling in the buffer cell. It was further postulated that accounting for this early settling might, at least partially, explain the high simulated inorganic Hg(II) results. Two different approaches were subsequently taken to accommodate the effects of the buffer cell, distinct from the remainder of ENR. The first approach was to move the boundary of the modeled area from the inflow of the buffer cell to the outflow of the buffer cell. Mercury loads via inflows were reduced by applying a reduction factor to the buffer cell mercury inflow. The second approach, discussed in later sections, was to use the linked-cells version of the model to distinguish the buffer cell from the remainder of ENR. The "correction factor" for the first approach was developed as follows:

Monitoring Site		Observed Mean Hg_t	Observed Mean MeHg	Estimated Mean HgII
		ng L^{-1} (unfiltered)		
ENR002	Inflow to Buffer Cell	1.96	0.21	1.75
G252C	From Buffer Cell to Cell 1	1.16	0.19	0.97
G252G	From Buffer Cell to Cell 1	1.18	0.17	1.01
G255	From Buffer Cell to Cell 2	1.75	0.16	1.59
ENR102	Cell 1	1.02	0.1	0.92
ENR103	Cell 1	0.74	0.05	0.69
ENR204	Cell 2	0.95	0.09	0.86
ENR203	Cell 2	0.83	0.14	0.69
ENR302	Cell 3	0.8	0.06	0.74
ENR303	Cell 3	1.04	0.05	0.99
ENR401	Cell 4	0.83	0.09	0.74

Table 5-1. Mean observed Hg concentrations in ENR from August 1994 to August 1997

Table 3-1 shows mean values for mercury concentrations for the period from August 1994 to August 1997 (SFWMD, 1999b). The total mercury mean value for the inflow, due to several outliers, was adjusted using detailed mercury data from the ENR mass balance spreadsheet

(SFWMD, 2002a) for station ENR002. Note the higher total mercury value for G255, relative to all other interior and buffer outflow sites. The two other buffer outflow concentrations (G252C and G252G) were almost identical. Values for the first interior monitoring sites ENR 103 and ENR204 also were low and more in the "ballpark" of G252C and G. Sixty percent of the flow from the buffer cell passes through G255, with the remaining forty percent passing through the other control structures. According to SFWMD, 1998 water discharged through G255 passed through a relatively straight flow path while G252C and G took a more circuitous path. It is likely that the G255 inflow is still carrying high sediment mercury load, perhaps due to higher flowrates, that settles out shortly after entering the ENR. As a result, the ratio of the Hg(II) inflows from G252C and G to the inflow Hg(II) (ENR002) was used to correct the ENR inflow time series at ENR002. This method produced a correction factor of 0.57 for Hg(II) inflow concentration; *i.e.*, the concentration leaving the buffer cell was 57% of that entering. MeHg concentrations from G252C, G252G and G255, and the 40/60 % flow ratio between buffer outflow to cells 1 and 2 respectively were used to obtain a MeHg correction factor of 0.82 (i.e. an 18% reduction in MeHg concentrations across the buffer cell). The ENR002 mercury inflow concentrations to the buffer were multiplied by these two correction factors to obtain corrected buffer outflow mercury concentrations. Figure 5-2 and Figure 5-3 show observed mercury concentrations at the inflow and outflow from ENR, as well as the estimated "effective" concentrations from the buffer cell to the modeled area.

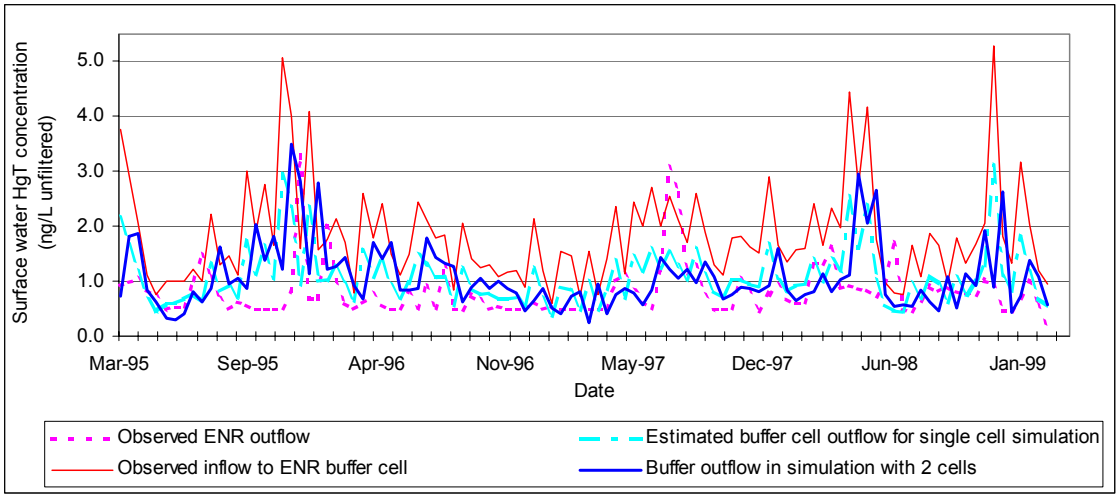

Figure 5-2. Total mercury concentrations in surface waters for 3 ENR locations (Data source: SFWMD 2000a)

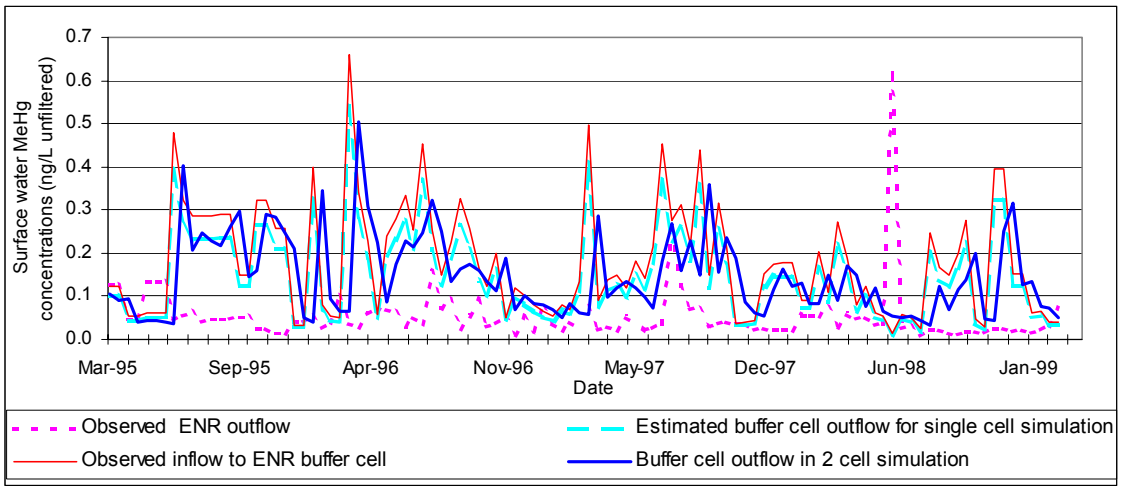

Figure 5-3. Surface water MeHg concentrations at 3 ENR locations. (Data source: SFWMD 2000a)

Initially simulations were run using the rate constants for methylation and demethylation calibrated from WCA 3A-15. Dr. Cynthia Gilmour has indicated (personal communication), however, that incubations using ^{203}Hg(II) suggest low sediment methylation rates at ENR, possibly due to the inhibitory effects of sulfide. We therefore also considered a scenario with no *in situ* biological methylation or demethylation. Since the model does not yet fully incorporate the effects of sulfide to inhibit methylation, we had to manually set the rate constants for *in situ* biological methylation and demethylation to zero. Net biological demethylation is a possibility that was not pursued in these simulations but is worthy of future consideration.

Two different approaches were ultimately tested in terms of estimating particle budgets for ENR. The first approach used was to tune the model simulations to arrive at sedimentation rates comparable to those estimated using a feldspar marker (SFWMD 2000d), on the order of 30 mm per year of bulk sedimentation. No mass sedimentation rates (g m^{-2} yr^{-1}) were available in connection with the feldspar data. The supply of settling matter from macrophytes and periphyton was estimated using empirical relationships developed by L. Fink (cited in Ambrose et al., 1997) that estimate biomass densities and turnover rates for sawgrass, cattails and periphyton. Decomposition in sediments and at the sediment water interface was adjusted to arrive at a bulk sedimentation rate consistent with the feldspar data. Note that it is preferable to tune the model sedimentation on the basis of mass fluxes (g solids m^{-2} yr^{-1}), but such information was not available with the feldspar data.

The second approach to deriving a particle budget for ENR was based on the use of a recently developed approach described in Tetra Tech (2003), a report in progress. This approach used the macrophyte biomass and turnover equations described above as well as a set of revised empirical equations to predict net particle accumulation rates as a function of surface water total phosphorus concentrations, based in part on the empirical relationships originally derived by Walker and Kadlec (1996). The mass sedimentation rates estimated with this 2nd approach were considerably less than the rates estimated with the feldspar data (406 versus 1778 g m^{-2} yr^{-1} sedimentation at a depth of 3 cm). The mass sedimentation rates from this latter approach were more consistent with rates estimated for WCA 2A and WCA 3A-15

ENR Model Results – Single Cell Deterministic Simulation

The mean predicted and observed mercury concentrations for critical water, sediment and biological parameters are shown in Table 5-2 for the simulated period March 1995-March 1999, for the single cell deterministic simulation with the ENR model cell boundary being the outflow from the buffer cell. This simulation had a particle budget based on feldspar data (SFWMD 2000d)

Figure 5-4 through Figure 5-10 show predicted and observed concentrations of total and methylmercury in various compartments. Reasonable fits between predictions with the single cell scenario and observations were obtained for total mercury in water, while predicted total mercury on sediment solids was at the low end of the observed range (Table 5-2, Figure 5-4 and Figure 5-6). It is important to note that for this particular single cell simulation, partitioning of inorganic Hg(II) on settling solids in the water column was underpredicted by more than an order of magnitude. Inorganic Hg(II) partitioning was adjusted to better match observations in subsequent model runs using 2 linked cells, as will be discussed in subsequent sections.

Methylmercury concentrations were somewhat overpredicted in water and sediments with the single cell scenario, even when there was no *in- situ* methylation invoked (Table 5-2, Figure 5-5 and Figure 5-7). Predicted concentrations in fish were low, consistent with observations. Predicted fish mercury concentrations were within the observed range for both scenarios run (Figure 5-8 through), but a simulation applying the *absolute* rate of methylation from WCA 3A-15 at ENR (6.4 $\mu g\ m^{-2}\ yr^{-1}$) would likely have resulted in a poorer fit between predicted and observed methylmercury levels in the system. This scenario should be simulated in the future as a further test of the relative importance of methylation rates versus other site factors affecting fish mercury concentrations.

Output Name	Units	Results for 3A-15 M/D constants	Results for Single Cell Deterministic Simulation	Results for Two Cell Deterministic Simulation	Observed	% Difference between Single Cell simulation and observations	% Difference between Two Cell simulation and observations
Surface water MeHg	ng/L unfilt	0.15	0.098	0.096	0.069	42.04%	36.72%
Surface water Hg(II)	ng/L unfilt	0.86	0.86	0.76	0.82	5.69%	-8.03%
Surface Sed MeHg	ug/g dry	0.00023	0.00011	0.00029	0.000069	52.90%	324.62%
Surface Sed Hg(II)	ug/g dry	0.033	0.033	0.077	0.078	-57.40%	-1.49%
Surface Sed porewater MeHg	ng/L	0.25	0.12	0.26	0.10	20.73%	171.19%
Surface Sed porewater Hg(II)	ng/L	0.44	0.45	1.14	2.53	limited observations (n=3)	limited observations (n=3)
Age 1 LMB	ug/g wet	0.05	0.03	0.030	0.04	-24.83%	-30.02%
Age 3 LMB	ug/g wet	0.13	0.089	0.099	0.075	17.14%	31.08%
Age 4 LMB	ug/g wet	0.14	0.09	0.12	0.14	-34.08%	-14.23%
Age 5 LMB	ug/g wet	0.15	0.11	0.15	0.09 (limited data n=2)	16.88%	54.39%

Age 1 Sunfish	ug/g wet	0.016	0.009	0.015	0.013	-31.33%	21.25%
Age 3 Sunfish	ug/g wet	0.06	0.04	0.042	0.03	51.94%	63.59%
Mosquitofish	ug/g wet	0.020	0.012	0.028	0.025	-49.21%	12.53%
Apparent MeHg partitioning in surface sediments		2.96	2.96	3.6	2.86		
Apparent Hg(II) partitioning in surface sediments		4.87	4.87	4.3	4.49		
Apparent total mercury partitioning in surface sediments		4.68	4.78	4.7	4.47		

Table 5-2. Predicted and observed means for selected parameters

(Data sources: Water concentrations: SFWMD, 2000a; sediment concentrations: Gilmour *et al.* 1998a, fish concentrations: Florida Fish and Wildlife Conservation Commission, 2000, and SFWMD 1999b)

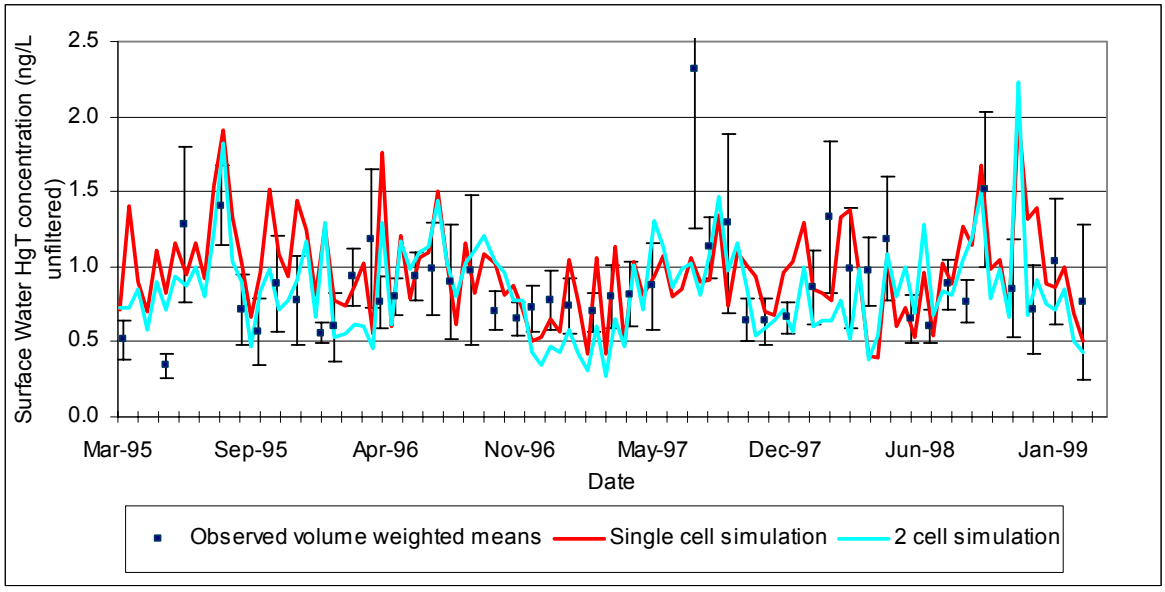

Figure 5-4. Observed and predicted total mercury concentrations in ENR surface waters. (Data source: SFWMD, 2000a)

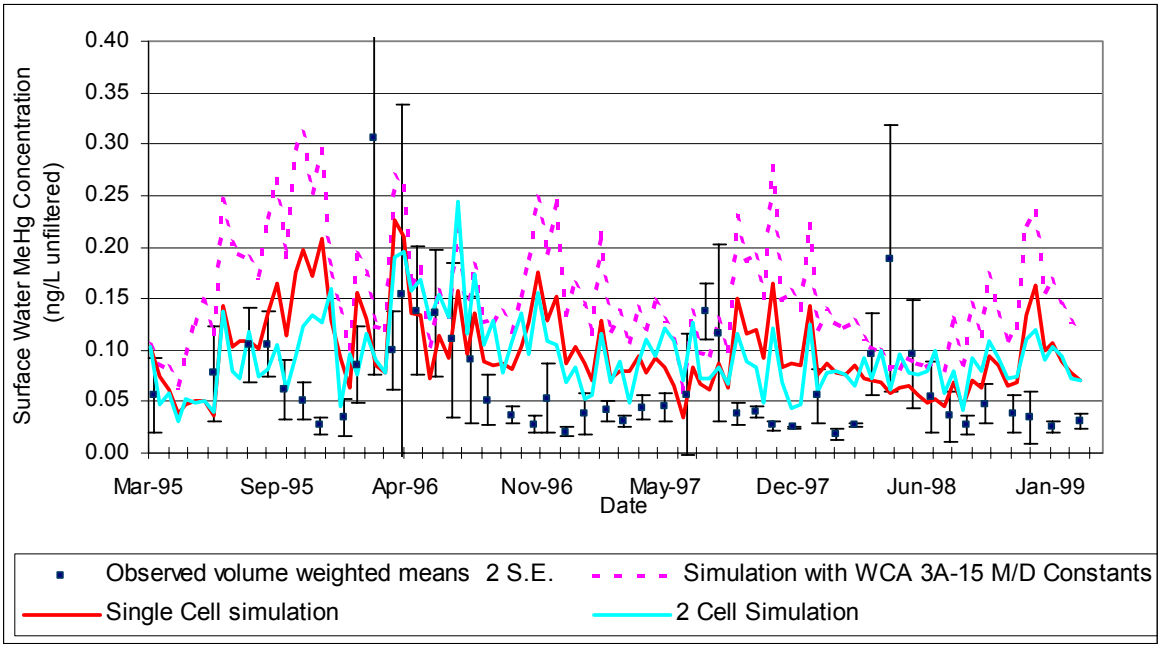

Figure 5-5. Observed and predicted surface water methylmercury concentrations at ENR. (Source of observations: SFWMD 2000a).

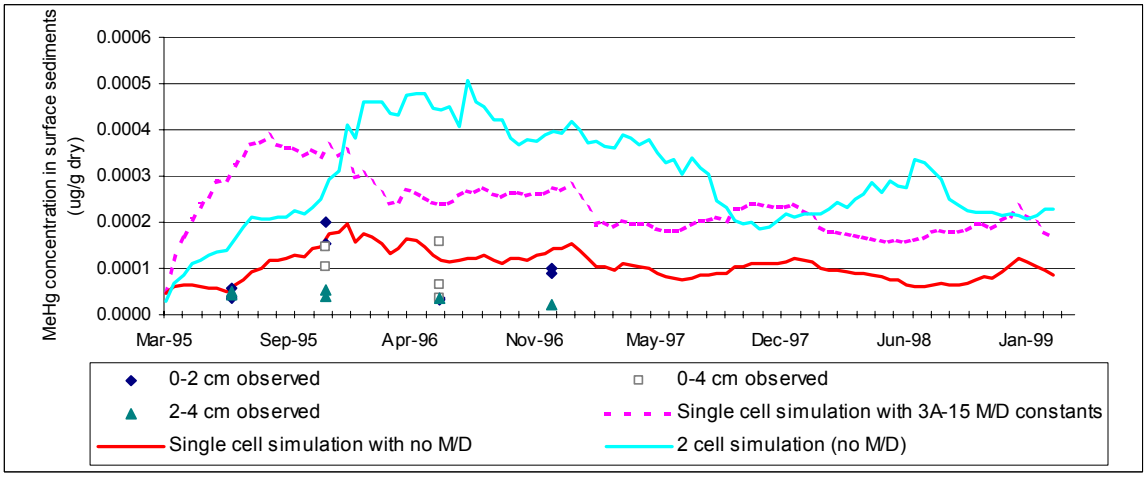

Figure 5-6. Observed and predicted total mercury concentrations for surficial sediments (0-3 cm) at ENR. (Source of observations: Gilmour *et al.,* 1998a)

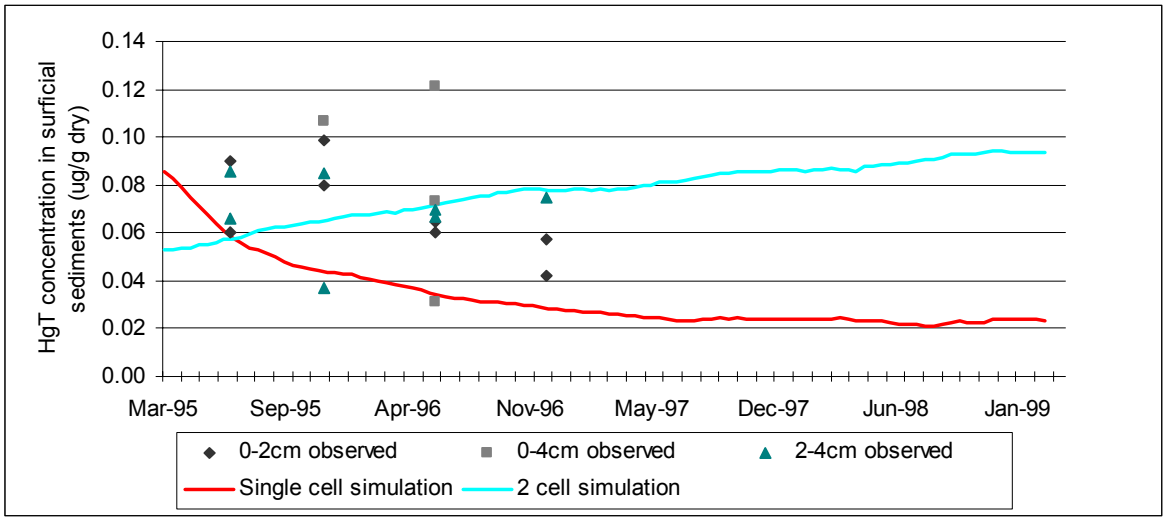

Figure 5-7. Observed and predicted methylmercury concentrations in sediment solids in surficial sediments (0-3 cm) at ENR. (Source of observations: Gilmour *et al.*, 1998a)

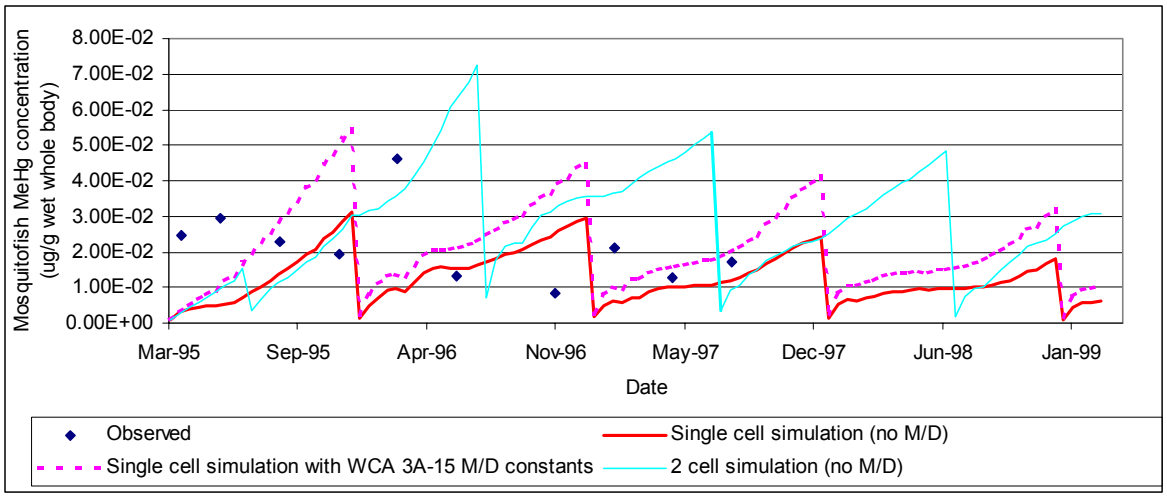

Figure 5-8. Observed and predicted mercury concentrations in ENR mosquitofish (Source of observations: SFWMD, 1999b)

Note that in the above figure the single cell and 2 cell runs had different assumed spawning dates.

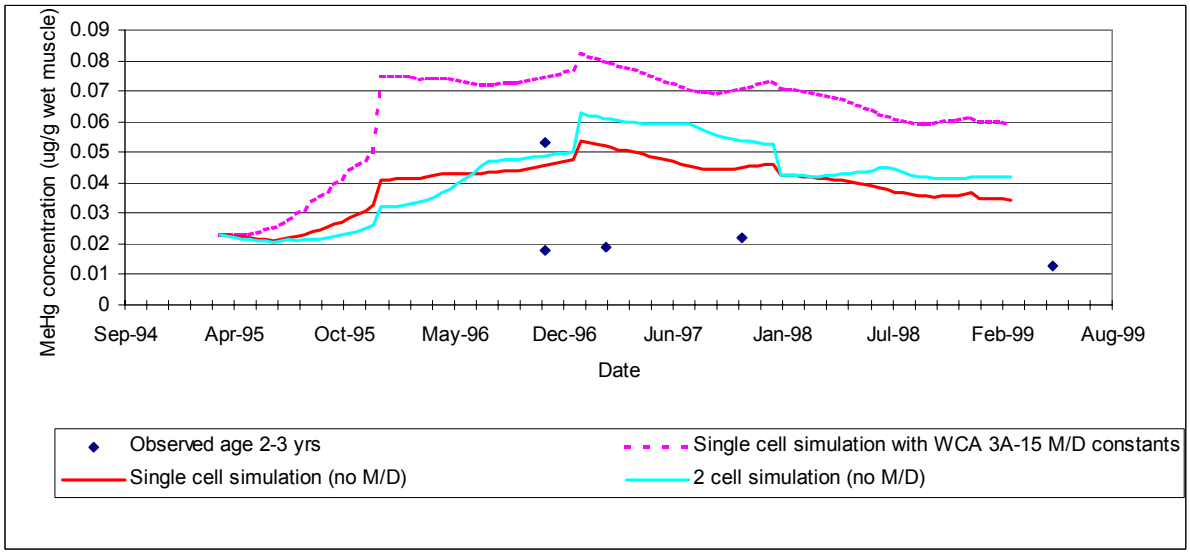

Figure 5-9. Observed and predicted mercury concentrations in 2-3 year old sunfish at ENR (Source of observations: Florida Fish and Wildlife Conservation Commission, 2000)

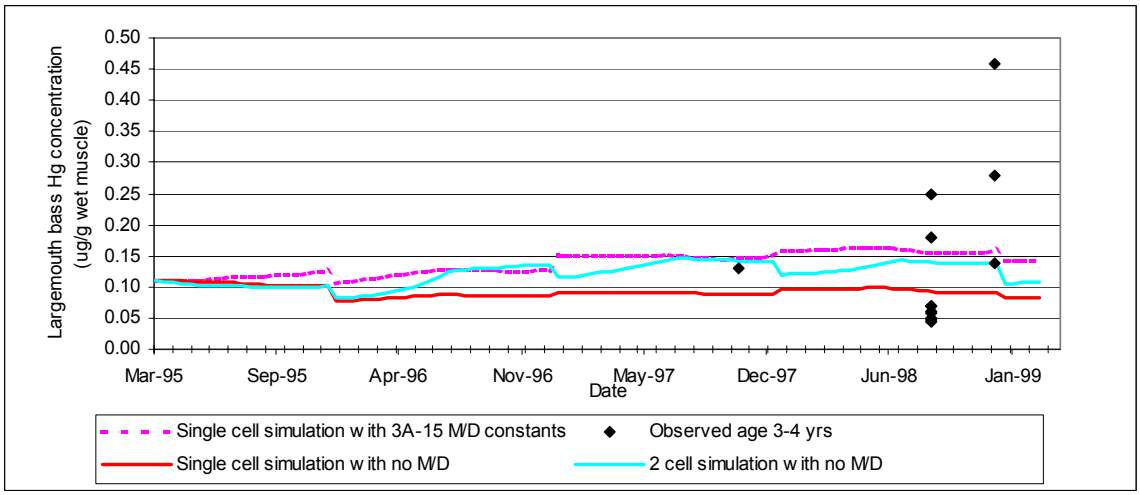

Figure 5-10. Observed and predicted mercury concentrations in largemouth bass (age 3-4 years) at ENR (Source of observations: Florida Fish and Wildlife Conservation Commission, 2000)

To examine sources and sinks for Hg(II) and methylmercury ENR, simulations were run with the single cell simulation until pseudo steady state conditions were achieved (~20 years). Since inputs were based on a four year period (1995-1999), the inputs were cycled on a four year basis, and the average fluxes for the last four year period are shown in Figure 5-11and Figure 5-12. Roughly three-quarters of the Hg(II) supply to ENR was predicted to be from the atmosphere (wet and dry/RGM deposition). Atmospheric loading of methylmercury was minimal however, with inflow accounting for almost all the MeHg supply to ENR in the simulation with no *in situ* methylation.

Field data clearly show that ENR acts as a trap for Hg(II) and methylmercury (Figure 5-2 and Figure 5-3). The entire ENR reduces the mean observed Hg(II) concentration 54% for the March 1995 – March 1999 period. Most of this reduction (43 out of 54%) occurs in the initial buffer cell, with the remainder occurring in the portion of the system downstream of the buffer cell. E-MCM predicts the portion of ENR excluding the buffer cell to act as a modest trap for Hg(II), reducing the inflowing Hg(II) concentration by about 10%. This is achieved in the model simulations primarily via burial (Figure 5-11).

Photoreduction of Hg(II) is of secondary importance as a loss mechanism in the model simulations at ENR. The mean annual predicted evasion rate for elemental mercury directly off the water surface at ENR is on the order of 2 ug m^{-2} yr^{-1}. This flux includes elemental mercury supplied by the predicted net rate of photochemical Hg(II) reduction, as well as a smaller component due to methylmercury photodegradation. Lindberg *et al.* (1999) estimated an evasion flux off the surface of ENR waters (not associated with vegetation) on the order of 50 g yr^{-1}, which translates into slightly more than 3 ug m^{-2} yr^{-1}, comparable with the model predictions. However, Lindberg *et al.* (1999) also estimated a much larger evasion rate of elemental mercury to the atmosphere from emergent vegetation, on the order of 1 kg yr^{-1} (equivalent to ~65 ug ug m^{-2} yr^{-1}). E-MCM does have a mechanism for macrophytes to take up Hg(II) from porewater, due to transpiration. The predicted magnitude of this flux was ~0.15 ug m^{-2} yr^{-1}, far less than the above field estimate. Even if all the inorganic Hg(II) predicted to be taken up by plant roots at ENR via transpiration was assumed to be reduced to elemental mercury and volatilized, the predicted flux would be on the order of 2.5 ug m^{-2} yr^{-1}. The discrepancy between our simulated results and Lindberg *et al*.'s measured volatilization rates over macrophytes was also noted

during simulations for WCA 3A-15 (Tetra Tech 2001). This may suggest an alternative mechanism unaccounted for in the model which could result in the localized reduction of Hg(II) at the root interface and subsequent flux through the plant to the atmosphere. Future attention to this topic is needed.

Overall, observations indicate that the ENR, as a whole, lowered MeHg concentrations in surface waters by approximately 72% for the March 1995 – March 1999 period. The buffer cell was responsible for only 17 of the 72% total, the remainder occurring downstream of the buffer cell. E-MCM also predicts the portion of ENR downstream of the buffer cell to act as a trap for MeHg, lowering the concentration of MeHg by 35%. This is achieved in the model simulations via a combination of MeHg photodegradation and burial Figure 5-12. Net biological demethylation is also a possibility. If the above predictions are combined with the observed reduction in MeHg concentration across the buffer cell, the total reduction in MeHg across ENR would be 46%.

Thus the buffer cell appears to be a better trap for Hg(II) than MeHg, while the portion of ENR downstream of the buffer cell appears to trap MeHg better than Hg(II).

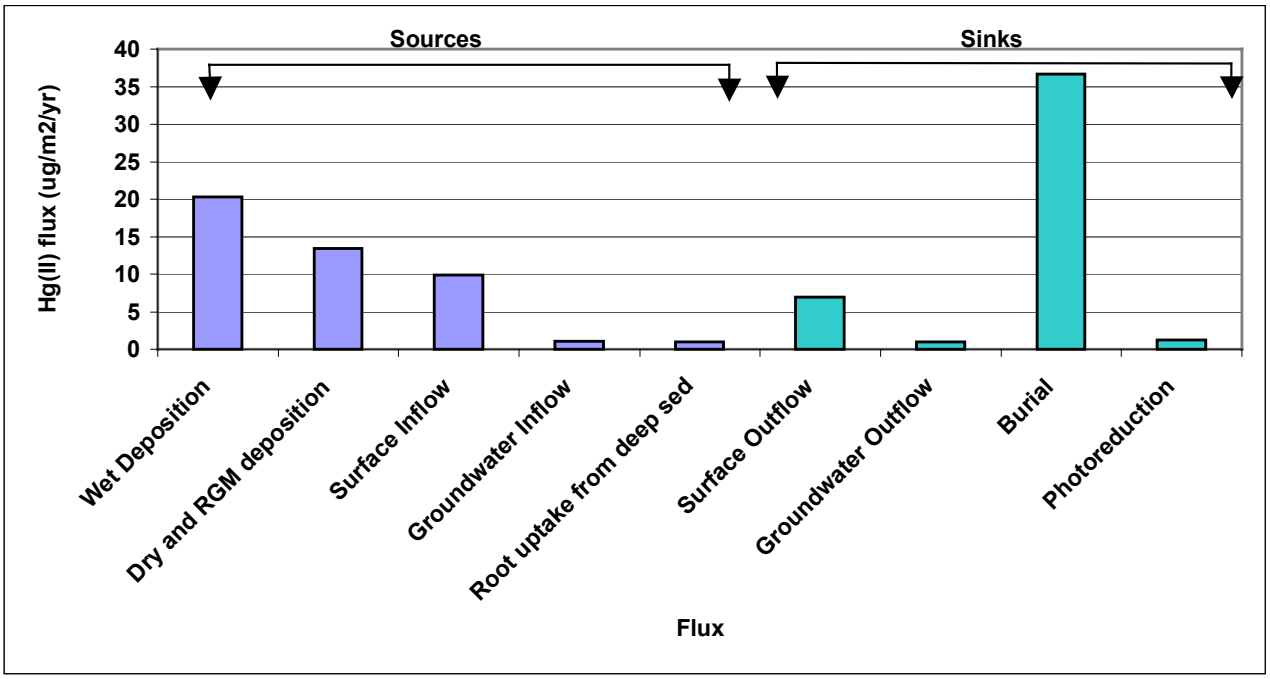

Figure 5-11. Predicted sources and sinks of inorganic Hg(II) for ENR at near-steady-state conditions

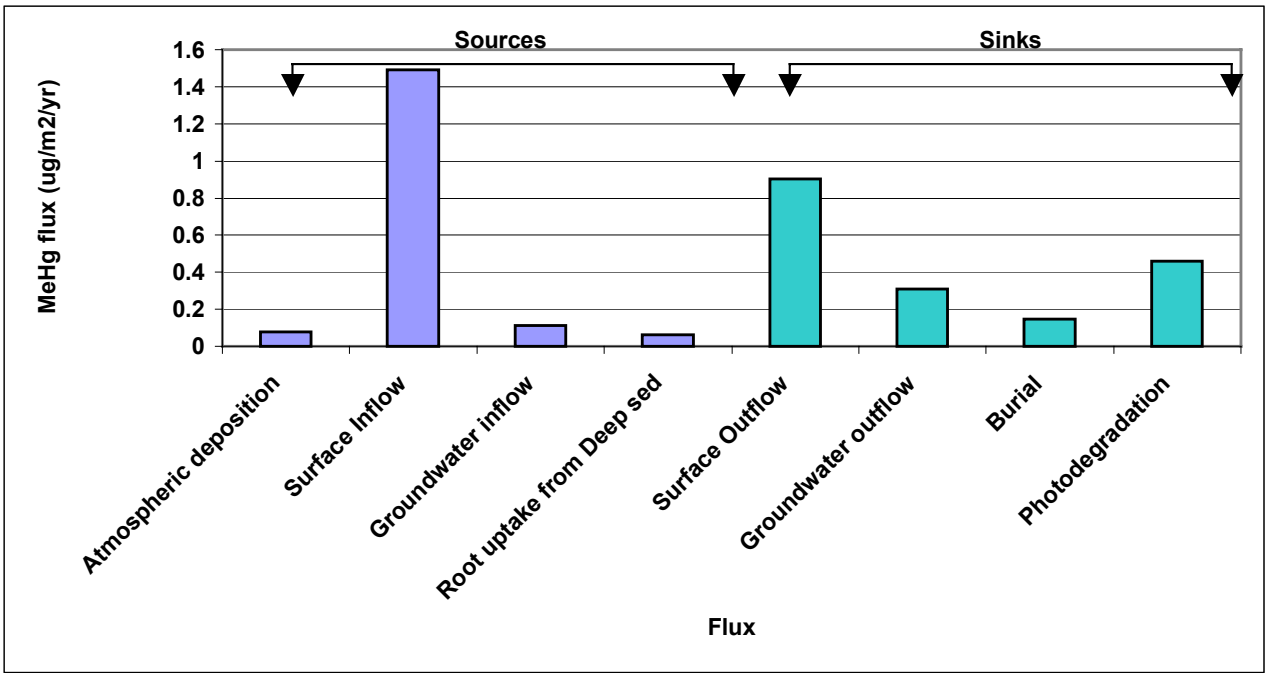

Figure 5-12. Predicted sources and sinks of methylmercury for ENR at near steady-state conditions

5.1.2.2 ENR Simulation with Two Linked Cells.

ENR simulations were also performed using two linked cells. In this scheme one cell represented the buffer cell, and the second model cell represented the combination of ENR Cells 1 through 4.

The approach taken to calibrate the buffer cell was to first match as best as possible the observed reductions in concentrations of total and methylmercury as waters passed through the buffer cell, prior to focusing on the 2nd model cell that represented ENR Cells 1 through 4. Given the very short period of time water spends in the buffer cell (0.8 days), and the particle trapping efficiency of the buffer cell, the most likely mechanism responsible for reductions of mercury concentrations across the buffer cell was sedimentation. The calibration of the buffer cell to obtain the desired total mercury and MeHg removal rates was done in two steps. First a particle budget was estimated to reflect the observed trapping of particles in the buffer cell. Then the associated reductions in mercury concentrations (total and methylmercury) were compared to mercury losses across the buffer cell, to see if reasonable mercury trapping efficiencies emerged.

Buffer cell particle budget

Available data were limited to establish a mass balance budget for particles in the buffer cell, but a preliminary budget was developed as follows:

- The mean annual concentration of suspended solids to the buffer cell was assigned a value of 7 mg L^{-1}, based on SFWMD (2000e).

- The mean annual concentration of suspended solids assigned for the buffer outflow was 3.26mg L^{-1}, based on SFWMD (2000e)). This was also assumed to be the mean TSS value within the buffer cell.
- Buffer cell water inflows and outflows were assumed to be equal. The mean annual flowrate was 400,495 m^3 day^{-1} (SFWMD, 2000a)

Using the above TSS and inflow values and assuming that gross particle settling rate is equivalent to the difference between inflow and outflow TSS fluxes, the gross settling rate is 985 g m^{-2} yr^{-1}. Assuming that the buffer cell TSS concentration was 3.26mg L^{-1}, a particle settling velocity of 0.82 m d^{-1} would produce the desired gross settling rate. Due to decomposition of particles in sediments and at the sediment interface, the resulting mass sedimentation rate at a depth of 3 cm was 819 g m^{-2} yr^{-1}.

Mercury removal in the buffer cell

The buffer cell water column distribution coefficients for HgII and MeHg were assumed to be the same as the ENR. Earlier simulations of ENR had somewhat underestimated the apparent partitioning for both Hg(II) and methylmercury in surface waters. For this two-cell simulation, partitioning was adjusted to better match observations for both total and methylmercury in surface waters. E-MCM was run for the buffer cell using the above estimated particle budget. The mean Hg(II) and methylmercury outflow concentrations that emerged compared favorably with the corrected concentrations derived using the method described in section 1.1.2.1 (see Figure 5-2 and Figure 5-1). Mean MeHg and Hg(II) concentrations flowing out of the buffer cell were essentially equivalent using the two methods.

Particle and mercury dynamics in the downstream ENR model cell

An initial 2 cell simulation was performed using the buffer cell calibrated as above in combination with a downstream cell that had inorganic Hg(II) partitioning in surface waters tuned to approximately field value, and the particle budget based on the feldspar data (SFWMD 2000d). This simulation underpredicted inorganic Hg(II) concentrations in surface waters and sediments (Table 5-3).

		Value	
Parameter	Units	Model Calibration	Observed mean
Inorganic Hg(II) concentration in surface waters	ng L^{-1} unfiltered	0.55	0.82
Inorganic Hg(II) concentration in surficial sediments (0-3 cm)	ng g^{-1} dry solids	0.03	0.08
Apparent partitioning for Hg(II) in surface waters	Log_{10}(L Kg^{-1})	6.03	5.95
Bulk sedimentation rate	cm yr^{-1}	3	3

Table 5-3. Predicted and observed inorganic Hg(II) concentrations in surface waters and sediments for ENR simulation using 2 linked cells, initial Hg partitioning and sedimentation based on feldspar data

Note: Feldspar observations are based on means of 24 samples taken from 1996 to 1997.

The rapid sedimentation imposed in the above simulation contributed to the underprediction of inorganic Hg(II) concentrations. A subsequent 2 cell simulation was carried out, again using the buffer cell calibration described above, and the inorganic Hg(II) partitioning the approximated field values, but using a slower rate of sedimentation, based on a recently developed approach described in Tetra Tech (2003), a report in progress. This approach used the macrophyte biomass and turnover equations described previously as well as a set of revised empirical equations to predict net particle accumulation rates based in part on the empirical relationships originally derived by Walker and Kadlec (1996). Mass sedimentation rates in this simulation were 406 g m^{-2} yr^{-1} at a depth of 3 cm, much lower than the value of 1778 g m^{-2} yr^{-1} imposed in the above 2 cell simulation.

This 2-cell simulation using the slower sedimentation rates predicted concentrations of total and methylmercury in surface waters for the ENR downstream of the buffer cell that were similar to the single cell run, as shown in Figure 5-4 and Figure 5-5. Figure 5-6 shows that predicted concentrations of total mercury in sediments are comparable to observations, although methylmercury concentrations in sediments are overpredicted by the two-cell scenario (Figure 5-7). Predicted fish mercury concentrations tend to be similar to the single cell run for fish at the 2nd and 3rd trophic levels ion the model (sunfish and largemouth bass, Figure 5-9 and). Mosquitofish concentrations however are somewhat overpredicted for the two cell ENR simulation Figure 5-8.

5.1.2.3 Discussion of deterministic ENR simulations (Single Cell and Two-Cell Scenarios)

Initial simulations of mercury cycling in ENR indicated that the assumption that the cells in ENR could be treated as single well-mixed entity was not appropriate. It was necessary to distinguish the buffer cell from the rest of ENR, due to the initial rapid sedimentation of Hg(II) in the buffer cell. This was done using two different approaches. The first approach moved the boundary of the modeled ENR area to exclude the buffer cell, and used the buffer outflow mercury concentrations as the inflows to the modeled area.. The single cell simulation used a high sediment accretion rate estimated from the sediment feldspar marker program (SFWMD 2000d). This rate was substantially higher than that used at all other sites (WCA 2A and 3A15). The second approach used a linked two cell scenario that treated the buffer cell distinct from the remaining ENR cells, which were still treated as a single entity. Furthermore, when model values for apparent inorganic Hg(II) partitioning in surface waters were tuned to better approximate field values, the simulation with less sedimentation than originally imposed improved the results. With these modifications, the model predicted surface water concentrations of total mercury well (0.76 to 0.86 ng L^{-1} predicted mean versus 0.82 ng L^{-1} volume weighted mean for stations within ENR) (Figure 5-4). Total mercury in sediments was somewhat underpredicted using the single cell approach (Figure 5-6), being significantly affected by the rate of sedimentation, which was based on field data from feldspar markers (SFWMD 2000d). The linked approach with a lower sedimentation rate from the Walker-Kadlec model better predicted total mercury concentrations on sediment solids.

Observations and E-MCM predictions both indicate ENR is a trap for methylmercury. The observed drop in MeHg concentration across the entire ENR from 0.18 to 0.05 ng L^{-1} for the 1995-99 period is somewhat greater than the drop predicted by E-MCM, to 0.097 ng L^{-1}. Part of this discrepancy is because E-MCM assumes well-mixed conditions horizontally, while the observations indicate a slight gradient for MeHg as one travels downstream through ENR. The observed outflow ENR MeHg concentration (0.05 ng L^{-1} for the 1995-1999 sample record) is

lower than the average MeHg concentration from several stations within ENR (0.069 ng L^{-1} volume weighted mean excluding the buffer cell). We could have increased rates of MeHg photodegradation and sediment accretion, or even invoked net biological demethylation to further reduce MeHg concentrations in ENR, but did not have a basis yet upon which to choose amongst these options. Finally it is possible that more of the inflowing MeHg to ENR is trapped in the buffer cell than we estimated (17% for MeHg, vs. 43 % for Hg(II)).

The MeHg trapping effect within ENR is likely due to a combination of site factors resulting in low methylation rates (or potentially even net demethylation), plus the net effect that loss mechanisms in the cell (photodegradation and burial) that generate fluxes of MeHg larger than that supplied by atmospheric deposition.

When the simulation was done to examine fluxes at near steady state conditions, it was found that the ENR system approached steady state more rapidly than was predicted at 3A-15. This is primarily a feature of the more rapid sediment accretion associated with the higher productivity conditions at ENR relative to 3A-15. ENR reached nearly steady state conditions within 15 years with the single cell simulation, as opposed to 25-30 years for 3A-15 in model runs.

Predicted sediment mercury concentrations tended to be higher for the two-cell simulation however, in comparison to the single cell simulation. This is likely partially a result of higher apparent partitioning between particle and dissolved phases assigned to methylmercury and Hg(II) in surface waters for the two cell scenario. These changes were made to better approximate field estimates of apparent mercury partitioning in ENR surface waters. One outcome of these changes is that settling becomes a more efficient mechanism to transfer total mercury and MeHg to sediments. Furthermore, particle sedimentation rates were significantly lower in the two cell scenario, which would also tend to increase sediment mercury concentrations. Overall, the two-cell ENR scenario performed better in some regards than the one cell scenario (improved prediction of sediment concentrations of total mercury), but overpredicted methylmercury concentrations in sediments and some fish (mosquitofish). As mentioned above, rates for mechanisms removing MeHg from the ENR system could be increased (MeHg photodegradation, sediment accretion, or net biological demethylation) in future simulations if data emerge to better constrain one or more of these fluxes.

5.1.3 Monte Carlo ENR simulation

Section 4.5 outlines the approach developed to add a probabilistic Monte Carlo capability to E-MCM. To demonstrate this feature, a Monte Carlo simulation was carried out for ENR. The scenario modeled was a derivative of the scenario discussed above where ENR was represented as a single cell that excluded the buffer cell. The simulation period was from March 15,1995 to February 24, 1999. Basically distributions were assigned to 104 inputs that were deterministic in the earlier simulation. These distributions are documented in Appendix B. A switch exists in the model interface that determines whether the model will operate in probabilistic or deterministic mode. If the probabilistic mode is selected, the input screen that is displayed to the user is shown in Figure 5-13.

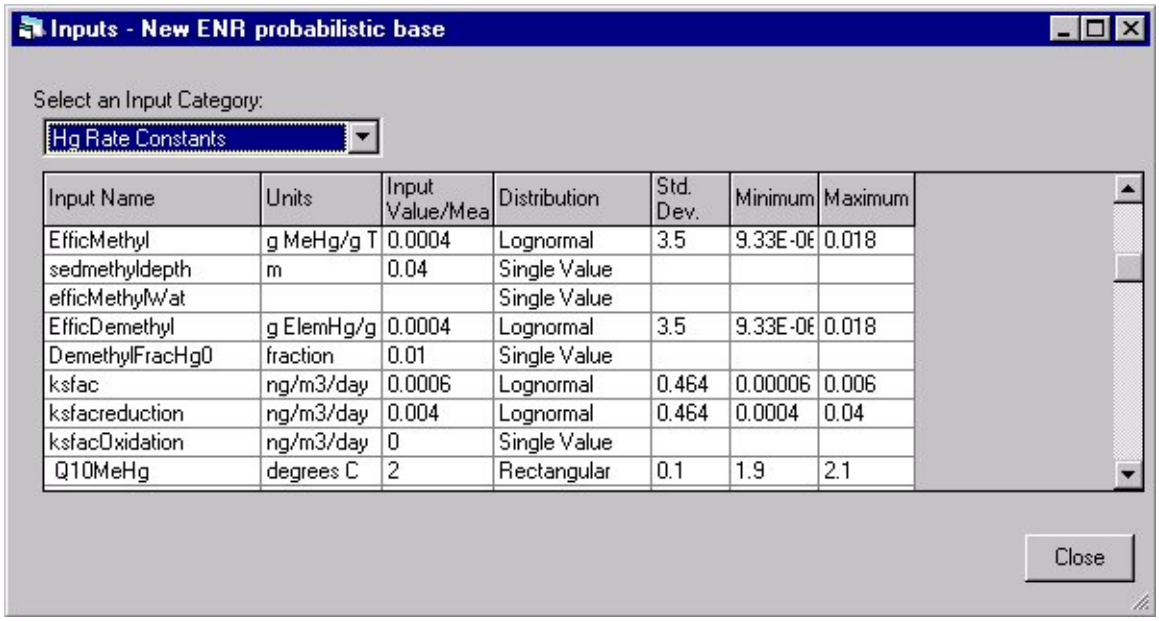

Figure 5-13. E-MCM sample input screen for Monte Carlo inputs

As noted earlier, a potential concern regarding Monte Carlo model applications is that unrealistic combinations of inputs can emerge if all inputs are assumed to behave independently, when in fact some inputs are often related to others. To help reduce the potential for this situation to occur, E-MCM has been designed such that some inputs can be made to depend on other inputs for probabilistic simulations. Dependencies between selected inputs can be switched on or off, but the relationships between inputs are "hard-wired" and can not be modified by general model users. Appendix C outlines dependencies between inputs that were programmed into E-MCM for the sample ENR application. It should be noted that coded relationship between surface inflows (independent variable) and surface outflows (dependent input) is specific to the ENR test case and would not be appropriate in any other situation. Macrophyte biomass and decay relationships used in the ENR sample application (Fink 2002a) are also derived from specific areas in the Everglades and may not universally applicable to the Everglades.

Many of the mean input values from the deterministic ENR runs (Tetra Tech 2002) were used for the probabilistic runs. There were detailed biweekly input time series spanning a four year period for several water quality inputs, wet mercury deposition and mercury inflows (via flowrates and inflowing concentrations of total and methylmercury) from this dataset. These 4 year input time series already had significant temporal variability. A probabilistic multiplier was used to scale these time series to produce additional variability. For example, the rate constant for methylation in sediments was assigned with the following distribution characteristics:

- Distribution type : Lognormal
- Mean value: 0.0004
- Standard deviation: 3.5
- Minimum allowable: 9.33E-06
- Maximum allowable: 0.018

The resulting distribution of sediment methylation rates constants for the sample ENR application is shown in Figure 5-14. Note that this is a lognormal distribution, but appears normal in the figure because the bins on the x-axis are based on a log scale.

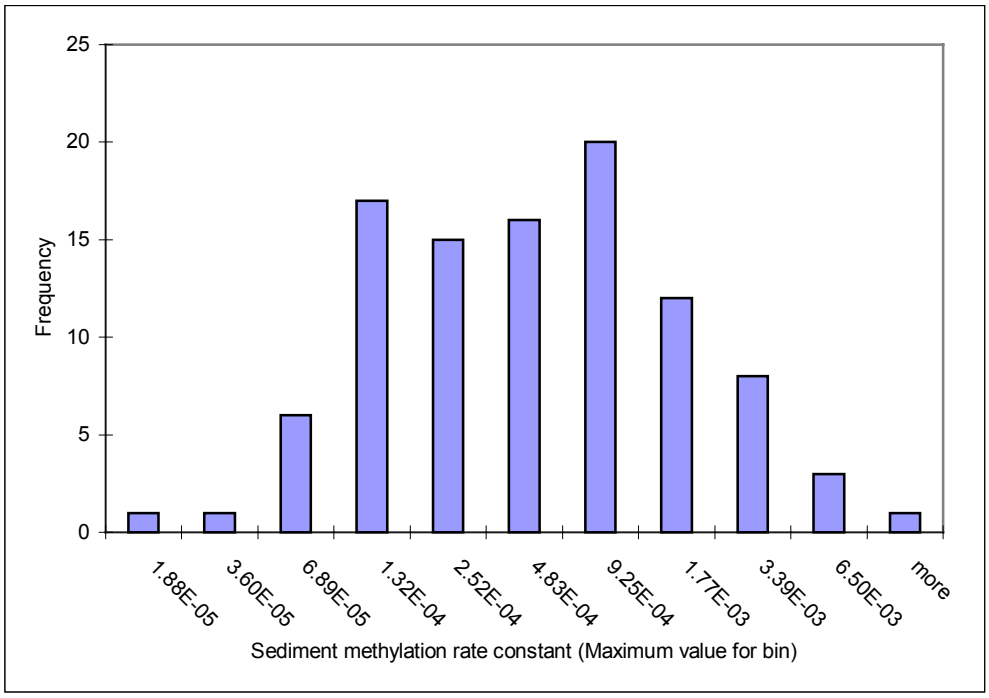

Figure 5-14. Methylation rate constants generated by E-MCM for sample ENR Monte Carlo simulation (n=100).

Macrophyte and periphyton biomass and turnover rates were set up to depend on the surface water total phosphorus concentrations. In turn the supply of detrital material and resulting particulate burial in sediments were dependent on macrophyte biomass and turnover. In this manner, sediment accretion and mercury burial were modeled for differing trophic conditions on the basis of probabilistically varying phosphorus levels.

For this sample application, the observed variability in surface water concentrations of total and methylmercury were reasonably reflected in the initial model simulations (see Figure 5-15 and Figure 5-16). Predictions for total and methylmercury concentrations in sediments were also reasonable. However the predicted variability in Hg levels for four to five year old largemouth bass was underpredicted initially (Figure 5-17). Since the variability in water and sediment MeHg concentrations was reflected in the initial simulations, this suggested that the variability in the fish mercury concentrations had a significant component due to biological variability above and beyond geochemical Hg cycling.

It was hypothesized that this biological variability causing widely varying mercury concentrations in largemouth bass came from the following

- variability in fish diet composition and mercury concentration,
- variability in fish growth rates

- variability in fish metabolic activity

Fish growth rates were varied as a direct function of surface water concentrations of total phosphorus. Phosphorus concentrations were assigned a range that varied from 0.67 to 1.33 of the mean ENR value (75 mg L^{-1}), using a rectangular distribution. Hence fish growth rates also had the same range about their mean values. Field measured fish weights as a function of age were highly variable (Table 5-4). Variable growth rates were applied simultaneously to all three fish species under the assumption that trophic status and resulting food availability would effect all three populations. Similarly respiration was varied inversely with phosphorus, with a value of 0.5 times mean respiration at the highest phosphorus level and 2 times mean respiration at the lowest phosphorus level. These numbers were used for illustrative purposes rather than having a quantititative basis. This was also done for all three fish species simultaneously. This was an attempt to account for the varying prey availability acquisition and general stress related metabolic levels that accompany changing trophic status.

Age	Minimum Weight (g)	Maximum Weight (g)
0+	21	147
1+	104	928
2+	182	1880
3+	349	2180
4+	268	2246
5+	493	811

Table 5-4. Minimum and maximum observed weight by age for largemouth bass at ENR (1995 to 1999) (Source: Florida Fish and Wildlife Conservation Commission. (2000)).

Due to the structure of E-MCM, it was beyond the scope of this study to make the fish diet probabilistic. However, as a surrogate approach for this illustrative example that would have a similar effect (although not mechanistically correct), the bioconcentration factors (BCF's) for zooplankton, benthos, shrimp and periphyton were made probabilistic to introduce additional variability in dietary mercury concentrations. The variability in the BCF's for zooplankton and benthos were adjusted until the predicted fish mercury concentrations showed the desired variability. This is somewhat a case of reverse modeling – *viz.,* calibrating the variability in dietary MeHg exposure to obtain the observed range of fish Hg concentrations.

The above changes in biological parameters resulted in an improved cumulative frequency distribution for age 4+ largemouth bass shown in Figure 5-18. A time series plot of predicted versus observed methylmercury in 4 to 5 year old largemouth bass is shown in Figure 5-19, including the range of concentrations predicted at a given time.

Discussion of Monte Carlo Simulation at ENR

The four years of field observations at ENR (March 15, 1995 to February 24, 1999) revealed a large amount of variability in fish MeHg concentrations. Model simulations suggest that while geochemical factors explain a portion of the variability in mercury concentrations measured in individual largemouth bass, there was also a significant contribution from factors related to the

food web. Variability in fish dietary mercury concentrations, fish growth rates and prey acquisition energy expenditure were introduced, with the result that predicted fish mercury concentrations better reflected variability in the field data. While this application of the model is not predictive, since some inputs were adjusted to generate a good fit for fish mercury variability, it does illustrate the potential of the model to be used in an R&D capacity to examine and develop hypotheses regarding factors affecting fish mercury concentrations. This initial exercise with the Monte Carlo version of the model suggests that spatially and temporally varying trophic conditions may result in varying diets, growth rates and stress-related metabolic levels, that would in turn affect fish mercury concentrations.

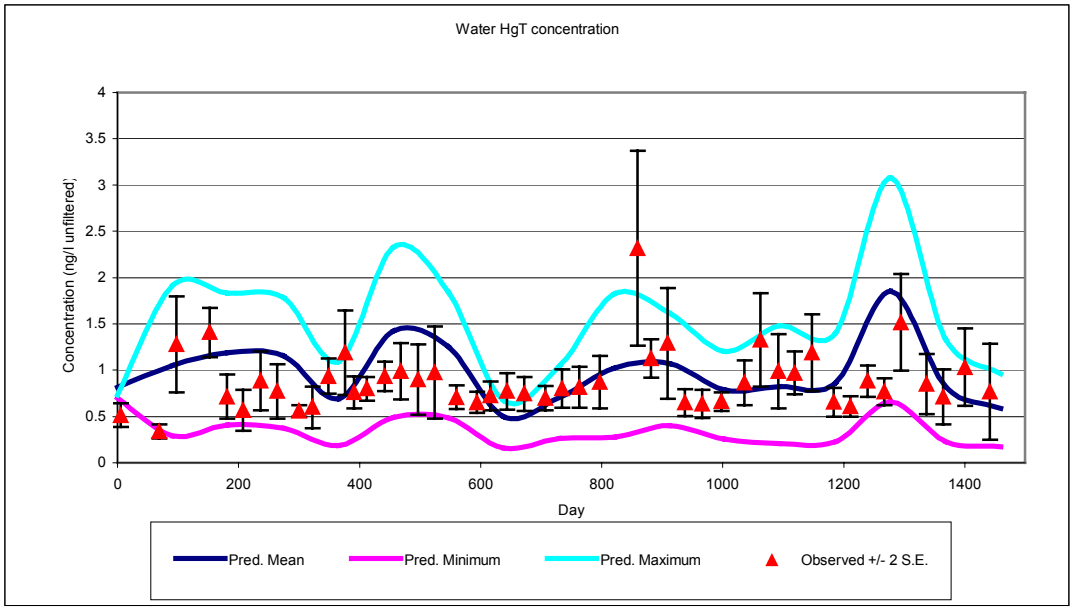

Figure 5-15. Predicted and observed concentrations of total mercury in ENR surface waters for sample Monte Carlo application.

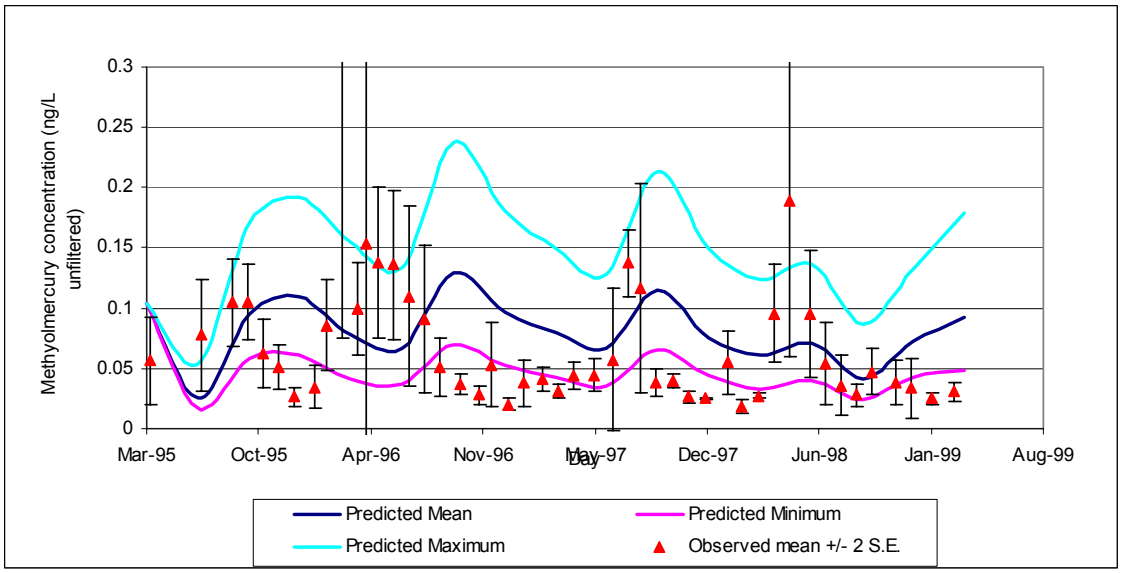

Figure 5-16 Observed and predicted surface water MeHg concentrations at ENR.

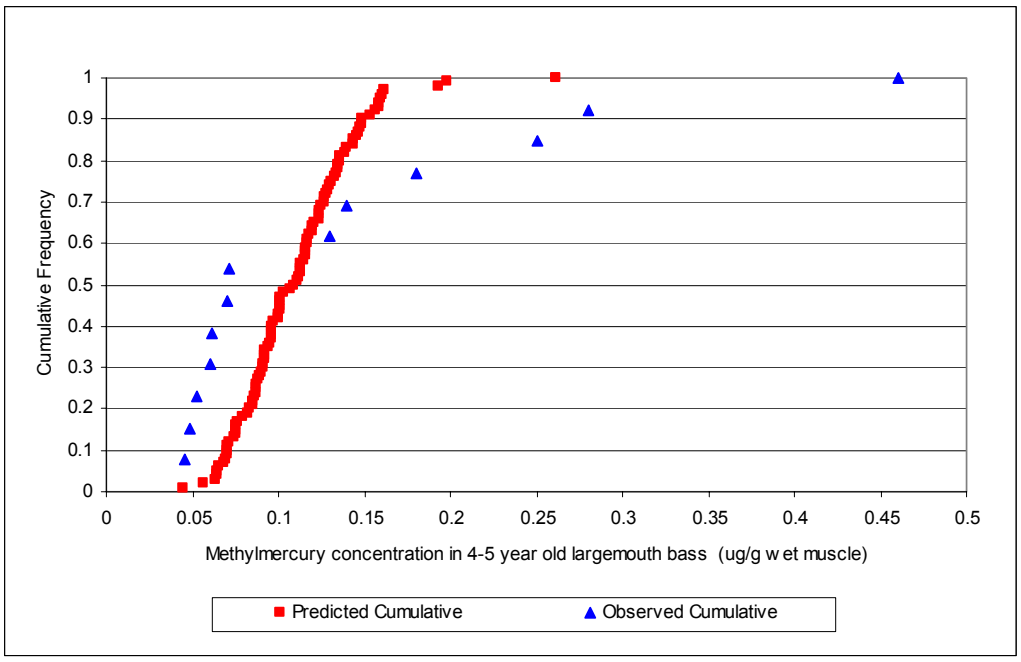

Figure 5-17 Predicted vs observed cumulative frequency distribution for age 4+ largemouth bass at ENR - initial simulation with low biological variability.

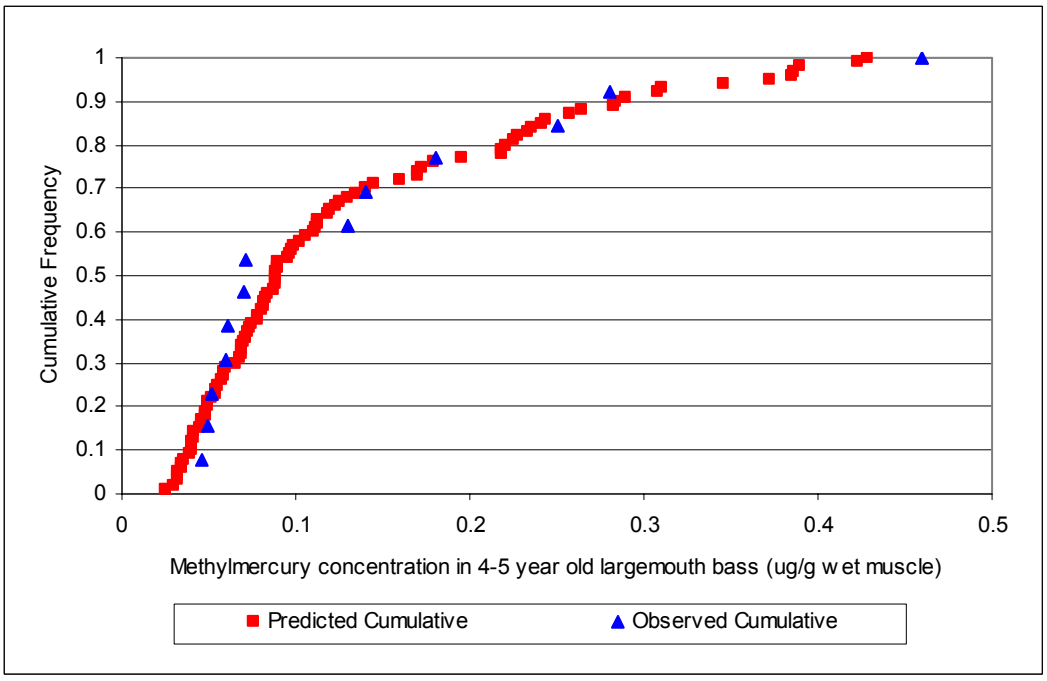

Figure 5-18. Predicted vs observed cumulative frequency distribution for age 4+ largemouth bass at ENR - initial simulation with high biological variability.

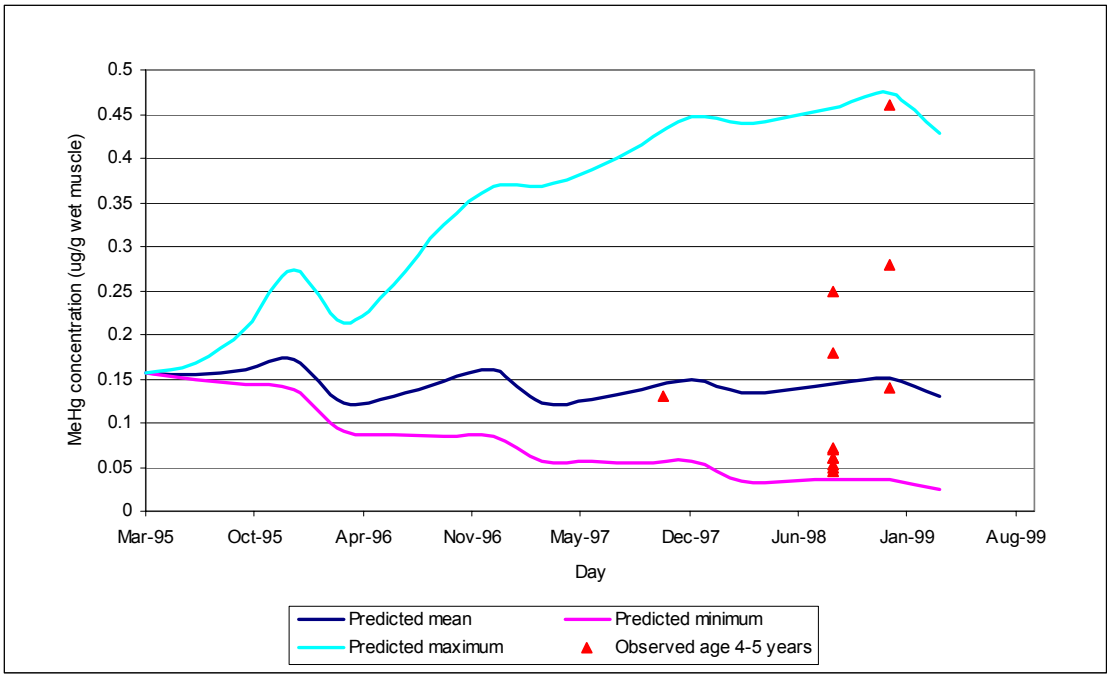

Figure 5-19. Range of predicted methylmercury concentrations in 4-5 year old largemouth bass at ENR (simulation with high biological variability)

5.2 Updated calibration of E-MCM to WCA 2A sites F1 and U3

E-MCM was applied to F1 and U3 during Phase II, and discussed in the Phase II report. During Phase III, the model calibrations for F1 and U3 were updated. In particular, estimates of particle budgets and methylation rates were revisited. This report presents the results of the final simulations carried out in Phase III of the study.

5.2.1 F1 and U3 Site Descriptions

Water Conservation Area 2A (WCA-2A) is a 450 square kilometer area in the Everglades. Water enters WCA-2A from the S10 inflow structures at the northern end of the marsh. The water from the S10 structures is largely runoff from agricultural land with elevated nitrogen and phosphorus levels. Much of the P and N entering WCA-2A is assimilated in the enrichment zones in the northern section of the marsh (Reeder and Davis, 1983). Thus a nutrient gradient exists in the marsh with steadily decreasing nutrient levels from north to south (Table 5-5), with relatively low productivity at the southerly end. F1 is a site in the eutrophied northern area of WCA 2A close (ca. 1.8 km) to the point of release of agriculturally impacted runoff through the S-10 structures. U3 is a much lower productivity site at the southern end of WCA 2A, approximately 10.8 km

downstream from the northern levees. Basic characteristics of the F1 and U3 sampling sites are shown in Table 2-1.

It should be noted that there is no systematic trend for DOC concentrations in surface waters in Table 5-5. During a recent meeting between the FDEP, SFWMD, ACME researchers and Tetra Tech in Reston, VA, the lack of a trend was questioned. Prior to future simulations, available datasets for DOC concentrations in surface and porewaters in the Everglades should be reviewed to see if the above values are appropriate.

Limited observations of surface water mercury concentrations (means derived from data collected from 1995 – 2000 [USGS, 2001]) on four dates with nearly coincident sampling at the different stations) suggest increasing Hg(II) concentrations as one moves from S10 to U3 (Figure 5-20). The concentration gradient trend for methylmercury in surface waters is weaker than for Hg(II). There were only four dates with essentially synoptic sampling at the four stations included in the figure, introducing uncertainty into the statistical confidence in the trends observed.

SITE	Dissolved Organic Carbon	Dissolved Oxygen	Total Phosphorus	NH3	Total Suspended Solids	Sulphate	pH
	All units mg L^{-1} except pH						
F0	36	2.3	0.10	0.62	9	54	7.3
F1	44	1.9	0.13	0.14	15	54	7.2
F2	42	2.0	0.07	0.11	4	54	7.3
F3	41	2.1	0.03	0.05	4	56	7.3
F4	37	1.9	0.02	0.03	4	57	7.3
F5	38	4.1	0.01	0.04	3	88	7.4
U3	39	4.4	0.01	0.05	3	52	7.5

Table 5-5. Water quality gradients across WCA-2A.

(Source of data: Mean values derived from SFWMD (2000g)).

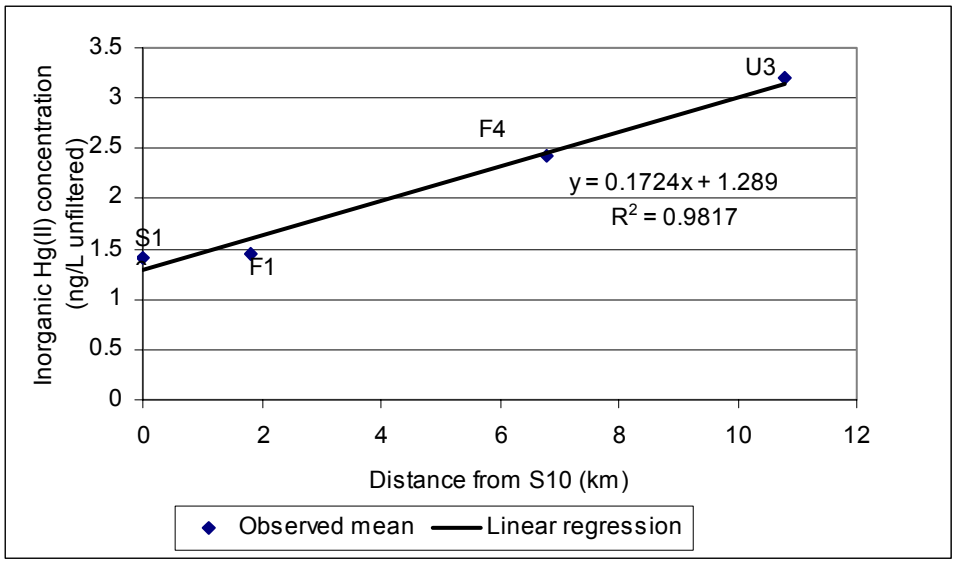

Figure 5-20. Surface water inorganic Hg(II) concentration gradient observed across WCA-2A.

(Data derived from USGS (2001), representing means of samples collected on 4 occasions from 1995 – 2000).

Flowrates out of the S10 control structure, and thus downstream, are highly variable. Depending in part on season and antecedent rainfall (and on how the control structures are managed), there are periods of high flows and periods of no flow from the S10 structures (see Figure 5-21)

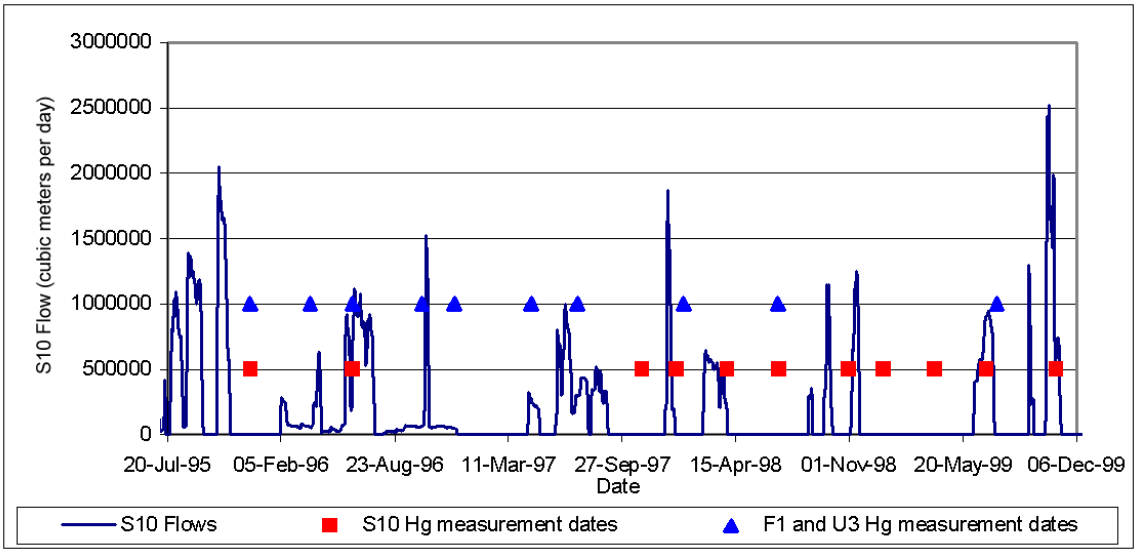

Figure 5-21. S10 flows and sampling dates for surface water Hg concentrations at S10, F1 and U3.

(Data Source: Flows: SFWMD (2000f), Hg concentrations: USGS (2001)).

The enriched site (F1) and the unenriched site (U3) are located 1.8 and 10.8 kilometers from the S10 structures, respectively. F1 is dominated by cattails with little periphyton and a detrital-based food web (Rawlik 2000). There are few predatory fish at F1 due to poor habitat (low dissolved oxygen, high sulfides, and dense macrophytes. The unenriched area at U3 is dominated by sawgrass with a fish community that includes predatory species (Rawlik, 2000).

5.2.2 Calibration Approach for F1 and U3 during Phase III

For Phase II and Phase III, F1 and U3 simulations were conducted using a simple three compartment linked wetland approach. During Phase II, the simulations for each cell had to be done independently. For Phase III, the linked-cell version of the model was used to run the three cells simultaneously. With the three-cell scheme, the outflow from one cell became the inflow to the next. F1 was the initial cell, followed by an intermediate cell and finally U3. The dimensions of the cells were selected so the three cells were contiguous and spanned the entire 12.6 km distance from S10 to the downstream end of the U3 cell. The F1 sample site is located at the middle of the F1 cell, which was 1 kilometer wide and 3.6 km long. S10 was the upstream boundary of the F1 cell. F1 outflows were assumed equal to inflows plus the amount of rainfall falling onto the cell. Evapotranspiration could not be included because it resulted in "negative outflow" from F1 when S10 was not releasing water. Alternative approaches to better consider the net loading of water through a cell are being considered for future simulations. A mass balance for water (as opposed to mercury) will likely be incorporated in a future version of the model.

The U3 cell was assigned the same dimensions as F1 (1 x 3.6 km), and the intermediate cell was 5.4 km long to span the gap between the F1 and U3 cells. Average water quality conditions from F3, F4, and F5 were used for the middle cell.

The high variability in S10 flowrates and the limited number of mercury sampling dates introduced uncertainty associated with mercury inflows to F1. Furthermore, the rapid water throughput makes this flux important in determining surface water concentrations at F1.

Treatment of Particle Budgets at F1 and U3.

During Phase III calibrations for F1 and U3, some inputs related to particle budgets were handled differently than for Phase II. During Phase II, inputs related to biomasses and turnover of macrophytes and periphyton were estimated using the equations of Fink (2002a) and decomposition rates at the sediment water interface were manually adjusted so the amount of particulate matter being buried in sediments (peat accretion) was consistent with field estimates from sites C1 and C6 near F1 and U3 respectively (Vaithiyanathan et al. 1996). The equations for macrophyte and periphyton biomasses used at F1 and U3 the same ones used at ENR, and can be seen in Appendix C.

For Phase III, inputs related to related to biomasses and turnover of macrophytes and periphyton continued to be estimated using the equations of Fink (2002a). Equations from Fink (2002a) were also used to estimate macrophyte and periphyton areal coverage as functions of total phosphorus levels. This is described in more detail later in the report (Section 6.3). Equations also were developed by Tetra Tech to predict decomposition at the sediment/water interface and decomposition within the upper sediment compartment as functions of phosphorus (Section 6.3). These equations were calibrated to provide peat accretion rates as similar as possible to

(Vaithiyanathan et al. 1996). These decomposition equations were also set up to reflect an assumption that peat accretion rates would continue to increase as phosphorus levels increased (see Section 6.3.3).

F1 simulations during Phase II were carried out with methylation occurring in sediments. During Phase III, results at F1 improved slightly when methylation was invoked in the water column instead of sediments, and this became the default condition for F1 simulations. Similar to Phase II, methylation rate constants were calibrated independently at F1 (in water) and U3 (in sediments) to obtain a good fit between observed and predicted methylmercury concentrations at the sites.

Finally, Phase II simulations involved some methylmercury partition constants on water column solids that were unrealistic but required at the time to generate reasonable MeHg concentrations in water and sediments. Adjustments were made in Phase III to reasonably reflect observed MeHg partitioning and still generate satisfactory results. Shifting methylation to the water column was one factor improving this situation.

5.2.3 Model Results for F1 and U3

The mean predicted and observed mercury values for critical water, sediment and biological parameters are shown in Table 5-6. The comparisons are based on mean values for the period January 1, 1995 through December 31, 1999.

Name	Units	F1 Predicted	F1 observed	F1 % Difference Predicted vs Observed	U3 predicted	U3 observed	U3 % Difference Predicted vs Observed
MeHg in surface waters (unfiltered)	ng L^{-1}	0.26	0.28	-8%	0.63	0.65	-3%
MeHg in surface waters (dissolved)	ng L^{-1}	0.22	0.19	16%	0.57	0.54	6%
Hg(II) in surface waters (unfiltered)	ng L^{-1}	2.15	2.53	-15%	3.47	3.60	-4%
Hg(II) in surface waters (dissolved)	ng L^{-1}	1.99	1.80	10%	3.29	2.25	46%
Hg(II) on settling solids in surface waters	ug g^{-1} dry	0.028	0.014	99%	0.049	0.015	229%
MeHg on surface sediment solids	ug g^{-1} dry	0.0014	0.0004	292%	0.0029	0.0011	157%
Hg(II) on surface sediment solids	ug g^{-1} dry	0.076	0.168	-55%	0.125	0.142	-12%
MeHg in surface sediment porewater	ng/L	0.46	0.13	250%	1.00	0.57	76%
Hg(II) in surface sediment porewater	ng/L	1.65	1.32	26%	2.32	3.31	-30%
Age 0-1 largemouth bass	ug g^{-1} wet muscle	0.24	NA	NA	0.37	0.25	47%
Age 1-2 largemouth bass	ug g^{-1} wet muscle	0.39	NA	NA	0.53	0.54	-1%
Age 2-3 largemouth bass	ug g^{-1} wet muscle	0.62	NA	NA	0.81	0.72	13%
Age 3-4 largemouth bass	ug g^{-1} wet muscle	1.05	NA	NA	1.35	0.92	47%
Age 4-5 largemouth bass	ug g^{-1} wet muscle	1.49	NA	NA	1.95	0.98	99%
mosquitofish	ug g^{-1} wet muscle	0.10	0.02	485%	0.09	0.10	-8%
Apparent Hg(II) partitioning on settling solids in surface waters	Log 10 value	4.17	4.67		4.21	5.03	
Apparent total Hg partitioning on settling solids in surface waters	Log 10 value	4.22	4.67		4.27	5.02	
Apparent MeHg partitioning on settling solids in surface waters	Log 10 value	4.48	4.53		4.47	4.41	

Table 5-6. Comparison of observed and predicted mercury concentrations and apparent partitioning at F1 and U3 .

(Observed data sources as follows: Water concentrations from USGS (2001); Sediment concentrations from Gilmour *et al*. (1998a); fish Hg data from Rawlik (2000) and Lange (2001)).

Predicted F1 Mercury Concentrations

Figure 5-22 through Figure 5-26 show predicted and observed concentrations of total and methylmercury in various compartments at F1. The model was calibrated to predict the mean concentrations of Hg(II) and MeHg surface waters F1 within 15%. There is high variability however on a day to day basis within, and between, concentrations in the field data and model. Predicted total mercury concentrations in F1 surficial sediments (0-4 cm) were within the observed range, while sediment methylmercury concentrations were overpredicted but still low to moderate in absolute terms (Table 5-6, Figure 5-24 and Figure 5-25).

The model strongly overpredicted F1 mosquitofish concentrations, with predictions in the range of 5-100 ng g^{-1} wet whole body, while the observations were typically 10 ng g^{-1} or less (Figure 5-26). No data were available for sunfish or largemouth bass mercury concentrations at F1.

Predicted U3 Mercury Concentrations

Figure 5-27 through Figure 5-33 show predicted and observed concentrations of total and methylmercury in various compartments at U3. The model was calibrated to predict the mean concentrations of Hg(II) and MeHg surface waters at U3 within 5%, although (similar to F1) there is high variability on a day to day basis within, and between, concentrations in the field data and model.

Similar to F1, total mercury concentrations in U3 surficial sediments (0-3 cm) were within the range of observations. Predicted U3 sediment methylmercury concentrations were also within the observed range but the mean value was overpredicted (Figure 5-30, Table 5-6)

E-MCM was calibrated to predict mercury concentrations in mosquitofish well at U3 (Figure 5-31). Some age classes of largemouth bass were well predicted (up to age 2-3 (Figure 5-32)), while older cohorts were overpredicted (age 3-4 and higher, Figure 5-33).

Figure 5-34 and Figure 5-35 show the predicted and observed surface water concentration gradients between F1 and U3 for Hg(II) and MeHg respectively. In all cases, concentrations were higher at U3 than F1.

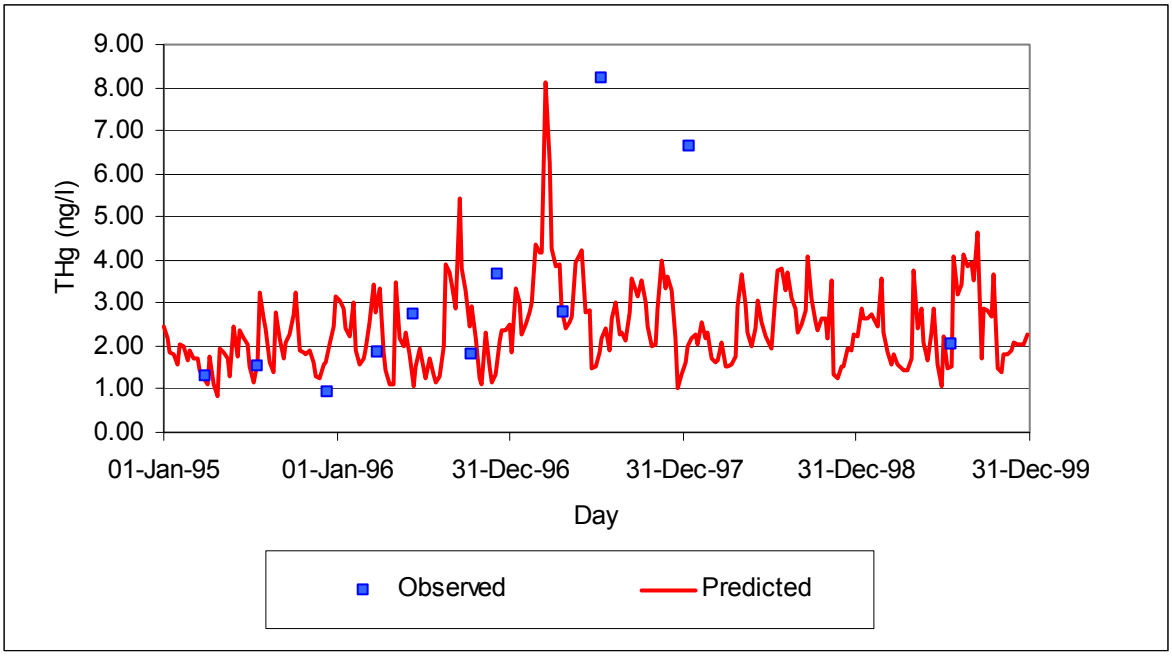

Figure 5-22 Observed and predicted total mercury concentrations in F1 surface waters. (Source of observations: USGS (2001)).

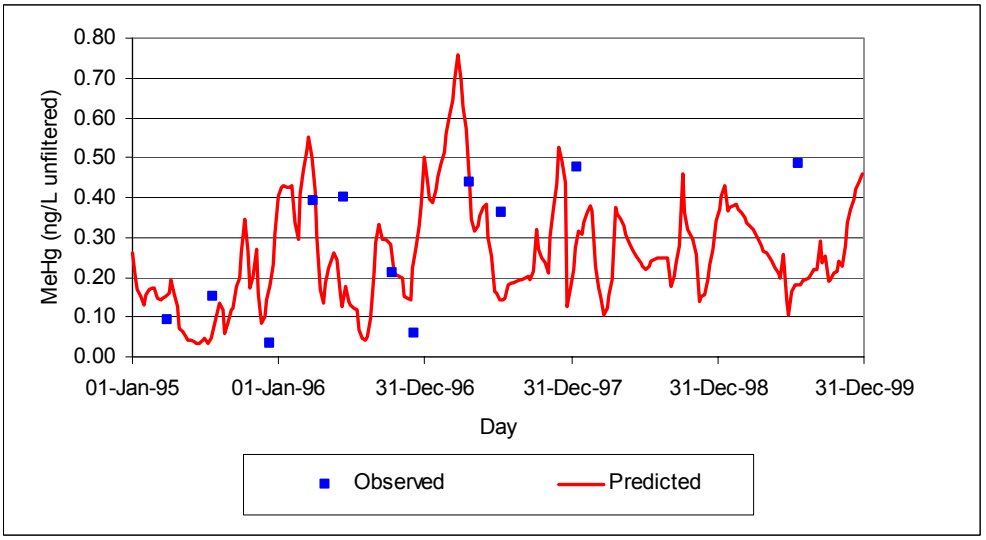

Figure 5-23 Observed and predicted methylmercury concentrations in surface waters at F1. (Source of observations: USGS (2001)).

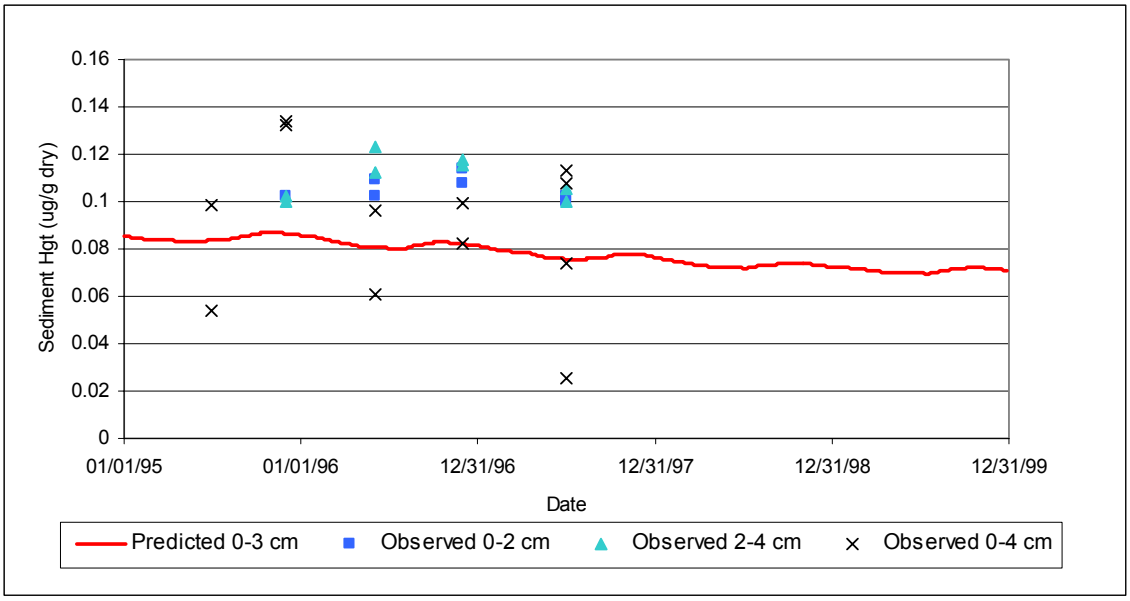

Figure 5-24. Observed and predicted total mercury concentrations in F1 sediments. (Source of observations: Gilmour et al. (1998a)).

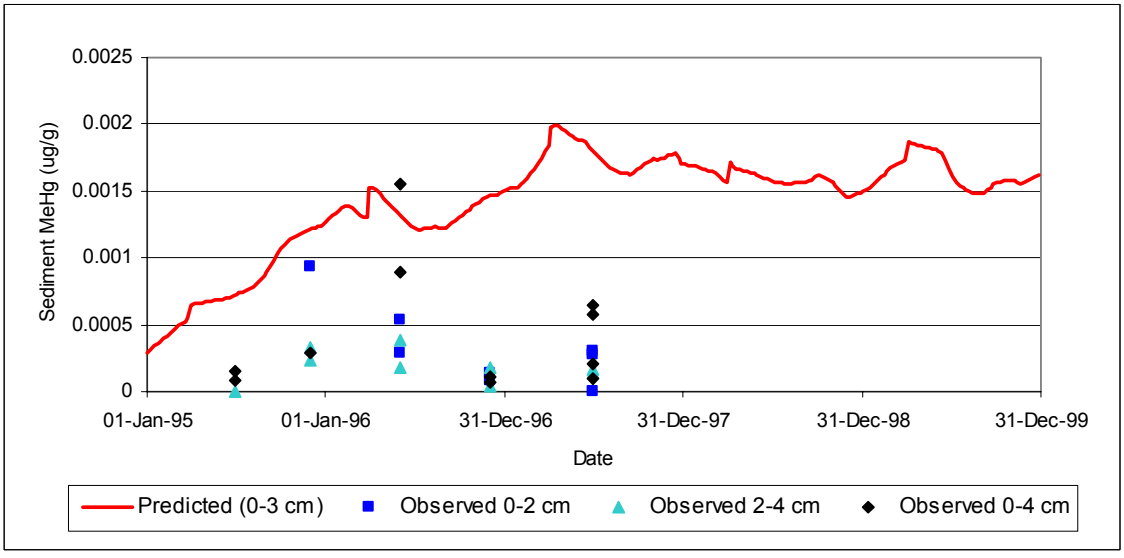

Figure 5-25. Observed and predicted methylmercury concentrations in F1 sediments. (Source of observations: Gilmour *et al.* (1998a)).

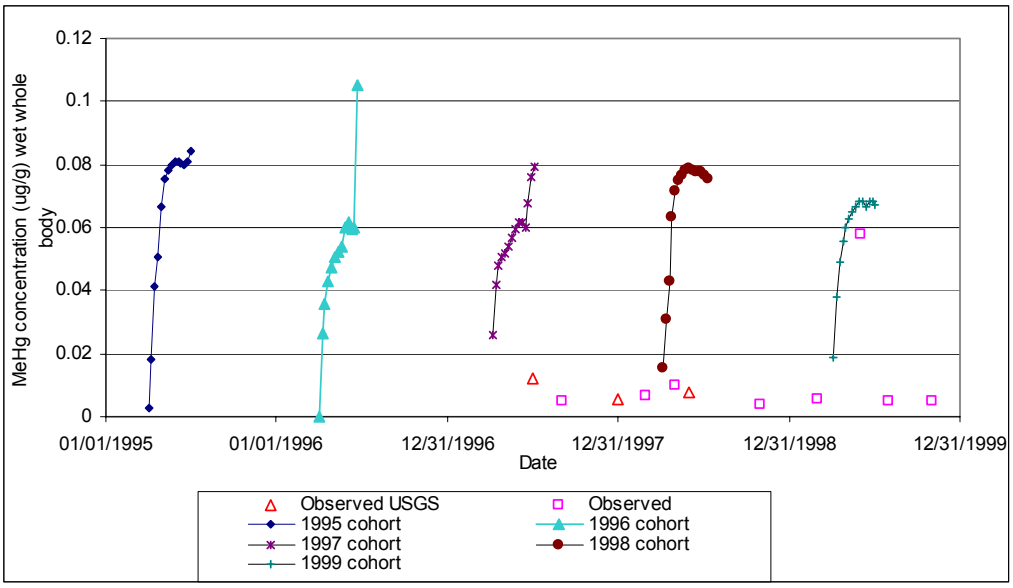

Figure 5-26. Observed and predicted Hg concentrations in mosquitofish at F1. (Observed data from Rawlik (2000))

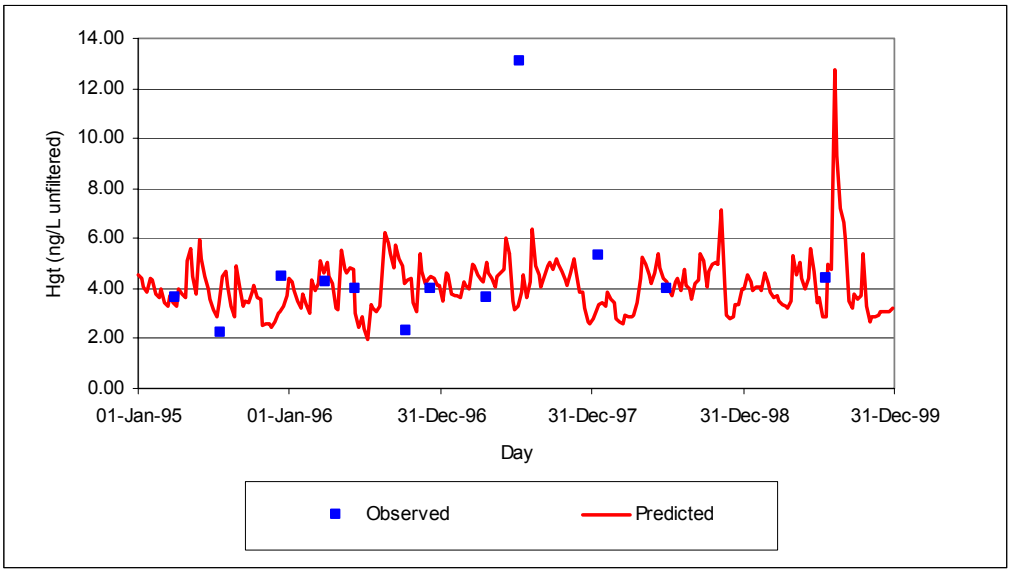

Figure 5-27. Observed and predicted total mercury concentrations in surface waters at U3. (Source of observations: USGS (2001)).

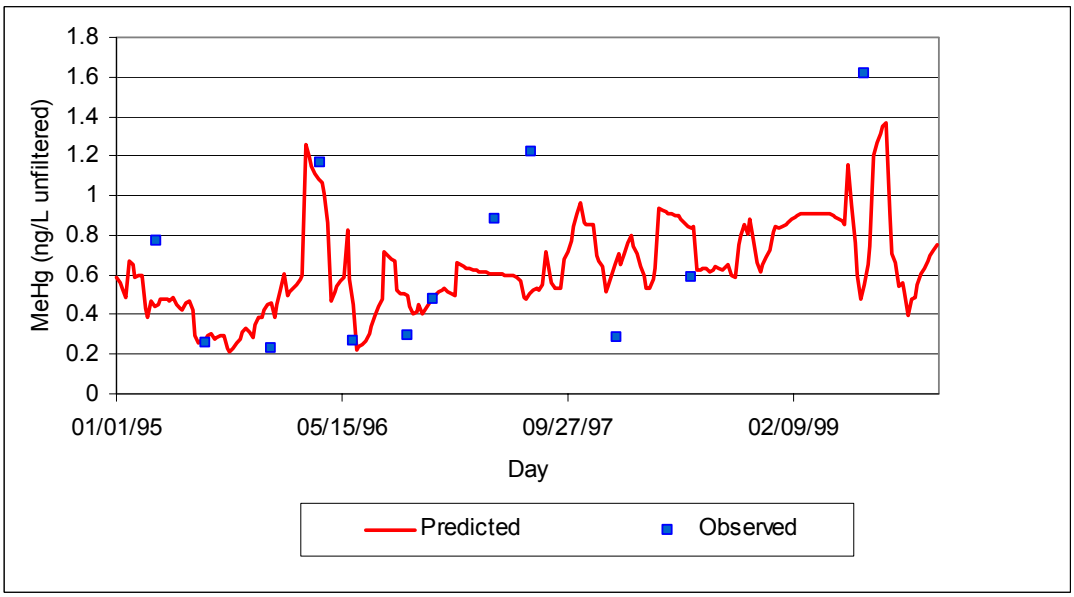

Figure 5-28. Observed and predicted methylmercury concentrations in surface waters at U3. (Source of observations (USGS (2001)).

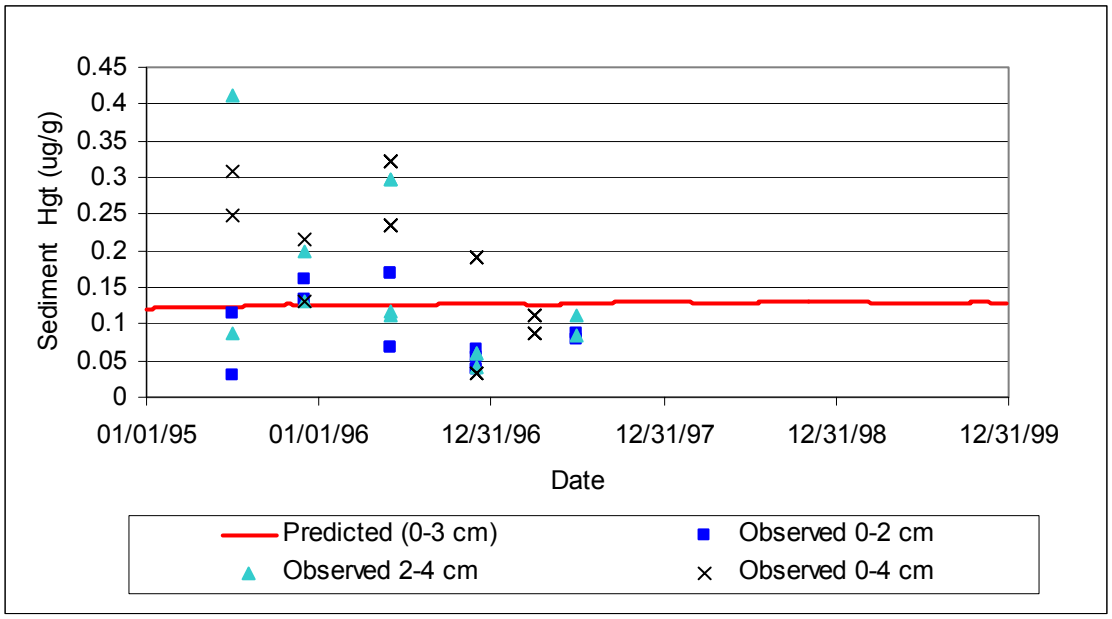

Figure 5-29. Observed and predicted total mercury concentrations in U3 sediments

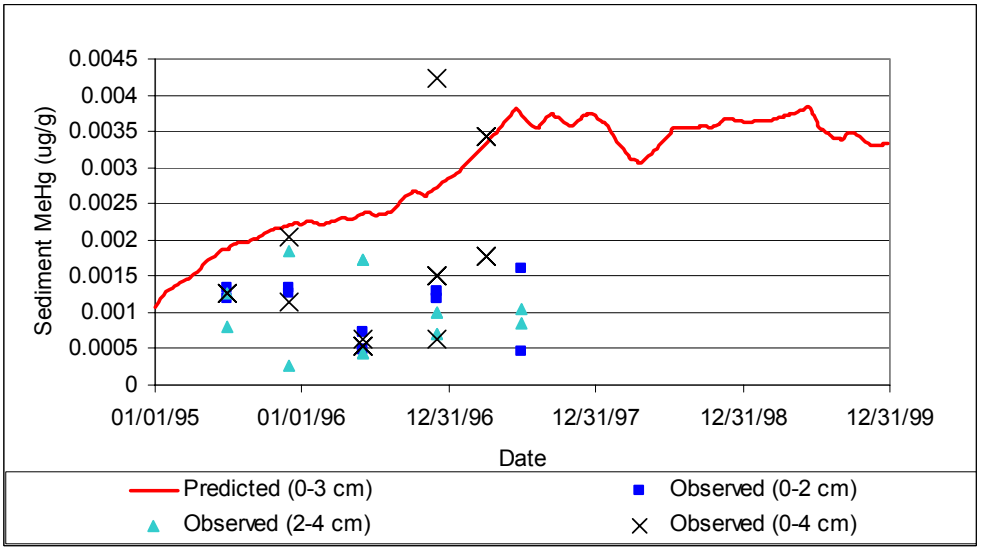

Figure 5-30. Observed and predicted methylmercury concentrations in U3 sediments. (Source of observations: Gilmour *et al.* 1998a)).

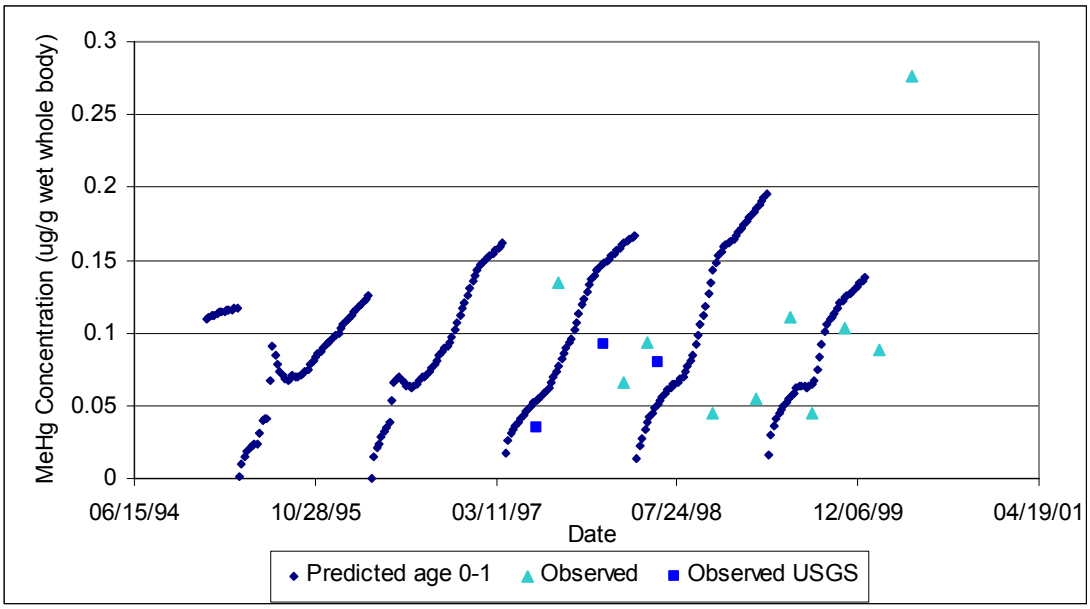

Figure 5-31. Observed and predicted mercury concentrations in mosquitofish at U3

(Source of observations: "Observed" series from Rawlik (2000); "Observed USGS" series from USGS (1999)).

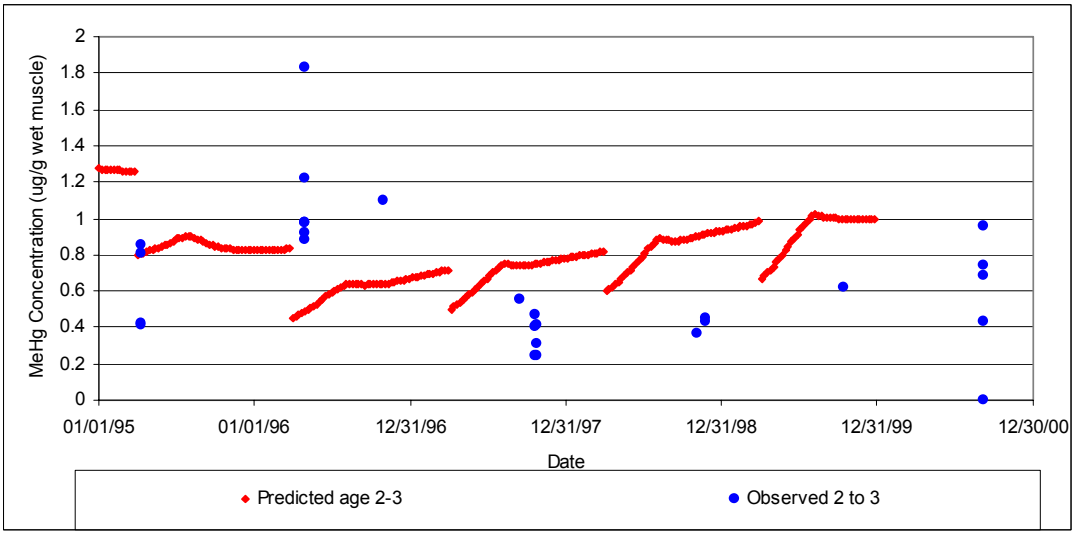

Figure 5-32. Observed and predicted mercury concentrations in age 2-3 largemouth bass at U3.

(Source of observations: Lange (2001)).

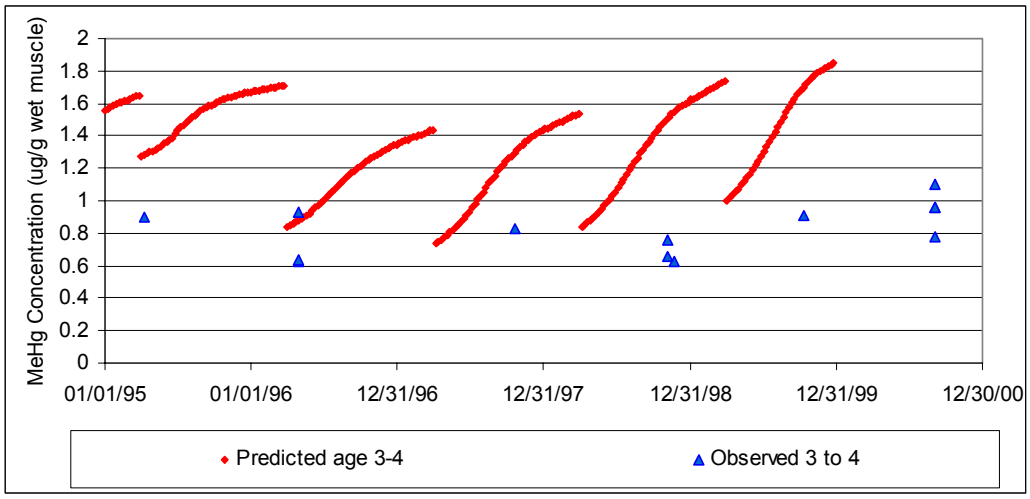

Figure 5-33. Observed and predicted mercury concentrations in age 3-4 largemouth bass at U3.

(Source of observations: Lange (2001)).

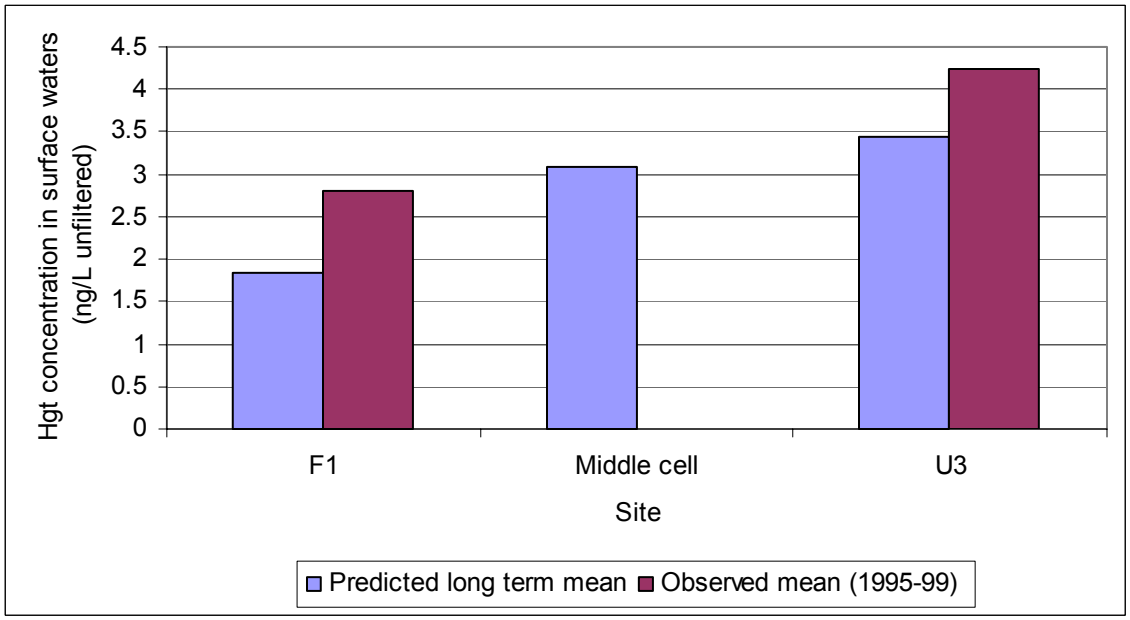

Figure 5-34. Predicted and observed surface water total mercury concentration gradient between F1 and U3.

(Source of observations: USGS (2001)).

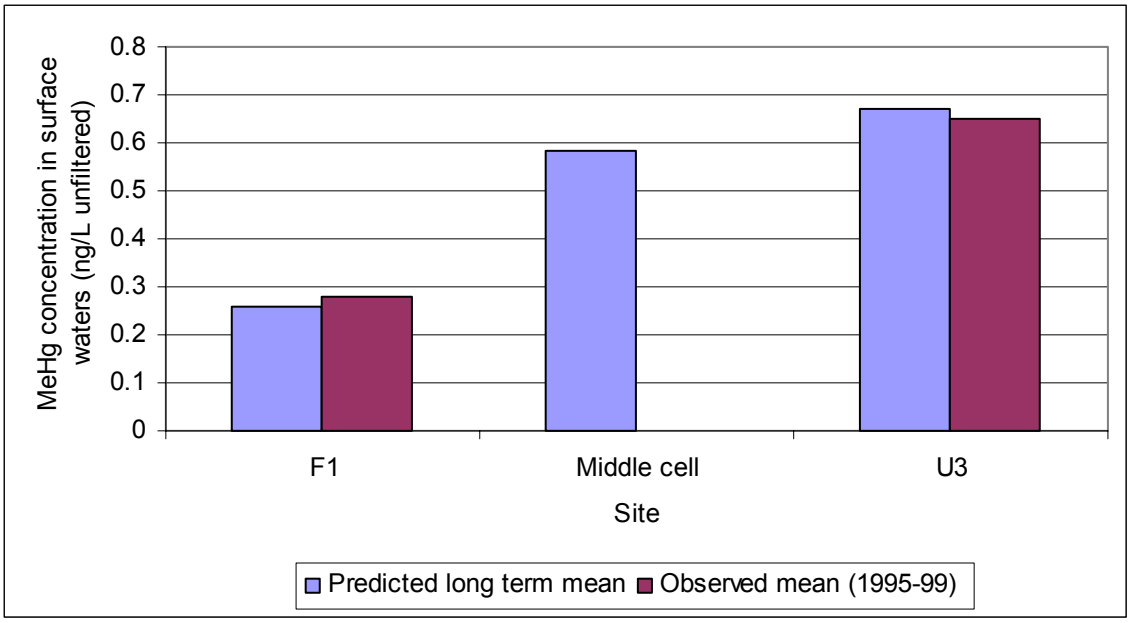

Figure 5-35. Predicted and observed surface water MeHg concentration gradient between F1 and U3.

(Source of observations: USGS (2001)).

5.2.4 WCA-2A Discussion

The field data tentatively suggest an increase in Hg(II) concentrations in surface waters between F1 and U3, although the extent of the data is insufficient to draw conclusions. E-MCM reflected these trends (Figure 5-34) and also predicted higher sediment Hg(II) concentrations at U3 than F1, consistent with observations.

An important factor causing an increase in predicted sediment Hg(II) concentrations as one travels downstream through WCA-2A was the estimated diminishing rate of sediment accretion. All other factors being equal, increased sedimentation would also translate into lower surface water Hg(II) concentrations, for example at ENR. There are other significant site-to-site differences however that can complicate this simple picture. For example, the rapid water throughput at F1 and U3 can dampen the effects of different sedimentation rates on water column mercury concentrations. The ultimate effects of different particle cycling regimes on water column mercury concentrations were still being assessed at the time of this report preparation.

E-MCM simulations at F1 suggest that a relatively high percentage of settling material at the site is decomposed rather than being buried. The effect of this in the model is that sedimentation is less effective as a mechanism to lower Hg(II) concentrations at the site than would be the case if most of the settling particles ended up contributing to long term peat accretion. Note that the ultimate sedimentation rate depends on the both of the production rate of plant material and the rate at which it is decomposed.

The model also predicted increasing surface water MeHg concentrations between F1 and U3, but there were differences to the calibrations of methylmercury kinetics at the sites. E-MCM thus

matched the trends for surface water methylmercury in WCA-2A at least partially by calibrating on a site by site basis as opposed to truly predicting them. Gross in-situ methylation rates at ENR, F1, U3 and 3A-15 respectively were calibrated to 0, 1.8, 5.7 and 6.4 μg m^{-2} yr^{-1}. Theses results support the well known hypotheses that (1) a set of local conditions in the vicinity of 3A-15 was better suited to methylation than other the other sites modeled, and (2) local methylation rates are an important factor affecting fish mercury concentrations, at least at some sites.

5.3 Model calibration at STA-2

Background

STA-2 is an artificial wetland constructed to remove phosphorus from agricultural runoff leaving the EAA. The site which is essentially was designed to remove phosphorus through hydraulic detention and vegetative uptake, consists of three cells (Figure 5-36). Flooding began in July 2000. Table 2-1 provides general characteristics of Cell 1within STA-2.

During the course of operational start-up, unacceptably high levels of methylmercury, with concentrations reaching up to 4.8 ng L^{-1} were measured in Cell 1 (Rumbold and Fink, 2001). In addition, methylmercury concentrations in the Cell 1 were found to far exceed those in the cell's inflow (Fink 2002b). Water levels in Cell 1 were low when flooding started in July 2000, but very high MeHg levels were detected by September 26, 2000 at which time outflow from the cell was shut off. The SFWMD requested Tetra Tech to use E-MCM to investigate the behavior of Cell 1 with the purpose of exploring possible mechanisms that could explain the anomalously high methylmercury levels found in Cell 1 of STA-2.

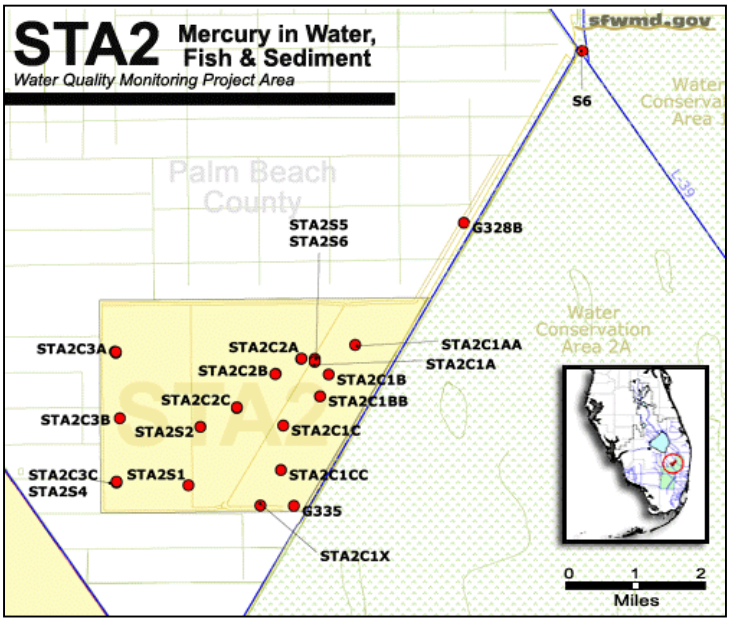

Figure 5-36. Site map and sampling stations for STA-2

(Map source: South Florida Water Management District).

Data sources for STA-2 Cell 1calibration

E-MCM was calibrated to the available data for methyl and total mercury concentrations in Cell 1 surface waters. Appendix E summarizes the data sources used to develop the inputs for the STA-2 calibration. Once site-specific data were entered for the scenario an initial simulation was carried out. The results for surface water methylmercury concentrations are given in Figure 5-37. The model provided reasonable predictions of the background level for methylmercury but was not able to account for the spikes in concentration at the beginning and end of the simulation period.

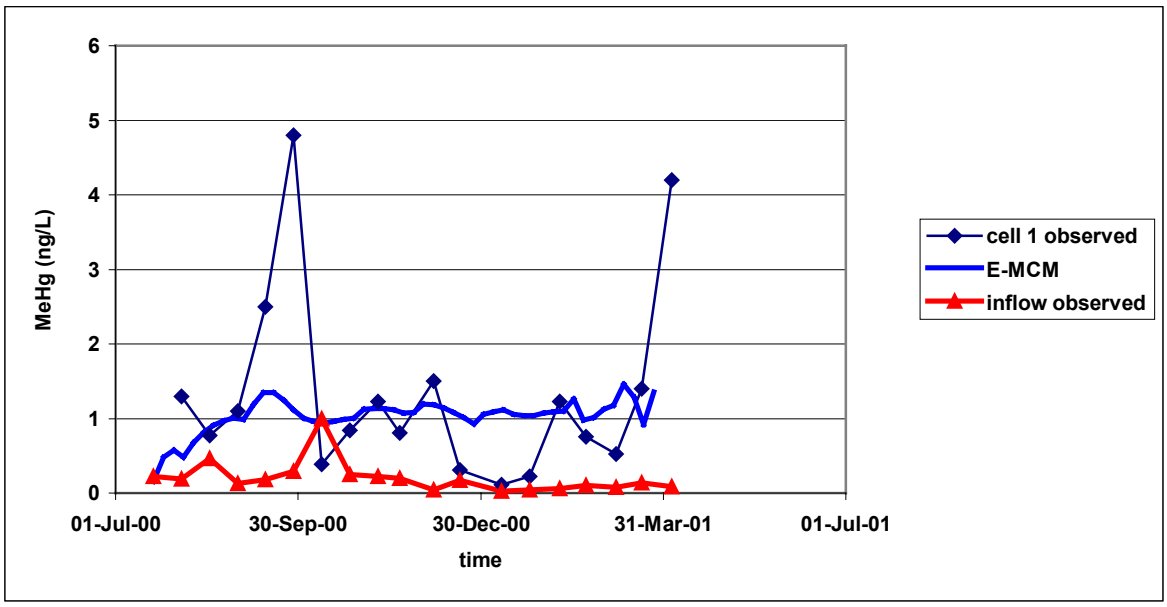

Figure 5-37. Preliminary predicted MeHg concentrations in STA-2 Cell 1 surface waters with methylation in sediments.

The rapid increases in surface water methylmercury concentrations observed at STA-2 could not be achieved when methylation was restricted to a sediment layer on the order of a few cm thick. It was hypothesized that methylation in the water column itself or at the sediment-water interface with rapid mixing in the water column could be invoked to describe the large spikes in methylmercury. E-MCM can be set up to include water column methylation. In the model, water column methylation is assumed to depend on the rate of decay of settling particulates and detritus at the sediment-water column interface, combined with a pool of Hg(II) to methylate, and a rate constant. In an effort to mimic the short term spike in water column methylmercury, we invoked high decomposition rates at the interface for a short period. The results for methylmercury and total mercury for the initial simulation with water column methylation are given in Figure 5-38 and Figure 5-39 respectively.

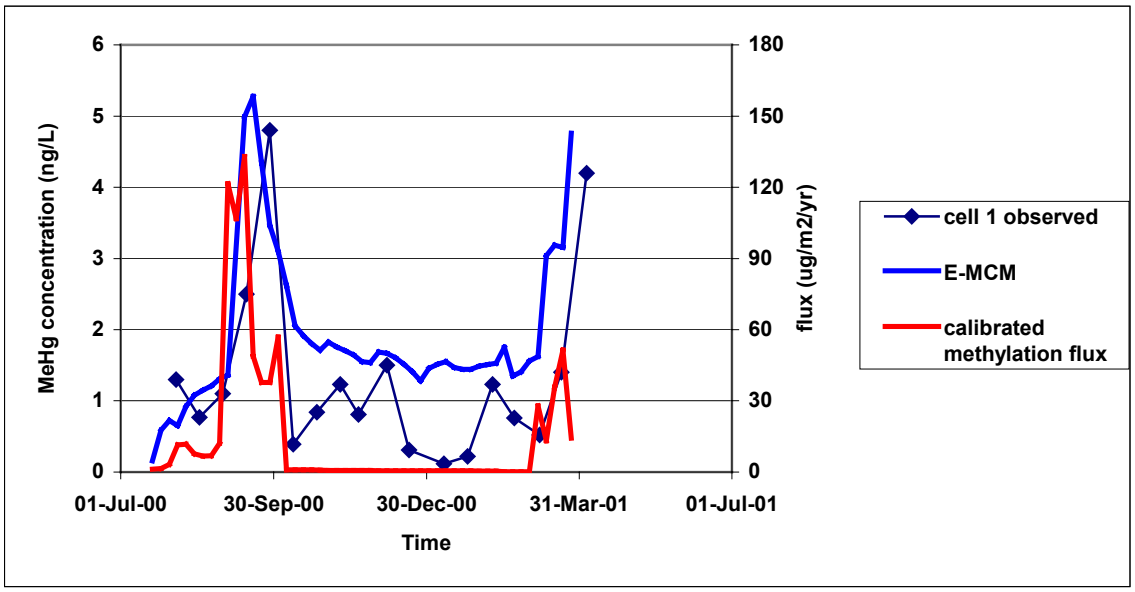

Figure 5-38. Predicted and observed MeHg concentrations in STA-2 Cell 1 surface waters, with water column methylation assumed.

(Source of observations. Fink (2002e)).

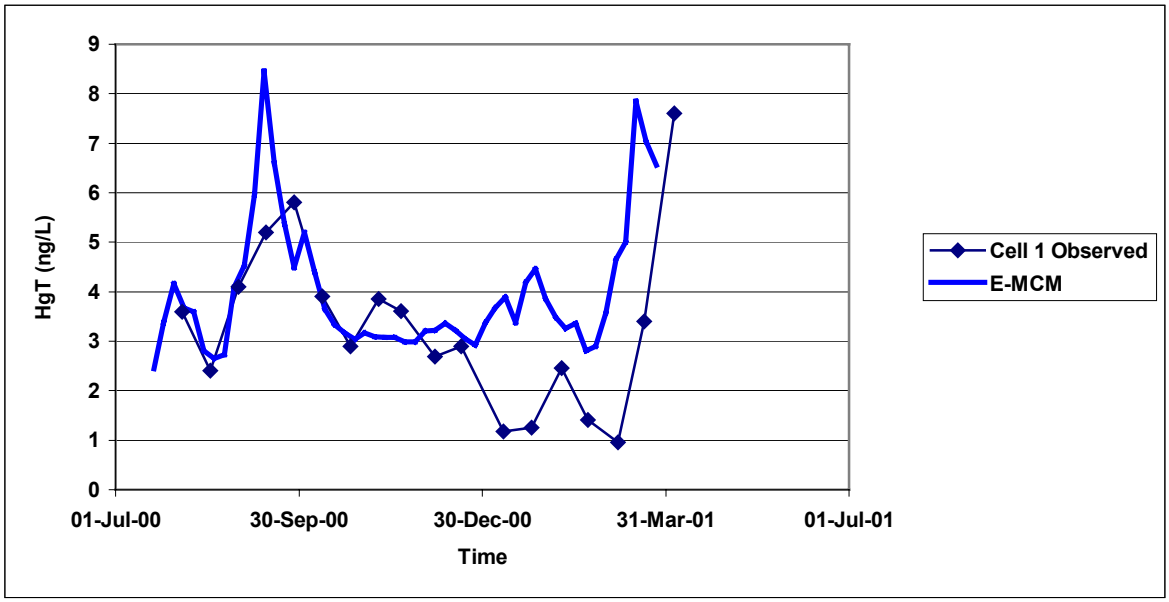

Figure 5-39. Predicted and observed total mercury concentrations in STA-2 Cell 1 surface waters, with water column methylation assumed

(Source of observations. Fink (2002e)).

Simulated total mercury concentrations compared reasonably well with observed levels (Figure 5-39). Good agreement between the simulated and observed methylmercury concentration spikes were obtained with the addition of water column methylation. It should be noted however, that in order to mimic the observed methylmercury spikes in E-MCM, extremely high short-term methylation rates on the order of 120 – 130 $\mu g\ m^{-2}\ yr^{-1}$ had to be imposed (Figure 5-38).

Simulated methylmercury concentrations in surface waters for the period between from December 2000 through March 2001 (the period between the two major concentration spikes) remained in the range of 1.3 – 2.0 $ng\ L^{-1}$, significantly higher than observed levels (Figure 5-38). Simulated methylation rates were close to zero during the period between spikes. This suggests that some other source was supplying methylmercury to the water column in the simulation at a rate sufficient to maintain the predicted elevated concentrations. The model predicted that the diffusion flux from the sediments to the water column was the most important source of methylmercury to the water column during this period with no in-situ methylation and was on the order of 10 $\mu g\ m^{-2}\ yr^{-1}$. Sediment mercury concentrations tend to change slowly with an active sediment layer on the order of 3 – 4 cm. This relatively slow response by sediments means that, for short-term simulations, the predicted sediment mercury concentrations and associated diffusive fluxes are highly dependent on the initial conditions specified for sediment methylmercury. Sediment methylmercury data for STA-2 were very limited and there is some uncertainty associated with the initial conditions used in the simulation.

Predicted methylmercury and Hg(II) fluxes averaged over the simulation in Figure 5-39 are given in Figure 5-40 and Figure 5-41, respectively. More than 90% of the methylmercury was estimated to originate with internal production.

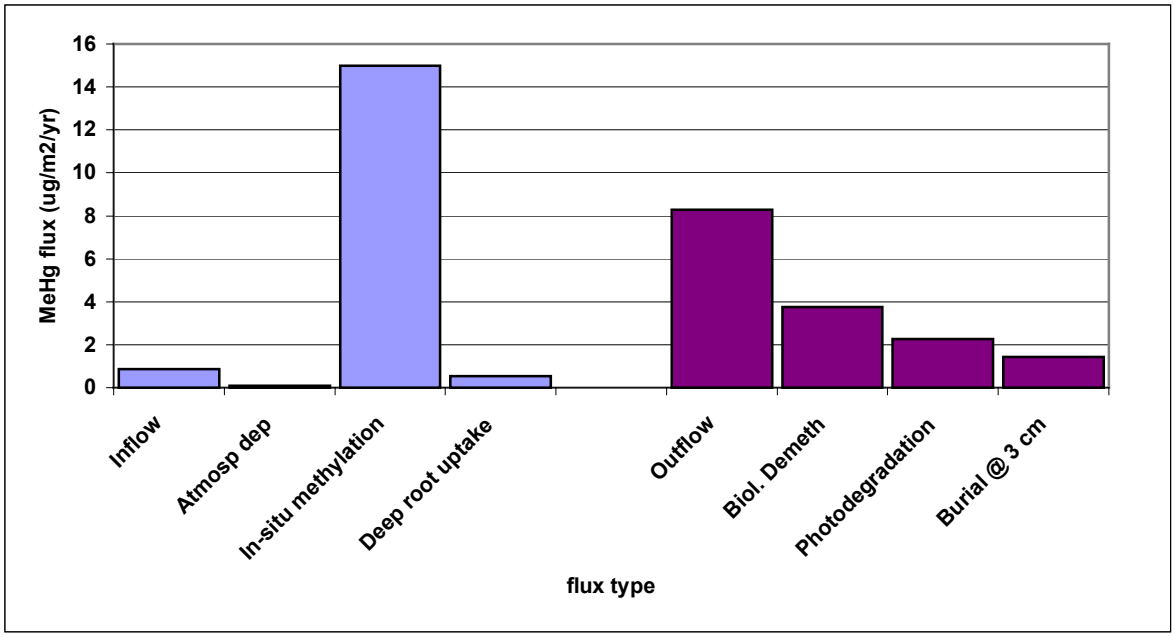

Figure 5-40. Simulated average MeHg sources and sinks for STA-2 from July 2000 – March 2001

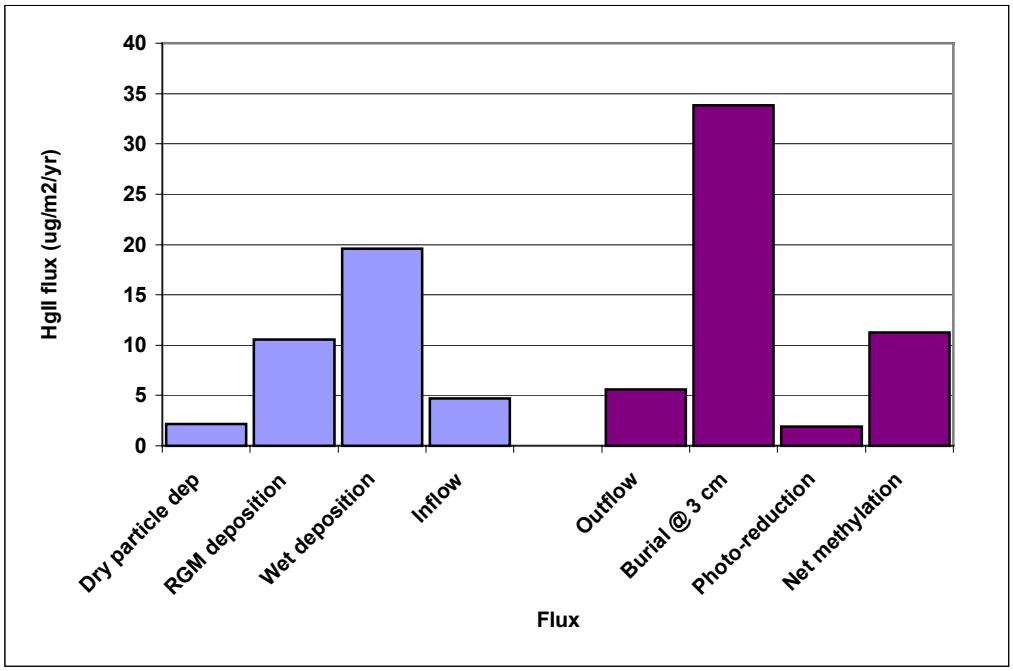

Figure 5-41. Simulated average Hg(II) sources and sinks for STA-2 from July 2000 through March 2001

A final hypothetical simulation was performed at the request of L. Fink to determine the impact, if any, that a periphyton bloom following flooding might have on surface water MeHg concentrations. The lower methylmercury concentrations observed during some periods might be explained by adsorption onto an increasing periphyton biomass. Periphyton levels were increased to about 7 times the background level for the period between mid December 2000 and mid February 2001. The magnitude of periphyton bloom was chosen to produce the desired drop in methylmercury concentrations and it should be noted that there were no periphyton data available for STA-2. No attempt was made to develop a mass balance for carbon/particulate fluxes in this scenario. The simulation results for methylmercury concentrations in surface waters are plotted in Figure 5-42 and illustrate an improved fit for the period between spikes. The results demonstrate that if the periphyton biomasses assumed were plausible, adsorption into periphyton biomass after the initial spike could potentially help explain reduced methylmercury concentrations observed.

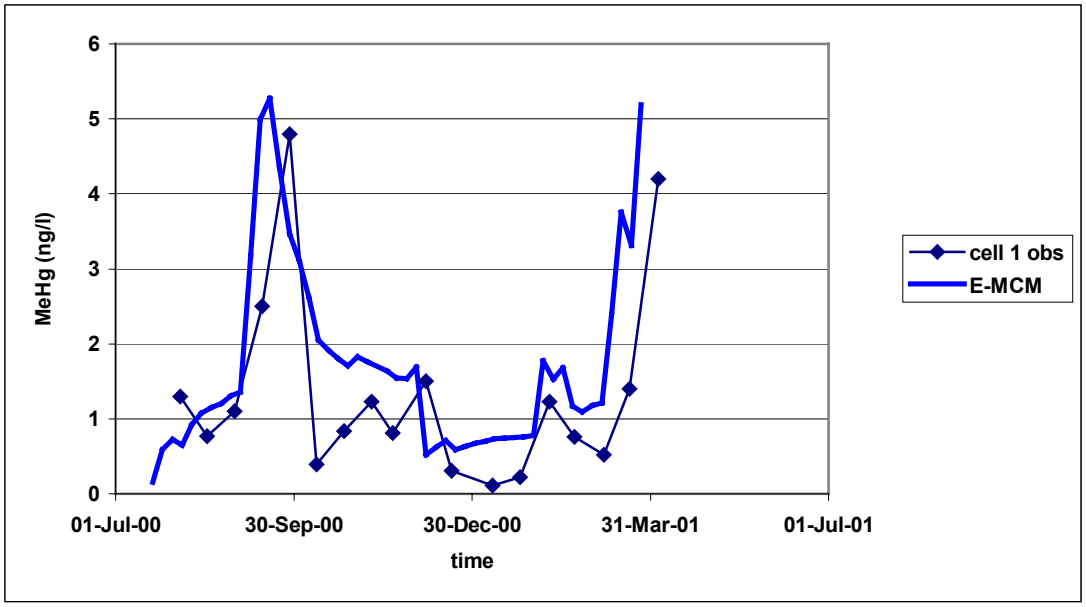

Figure 5-42. Simulated MeHg in STA-2 surface waters with the addition of a periphyton bloom in December 2000

(Source: Fink (2002e)).

Conclusions for STA-2 Cell 1 simulations

The results of the application of E-MCM to STA-2 Cell 1 should be considered at this point to be speculative in nature. There were substantial gaps in the data available to use in the calibration of E-MCM. For example, no data were available for water column particulates, sedimentation rates or periphyton coverage, all of which may impact mercury fluxes and concentrations in model runs. The simulation results, with the above caveat, suggest the following:

- E-MCM could be tuned to provide a good fit to dynamic water column mercury concentrations for STA-2. This required specific adjustments to methylation rate constants, both in magnitude and timing, and assumptions about possible periphyton growth and die-off patterns. These results are not predictive in nature, instead representing hypothesis testing.

- Internal methylation in the water column or at the water column-sediment interface had to be invoked to produce the observed short-term MeHg spikes in water column concentrations.

- The principal source of methylmercury to STA-2 appeared to be internal production. More than 90% of the methylmercuy originated with methylation within the STA-2 cell.

- The cycling of periphyton biomass could plausibly play a significant role in moderating short term methylmercury concentrations in the water column through growth and die-off patterns.

6 Management Scenarios

Tetra Tech was requested to run a set of model simulations in Phases II and III to examine the possible implications of management options on mercury behavior and concentrations in Everglades marsh areas. This section of the report focuses on the Phase III scenarios, with summary information provided on earlier management scenarios simulated.

6.1 Background

The Everglades Construction Project (ECP) is modifying existing and adding new structures to redirect all Lake Okeechobee makeup water and all stormwater runoff from the Everglades Agricultural Area (EAA) through constructed wetlands. The wetlands are intended to remove phosphorus and restore a more natural sheet flow to the northern remnant Everglades. Resource managers would like to know whether these changes to flow, stage-duration, or quality of the water being supplied to the northern Everglades will adversely impact Everglades mercury levels.

During the period when previously impacted areas are transitioning from eutrophic to oligotrophic conditions, it is also likely that local air sources of Hg(II) in wet and dry atmospheric deposition will be further reduced, following a 90% reduction over the previous decade (L. Fink pers. comm.).

The net effect of this complex interaction of decreasing mercury loads and changing water flow, depth, and quality on downstream MeHg production and bioaccumulation is difficult to unravel. Simulation models offer a systematic framework to attempt to examine the effects of factors, both individually and in combinations. L. Fink of the South Florida Water Management District provided a set of 10 management scenarios that were run during Phase II. These scenarios involved various combinations of atmospheric Hg deposition, flowrates, methylation rates and total phosphorus levels at ENR (3 scenarios) and WCA 2A (7 scenarios). During Phase II of the project, total phosphorus concentrations in surface waters were not a model input however. It was necessary to make assumptions about the effects of changes in total phosphorus (TP) levels on selected model inputs during Phase II. Inputs assumed to be impacted by total phosphorus concentrations in surface waters included those related to macrophyte and periphyton coverage and turnover, decomposition, sediment accretion, surface water chemistry and fish growth and diets. The effects of changing TP concentrations on these inputs were estimated by using conditions measured at sites with the desired TP level (e.g., applying U3-like conditions when total phosphorus concentrations in surface waters were circa 10 $\mu g\ L^{-1}$). Some of the management scenarios also involved changes to methylation rates, specifying rates that are "F1 like", "U3 like" or "3A-15 like". For these Phase II scenarios we applied the methylation *rate constants* calibrated from F1, U3 or WCA 3A-15.

Finally, managements scenarios for WCA-2A were run in a manner which simultaneously considered the effects at F1 and U3. For example, if a scenario changed the predicted concentration of Hg(II) in F1 surface waters and outflow, these changes were fed into the simulation for an intermediate cell between F1 and U3, and again for the U3 cell. Thus the Phase II WCA scenarios represented a first attempt to address the impacts of management actions on mercury concentrations between F1 and U3.

Overall, the following trends emerged from the Phase II WCA 2A management scenarios:

- Reduced atmospheric deposition of mercury resulted in lower predicted levels in water and fish, as expected.
- Reduced flows tended to increase predicted concentrations of mercury in water (total and methylmercury) and fish at F1 and U3.
- Particle budgets exerted an important influence on predicted mercury levels. In particular, sediment accretion rates and the extent to which settling material decomposes at the sediment/water interface, instead of being incorporated and buried in sediments, had important implications for predicted mercury levels.
- F1 management scenario results suggested that system productivity can impose multiple, competing influences on mercury cycling, confounding simple relationships between system productivity and mercury levels.
- The highest predicted concentrations of mercury occurred for a scenario that included reduced sedimentation rates at F1 and U3, reduced flows, and increased methylation rates, all combining to generate fish mercury concentrations higher than the base case simulations.

During Phase III, additional management scenarios were undertaken that focused on the effects of nutrient status and flowrate on fish mercury concentrations in WCA 2A. Furthermore, simple relationships were developed to try to estimate the effects of phosphorus levels on particle budgets (e.g., peat accretion) and methylation rate constants. These relationships were embedded in the Phase III management scenario simulations. Details on the Phase III management scenario simulations are provided below.

6.2 Description of Management Scenarios for Phase III

Sixteen management scenarios for WCA-2A were provided by the South Florida Water Management District (Table 6-1) . These scenarios included 9 scenarios under conditions with currently estimated flowrates. Seven additional scenarios examined the effects of 50% flow reductions under various nutrient regimes. Note that the effects of flow and nutrient levels were treated as independent for this analysis, although it is recognized that changing the flow could well affect nutrients and system productivity.

For the base case flow scenarios, three scenarios were run with different concentrations of total phosphorus at U3 (4, 7 and 10 $\mu g\ L^{-1}$), and assuming low phosphorus concentrations at F1 (10 $\mu g\ L^{-1}$). The remaining base case flow scenarios run so that the following phosphorus concentrations at F1 were examined: 10, 20, 30, 50, 75, 120 and 127 $\mu g\ L^{-1}$, while assuming a U3 phosphorus concentration of 10 $\mu g\ L^{-1}$.

Simulations with reduced flows followed the same basic pattern as the base case flow scenarios, with the following F1 phosphorus concentrations: 10, 20, 30, 50, 120 $\mu g\ L^{-1}$.

Scenario number	Flowrate		F1 TP concentation (μg/L)							U3 TP concentration (μg/L)		
	Base flow	50% of base flow	10	20	30	50	75	120	127	4	7	10
1	X		X							X		
2	X		X								X	
3	X		X									X
4	X			X								X
5	X				X							X
6	X					X						X
7	X						X					X
8	X							X				X
9	X								X			X
10		X	X							X		
11		X	X								X	
12		X	X									X
13		X		X								X
14		X			X							X
15		X				X						X
16		X						X				X

Table 6-1 . Phase III management scenarios.

Simulations were run for 20 years, adequate time for the systems to reach apparent steady state. The primary endpoints we examined were water column concentrations of total and methylmercury, and fish mercury levels in 3 year old largemouth bass. F1 does not currently support a predatory fish population due to poor habitat, but it was assumed for the purpose of the management scenario analysis that F1 would support one. In addition to the key endpoints, we also made use of available data for mercury concentrations in several other compartments, including total and methylmercury in surface waters and sediments, methylmercury in the lower food web, and apparent mercury partitioning between solid and dissolved phases. Finally, field data were used to calibrate particle budgets as well, particularly for the F1 and U3 sites.

Water quality field data from (SFWMD 2000g) indicated that there was a strong relationship between total phosphorus and dissolved oxygen in the water column; hence this parameter was adjusted as a function of total phosphorus concentrations in surface waters. The relationship between other water quality parameters and phosphorus was weak across WCA-2A sites examined (e.g., see Table 5-5) using the datasets available; hence these values were held constant at WCA-2A sites.

The scenarios provided by the SFWMD involved changes to total phosphorus levels at F1 and/or U3. To address the potential for cascading effects downstream of F1 towards U3, the model was run with 3 linked cells, using a linked-cell version of the model. F1 was assumed to cover the terrain from the S10 flow structures downstream 3.6 km, such that the actual F1 sampling site was in the middle of the modeled cell. U3 was modeled as a cell 3.6 km long, again with the U3

sampling station in the middle of the cell. Bridging these two cells was an intermediate "middle cell". It was necessary to assign phosphorus levels to this middle cell as well for simulations. Table 6-2 shows the surface water concentrations of total phosphorus applied to all cells for the management scenarios.

Scenarios	Total Phosphorus Concentration applied to Model cell ($\mu g\ L^{-1}$)		
	F1	**Middle Cell**	**U3**
1 &10	10	10	4
2 & 11	10	10	7
3 & 12	10	10	10
4 & 13	20	10	10
5 & 14	30	10	10
6 &15	50	15	10
7	75	15	10
8 & 16	120	20	10
9	127	20	10

Table 6-2. Surface water phosphorus concentrations applied to F1, Middle, and U3 cells in model scenarios (Source SFWMD 2000g)

The following model inputs were modified as a result of changes to total phosphorus levels:

- Inputs related to particle budgets (marsh coverage by plants, productivity, sedimentation, decomposition).
- Rate constants for biological methylation and demethylation.
- For scenarios with TP levels less than 120 $\mu g\ L^{-1}$ the fish diet used for U3 simulations was applied. For scenarios with TP levels greater than or equal to 120 $\mu g\ L^{-1}$, the F1 fish diet was applied.

Input values for these phosphorus-dependent inputs were estimated internally within the model, using relationships "hard-wired" into the model for the purposes of these simulations. These relationships are described in more detail in subsequent sections.

6.3 Trophic State Considerations

To predict the effects of changing phosphorus dynamics on mercury cycling in the Everglades, changes in nutrient concentrations must in essence be translated into changes in trophic state and related site conditions. A number of key processes related to changes in trophic state need to be considered by E-MCM with respect to possible effects on mercury cycling. These include:

- Changes in particle dynamics. These include changes in the fractional coverage of marshes with respect to open water and key macrophytes (sawgrass and cattails); changes in the sizes of macrophyte and periphyton biomass pools and the supply of detrital matter; changes in sedimentation (peat accretion) rates; and changes in decomposition rates both at the sediment-water interface and in sediments.
- Development of relationships between total phosphorus and methylation rate constants for management scenarios. Adjustments to methylation rate constants as a function of total phosphorus may contribute to predicting desired trends in terms of methylation rates under differing system productivity, but may not be mechanistically correct. For

example, trophic status may affect bioavailable pools of inorganic Hg(II) to methylate, rather than the actual rate constant for methylation. However the model is not yet fully able to predict concentrations of bioavailable Hg(II), nor the effects of system productivity on these concentrations.

- Food web changes also would be expected (growth rates, structure and length of food web, diet composition, etc.) with changing trophic state. Although a "bottom-up" food web module has been built into E-MCM, this module has not been adequately tested, and was not used for the management scenarios.

The original goal of this study was to link E-MCM to an independent model that would provide most of these relationships, particularly with respect to particle dynamics. However, because the use of ELM proved not feasible at this juncture, we developed a series of comparatively simple relationships between concentrations of total phosphorus in surface waters and particle-related parameters. The following sections provide brief overviews of the approaches and resultant relationships that were used to link changing surface water TP concentrations with changes in: (1) vegetative cover; (2) the sizes and turnover rates of macrophyte and periphyton biomass pools; (3) sedimentation (peat accretion) rates; and (4) sediment decomposition rates. These relationships cannot be viewed as robust – they are empirical in nature and are, in part, developed with very limited data. They do, however, serve the purpose of demonstrating the science-based usefulness of the conceptual model for this report.

6.3.1 Fractions of marsh areas with open water, sawgrass, and cattails

Within the Everglades, it is well established that sawgrass (*Cladium jamaicense*) dominates the vegetative cover at low productivity marsh sites, while cattail (*Tyhpa domingensis*), although present as sparse colonies in some portions of the unimpacted Everglades, now dominates at eutrophic sites. Unfortunately, what has not been clearly established is the functional relationship between a change in the long-term average water column total phosphorus concentration and the corresponding change in long-term average vegetative cover. While there is are extensive sets of surface water, pore water, and soil total phosphorus data extending back almost a decade in some areas of the northern Everglades, the corresponding coverage data are more limited and confined almost exclusively to estimates based on photogrammetric interpretation of false-color infra-red aerial photographs or statellite images taken at infrequent, irregular intervals (Rutchey and Vilchek, 1999). However, a limited number of ground-based data are also available. To quantify the functional relationship between water column TP concentration and vegetation coverage in the northern Everglades, data were gathered from two studies. The first involved the collection of data on the frequency of occurrence of sawgrass and cattails along north-south "D" transect every two years between 1990 and 1996 published by Paul McCormick *et al.* in the Everglades Consolidated Report (2000). The results from the September 1996 campaign were selected for this exercise because it fell within the timeframe of the mercury studies (Aquatic Cycling of Mercury in the Environment) carried out by the U.S. Geological Survey along the "F" Transect from July 1995 through July 1998. These data were then paired with the average TP concentrations at the nearest routinely monitored site along the adjacent "F" Transect for the period 1994-1997. Data were also obtained from the same source on the fraction of the surface area covered by open water, emergent macrophyte, floating macrophyte, and periphyton as a function of distance from the L-39 levee based on low-altitude aerial photographs taken along the "F" transect in 1998 or 1999.

Because the vegetative cover sampling and nutrient monitoring locations do not match-up identically, it was initially important to develop a predictive relationship between surface water concentrations of total phosphorus (TP) along the "F" transect and the distance downstream from the S-10 structures. The following non-linear model (Equation 1) was fitted to the data using least squares regression (SAS Institute, 1998):

$$TP = B_1 \cdot e^{-(\frac{Dist - 1.8}{B_2})} + B_3 \qquad (1)$$

where TP is expressed in μg L^{-1}, *Dist* = distance downstream from the S-10 structures, and B_1, B_2, *and* B_3 are fitted parameters (0.1805, 2.5254, and –0.0030 respectively). With this relationship, it was possible to estimate the phosphorus concentration for each location where surface reflectance data were available. This led to the following equation (Equation 2) developed by Fink (L. Fink, personal communication), which was "optimized" to produce predicted fractions of open water at sites with low TP concentrations that fit *a priori* expectations for the tail of the distribution at the measured lower concentration range for TP (as opposed to a best fit procedure using all the data):

$$Frac_{open} = 1 + \frac{(4.55 \cdot \mathrm{ATANH}\{1.25 \cdot (\frac{\mathrm{TP}}{180}) - 1\})^4}{110} \qquad (2)$$

where $Frac_{open}$ is the fraction of marsh area that is open water; TP equals the total phosphorus concentration in the surface water (μg P L^{-1}); and ATANH is the inverse hyperbolic tangent function.

The next step was to estimate how the proportions of vegetative cover dominated by sawgrass and cattail change with surface water TP concentrations. In order to use the "D" transect data for vegetative cover, it was necessary to infer corresponding nutrient concentrations from nearby "F" transect nutrient monitoring stations. In other words, we assumed that the total phosphorus concentrations in surface waters were comparable for the following suite of paired stations: F1 and D2; F2 and D3; and F3 and D4. Using the data measured in 1996 across transect "D" to estimate the fraction of vegetated area covered by sawgrass, we developed estimates for the fractions of vegetated marsh area covered by sawgrass at F1, F2 and F3 (Table 6-3).

D transect site*	September 1996 field estimate of fraction of vegetated area covered with sawgrass*	F transect station assumed comparable to D transect site	Distance along F transect from S-10 structure (km)	Average TP concentration measured at F transect station between 1994-97 (μg L^{-1})
D2	0.075	F1	1.8	175
D3	0.35	F2	3.8	90.8
D4	0.8	F3	5.6	25.5

Table 6-3. Estimated fraction of vegetated marsh area covered with sawgrass, and associated F transect sites and total phosphorus concentrations in surface waters.

A hyperbolic function was fitted through the above three points (F1, F2, F3) to estimate the fraction of vegetated area covered by sawgrass as a function of TP, as shown in Figure 6-1. It was further assumed that the remainder of the vegetated area was essentially cattails, which was then calculated by difference (also shown in Figure 6-1). Using this approach, the TP concentration that corresponds to a 50:50 mix of sawgrass and cattails on an area basis would be approximately 63 µg L^{-1}.

Using the hyperbolic function for open water (Equation 2) and the relationship shown in Figure 6-1, the fractions of total marsh area covered with open water, cattails and sawgrass as a function of total phosphorus concentration in surface waters were estimated and plotted (Figure 6-2).

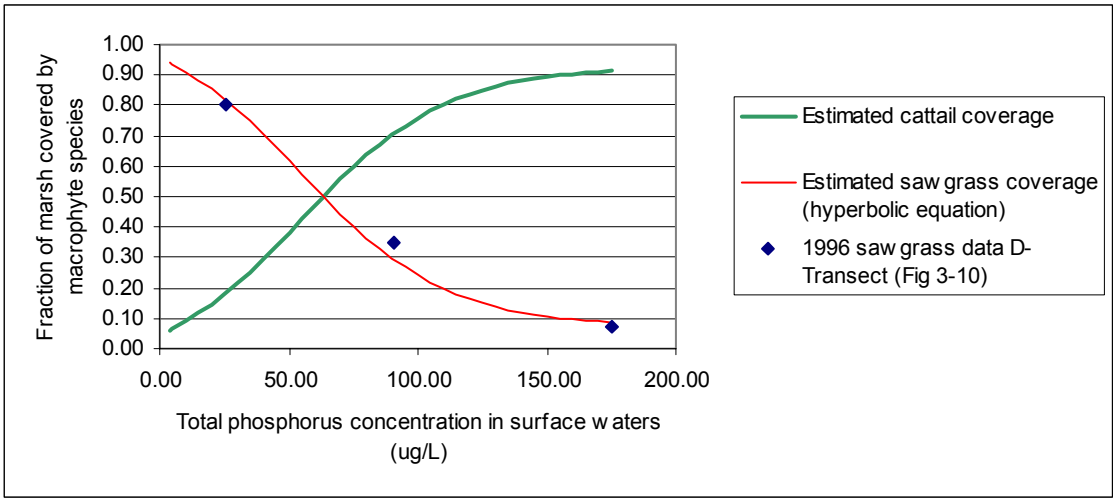

Figure 6-1. Estimated fractions of vegetated areas covered by cattails and sawgrass as a function of surface water total phosphorus concentration (mg L^{-1}).

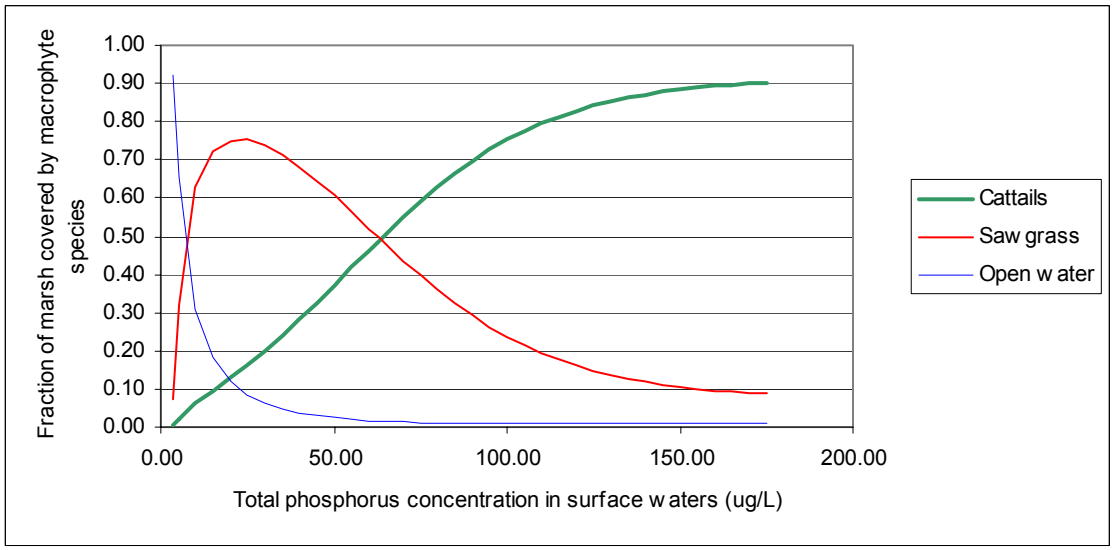

Figure 6-2. Estimated fractions of total marsh area covered by cattails, sawgrass and open water as a function of surface water total phosphorus concentration (μg L^{-1}).

6.3.2 Estimation of macrophyte and periphyton particle pools and the supply of detrital matter

There are several factors that combine to dictate the supply of litter to a marsh from macrophytes and periphyton. These include the areal coverage of the marsh by different plant species, as well as the biomass densities and turnover rates of these plants. Aerial coverage was estimated as discussed previously. We used the empirical relationships developed by Fink (cited in Ambrose et al., 1997) to estimate biomass densities and turnover rates for sawgrass, cattails and periphyton. Since more specific data were not available, we assumed similar to Ambrose *et al.* (1997) that water lily turnover rates were functionally equivalent to the empirical relationship derived by Fink for sawgrass, and that the relationship between lily biomass and TP concentration was equivalent to 20% of the sawgrass biomass relationship.

Previously determined estimates of total marsh areal coverage were then combined with the biomass densities and turnover estimates for sawgrass, cattails, lilies and periphyton to yield the relationship between rate of supply of settling detrital matter and TP concentration in surface water shown in Figure 6-3. Note that external inputs of settling material (e.g., from total suspended solids), and other sources contributing to internal production of particles (e.g., from algal production) are currently ignored in this model relationship.

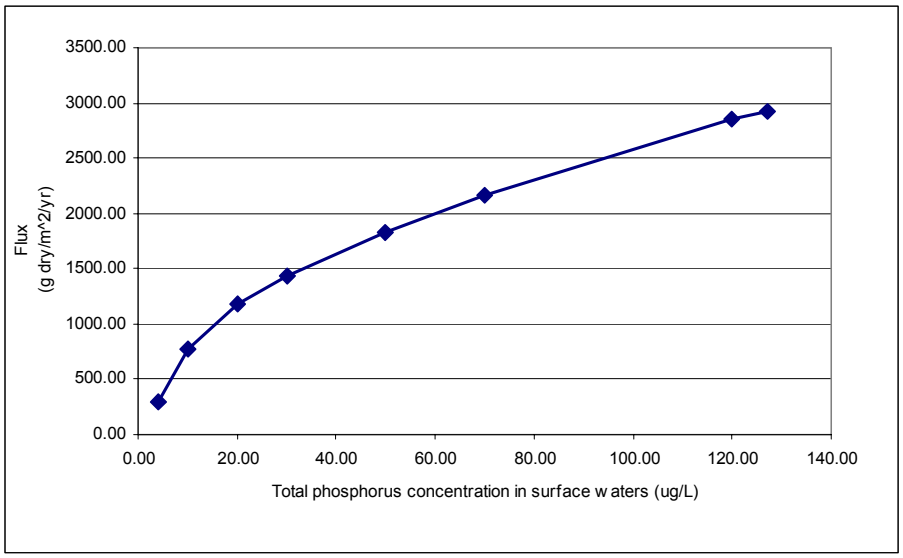

Figure 6-3. Predicted supply of detrital matter as a function of phosphorus concentrations in surface waters

6.3.3 Estimation of sedimentation (peat accretion) rates

Estimated field sedimentation rates were available for WCA-2A from Vaithiyanathan et al. (1996) from transect locations C1 (eutrophic) and C6 (oligotrophic) in June 1990. Peat accretion rates were estimated using ^{210}Pb and ^{137}Cs dating. The estimated rates for the upper 25 cm of the sediment/soil profile (post 1960's) were 7.1-7.5 mm yr^{-1} at C1 and 1.9-2.5 mm yr^{-1} at C6 (Vaithiyanathan et al. 1996).

Using these rates as a guide, we sought to calibrate the particle budgets to arrive at a peat accretion rate at F1 and U3 similar to the field estimates for C1 and C6 respectively (Vaithiyanathan et al. 1996). Although C1 and C6 lie on a different transect than F1 and U3, they are at similar distances from the S-10 canal. C1 is characterized as an enriched site while C6 is unenriched. Also of critical importance was the shape of the curve connecting these two points: in other words, how did sedimentation change as a function of surface water TP level between F1 and U3? Based on data from Walker and Kadlec (1996), we attempted to calibrate the model so that as surface water TP levels increased, so did sedimentation rates, but at an ever slowing rate of increase. This trend can be explained in part by a shift from sawgrass to cattails as the surface water TP levels increase; sawgrass decomposes less readily than cattails, and thus contributes more to net sedimentation than cattails when net sedimentation is normalized to gross productivity (Reeder and Davis, 1983).

6.3.4 Estimation of decomposition rates

Sedimentation rates at the bottom of the surficial sediment layer (*i.e.,* 0-4 cm) were calculated by difference using the supply of settling material, minus the amounts of decomposition at the sediment water interface and within the sediment layer, minus any resuspension (Equation 3):

$$S_{4cm} = S_{0cm} - Decomp_{0cm} - Decomp_{0\text{-}4cm} - Resusp \qquad (3)$$

We assumed that the relationship depicted in Figure 6-3 for the supply of detrital material was valid, and that resuspension of sediment particles is a secondary consideration (as opposed to resuspension of particles at the sediment-water interface, which may be more significant). We also developed rates of decomposition at the sediment-water interface and within the sediment layer (see below) to arrive at the desired peat accretion rates as a function of surface water TP concentrations. In lieu of data, we also assumed that the general pattern suggested by Walker and Kadlec (1996) for sedimentation as a function of surface water TP level also applied to decomposition – *i.e.*, increasing decomposition rate as a function of increasing TP concentration, but at a slowing rate. We assumed this relationship applied to both the sediment-water interface and within the sediment layer, again in lieu of actual data to serve as a guide.

The net results of our assumptions regarding the supply of particulate matter, decomposition and peat accretion are shown in Figure 6-4. Note that the term "flux into sediments" refers to the net amount of material entering into the sediments after some of the settling material has decomposed at the sediment-water interface, or has been resuspended. Figure 6-5 shows the same estimated sedimentation rates as in Figure 6-4 above, but at a finer scale to better show the shape of the curve. The predicted relationship between fish Hg levels and surface water TP concentration is very sensitive to our assumed relationship between surface water TP concentrations and particle fluxes (Tetra Tech, 2002), and it should be recognized that this is an area of uncertainty that requires further critical study and analysis.

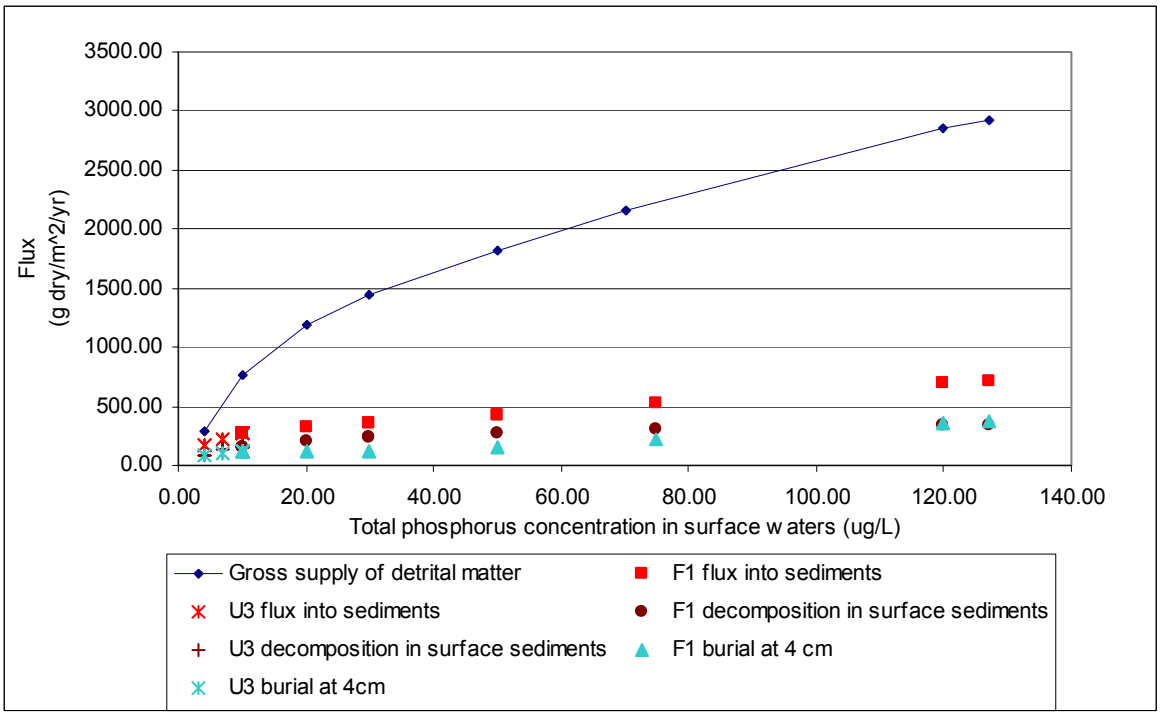

Figure 6-4. Predicted particle fluxes as a function of phosphorus concentrations in surface waters

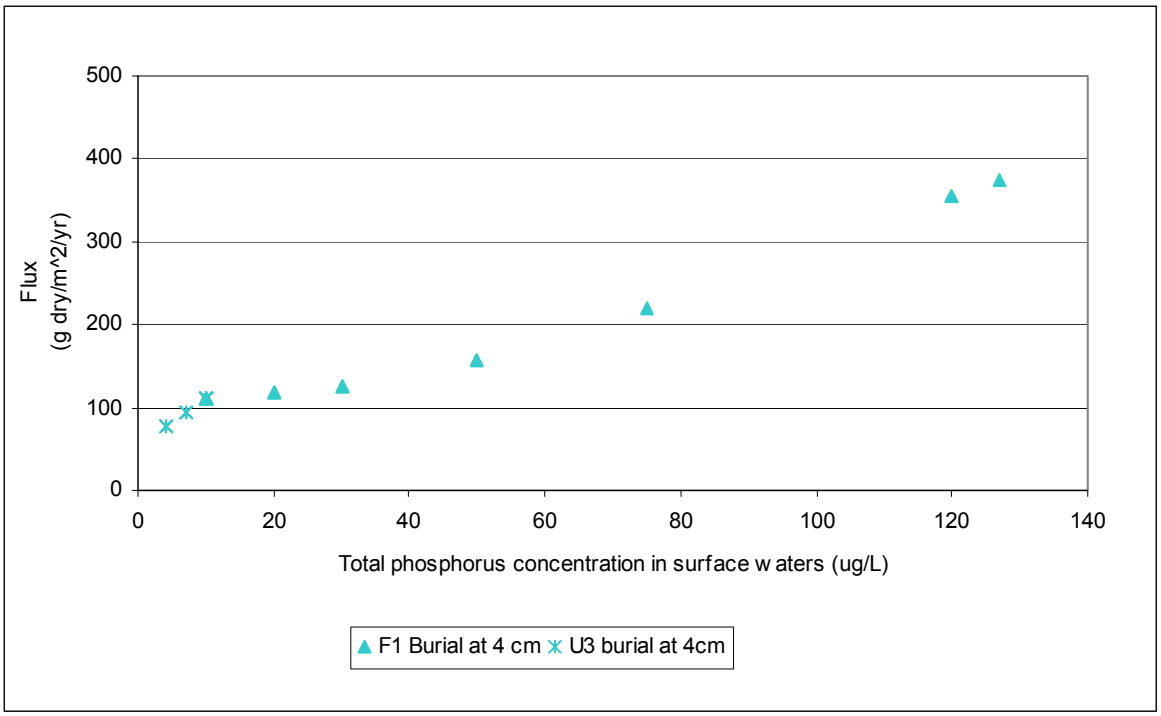

Figure 6-5. Predicted particle burial rate as a function of total phosphorus concentration in surface waters

As will be shown later in the document, the predicted relationship between fish mercury levels and total phosphorus was affected by the assumed relationship between phosphorus and particle fluxes. An alternative example of a particle budget was tested in the management scenarios and is shown in Figure 6-6. For this particle budget, we used the same equations to estimate the supply of detrital matter, and used nearly the same peat accretion rates at F1 and U3. Rather than assume a desired shape of the sedimentation/phosphorus relationship though, we used information on decomposition rates from Fink (2002a) and Reeder and Davis (1983). Dead leaf material from sawgrass and cattail was placed in litterbags at enriched and non-enriched sites in WCA2A and observed over roughly a six month period. Decay rates for the model were derived from these experiments as a function of total phosphorus (Reeder and Davis, 1983) and resulted in the relationship between phosphorus concentrations and sedimentation rates shown in Figure 6-6. In this example of a particle budget there was actually a peak sedimentation rate when surface water total phosphorus concentrations were on the order of 50 μg L^{-1}. While we are not suggesting this is actually the case, it does serve later in the document to show the potential for particle budgets to affect the predicted relationship between fish mercury concentrations and total phosphorus levels.

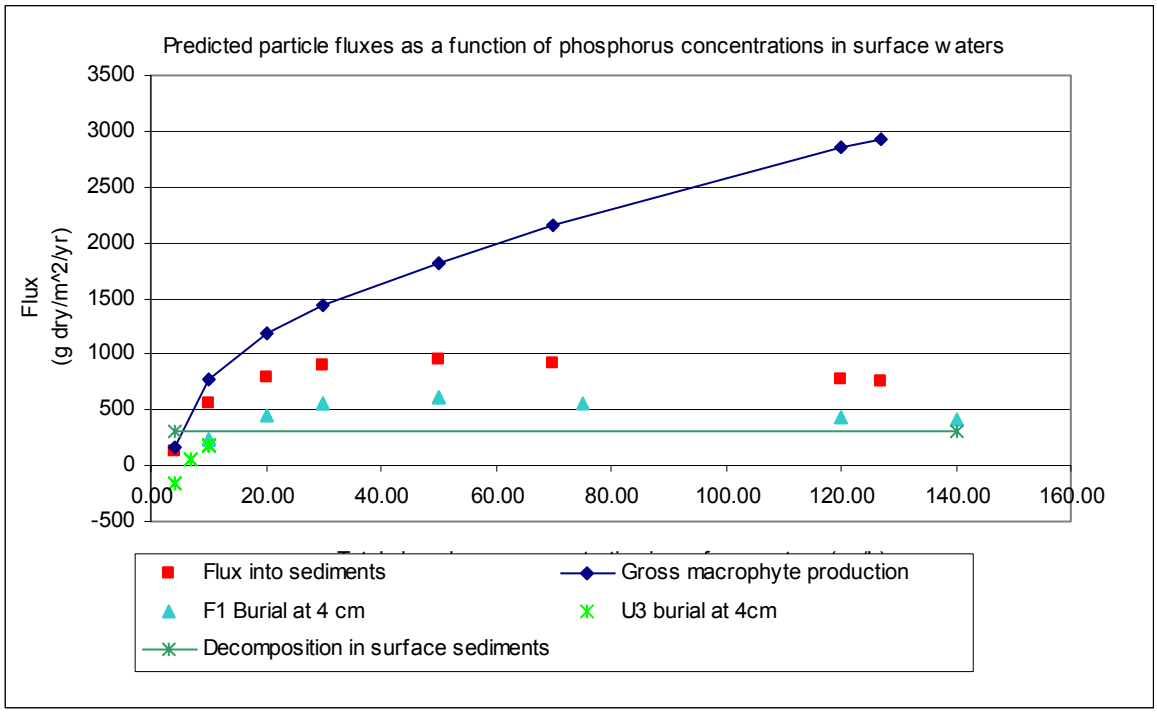

Figure 6-6. Alternative particle budget used to show sensitivity of model to particle fluxes

6.4 Development of relationships between total phosphorus and methylation rate constants for management scenarios

The relationship between true gross methylation (and demethylation) rates and system productivity has not yet been fully quantified. In fact it is not yet possible to measure true methylation rates, nor has the pool of Hg(II) bioavailable for methylation been clearly identified. For Phase II management scenarios, the South Florida Water Management district provided an approach to estimate methylation rates. Some of the Phase II management scenarios involved changes to methylation rates, specifying rates that are "F1 like", "U3 like" or "3A-15 like". For these scenarios Tetra Tech Inc. applied the methylation *rate constants* calibrated from F1, U3 or WCA 3A-15.

For Phase III management scenarios, Tetra Tech was requested to estimate methylation rates on the basis of total phosphorus concentrations that might exist under a given management scenario. Both water column and sediment methylation needed to be considered. For sediments, options considered included (1) using published rates for methylation and demethylation at sites with different phosphorus levels, determined with radiotracer or stable isotope incubations from intact cores, or (2) to use methylation and demethylation rates calibrated with E-MCM at sites with different phosphorus concentrations. For the water column methylation, no incubation data were found from the literature, and only one site has been calibrated with E-MCM to date with water column methylation (site F1).

Interestingly for sediments, the relative ranking of sites with high or low methylation rates was very similar for incubations and E-MCM calibrations, but the absolute magnitudes of the rates were orders of magnitude different for the two approaches. Figure 6-7 shows a comparison of estimated gross methylation rates in sediments based on (1) E-MCM calibrations and (2) laboratory incubations for sites with a range of phosphorus concentrations in surface waters. The rates are generally higher at the lower phosphorus sites. It should be noted though that some water column methylation was calibrated to occur at F1, a highly productive site. The graph refers only to sediment methylation rates. The units on the Y axis are different ($\mu g\ m^{-2}\ yr^{-1}$ for E-MCM calibrations; $ng\ g^{-1}\ day^{-1}$ for incubations. When compared in like-units, the rates are orders of magnitude higher for the incubation estimates than the E-MCM calibrations (Table 6-4). While this may at first indicate that at least one of these methods is utterly incorrect, it is in fact encouraging that in relative terms both methods end up with similar rankings of sites that are potentially hot spots, or not, for methylation. Furthermore, the E-MCM gross methylation rates could be higher if the demethylation rates were also faster, but generated the same net methylation. Also the ^{203}Hg incubations may represent rates that apply to highly bioavailable Hg(II), and when extrapolated to the entire sediment Hg(II) pool, could generate high estimates for ambient methylation rates. The authors of this document and many others have often commented that it would be very useful to determine the truly bioavailable pool of Hg(II) for sediment methylation, and to thus be able to determine a rate constant applicable to this pool. Note that if typical methylmercury concentrations on solids are taken to be on the order of 0.1 to 10 $ng\ g^{-1}$, then the 203Hg incubation rates would be turning over the entire pool of methylmercury in surficial sediments daily, which is possible but seems very fast.

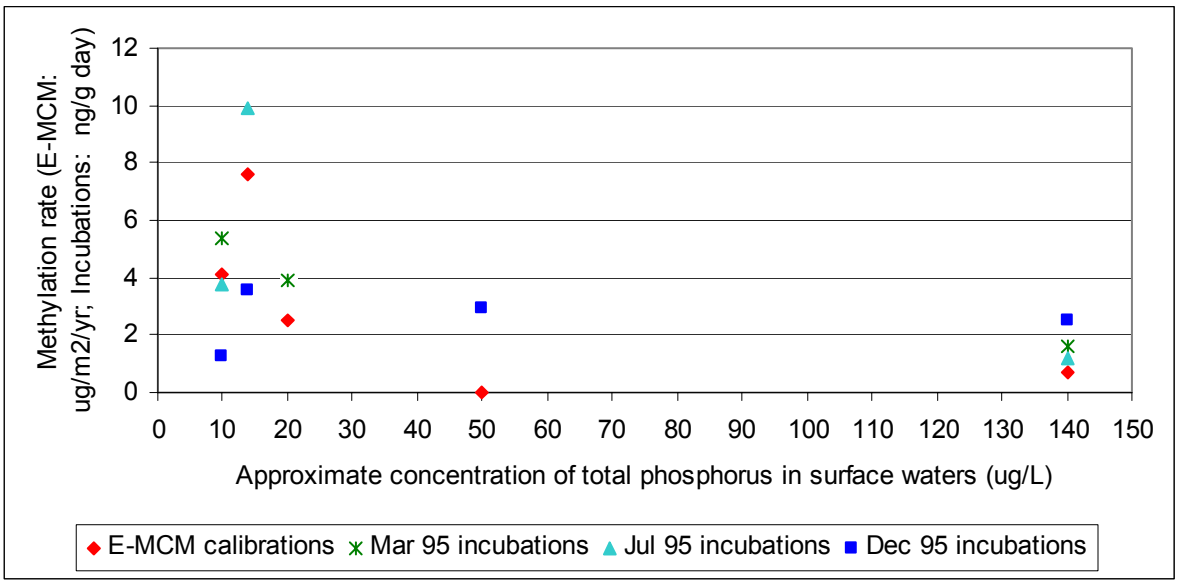

Figure 6-7. Estimated sediment gross methylation rates as a function of total phosphorus in surface waters at 4 Everglades sites - estimated by (1) E-MCM calibration and (2) ^{203}Hg incubations by Gilmour *et al.* (1998b)

Flux units	E-MCM estimate for WCA 3A-15 (high production site)	Estimated range of ambient rates using 203 Hg incubations for sites spanning a nutrient gradient*
% of Hg(II) on solids methylated per day	0.005	0 to 12, average ~2
ng methylated/g solids/day	0.008	~1 to 10

Table 6-4. Comparison of sediment methylation rate estimates using (1) E-MCM calibrations and (2) sediment core incubations with 203 Hg (derived from Gilmour *et al.* (1998b))

For the purposes of the Phase III management scenarios, we developed a relationship between methylation rate constants and surface water phosphorus concentrations. The relationship can be summarized as follows:

- For TP>120 μg L^{-1} the water column methylation constant calibrated for F1 was used. Methylation in sediments was shut off.
- For TP between 10 and 75 μg L^{-1} we fitted a curve to the sediment methylation rate constants calibrated for F1, the middle cell and U3. Water column methylation was shut off.
- For TP <10 μg L^{-1} we held the sediment methylation rate constant calibrated for U3. Water column methylation was shut off.

The relationship for rate constants for gross methylation in sediments is shown in . Since exponential curves can change rapidly outside the range of fitted values, we maintained the same value for the methylation rate constant when total phosphorus concentrations were at or below 10 $\mu g\ L^{-1}$.

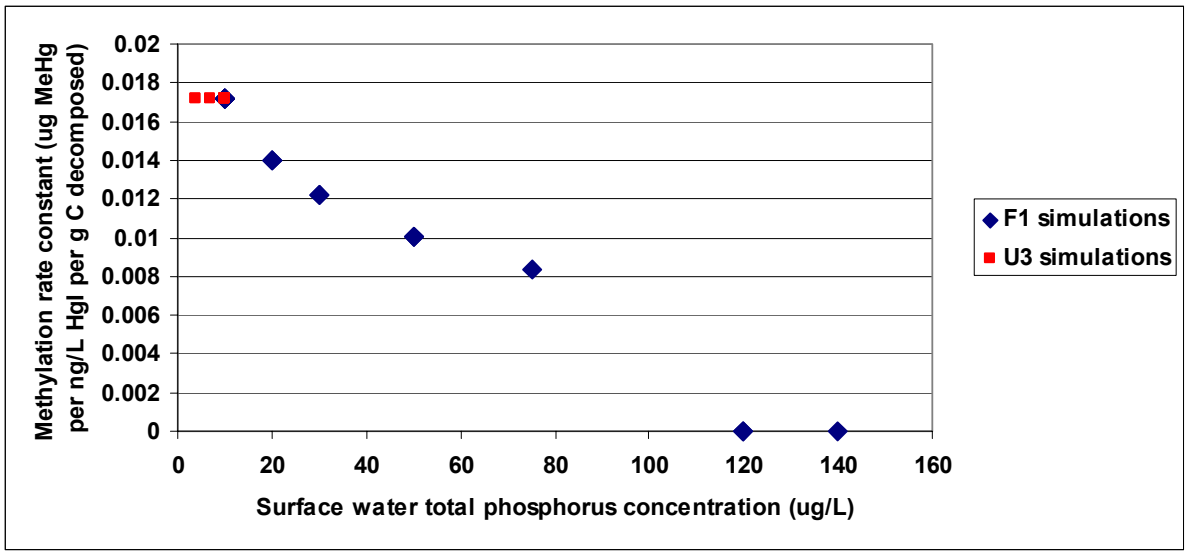

Figure 6-8. Estimated relationship between total phosphorus in surface waters and sediment methylation rate constants for Phase III management scenarios

It is interesting that the sediment methylation rate constant was calibrated to decline as phosphorus levels increased. This means that for a given amount of decomposition, and a given concentration of sediment porewater Hg(II) to act upon, the methylation process is predicted to be more effective in low phosphorus environments. This does not imply a direct cause-effect relationship between phosphorus and methylation constants. It could show an indirect relationship though, for example if higher productivity sites generated more sulfides, reducing the fraction of total dissolved porewater Hg(II) that is available to methylate. Note also that the relationship assumed between phosphorus and the methylation rate constant is not necessarily the same as the relationship that might emerge for methylation *rate* and phosphorus. This is because other factors beyond the rate constant also affect the predicted methylation rate (porewater Hg(II) concentration and decomposition rates).

6.5 Results of Management Scenario Simulations

The management scenarios focused on the potential effects of changes to nutrient levels and water flowrates across Water Conservation Area 2A, specifically from F1 to U3. Figure 6-9 through Figure 6-18 summarize the results of the management scenario simulations for the particle budget shown in Figure 6-4.

6.5.1 F1 Management Scenario Results

Figure 6-9 shows the predicted relationship between surface water Hg(II) concentrations and phosphorus concentrations. The Y-axis unit in this graph is the concentration predicted for a given scenario, divided by the concentration predicted for the base case. Thus a value of 2.0 would mean the scenario had a predicted concentration twice as high as the base case. The base flow results represent simulations with estimates of current flow conditions based on measured

flows from the S10 control structure from 1995 to 1999. Results are also shown for scenarios identical to the base cases, but with flowrates reduced by 50%. The results are representative of near-steady state conditions after 20 years of simulation at a given phosphorus level. The remaining figures for management scenarios are presented in the same manner.

Figure 6-9 and Figure 6-10 suggest that surface and porewater concentrations of Hg(II) are predicted to drop at F1 as phosphorus levels increase, but there is a slight decline for predicted Hg(II) in surface waters at the lowest phosphorus level (10 μg L^{-1}), and a peak at a phosphorus concentration of 20 μg L^{-1}. Under base flow conditions, the range of phosphorus levels simulated resulted in approximately a 40 – 50% change in predicted surface and porewater Hg(II) concentrations.

Similar to the effects of phosphorus on predicted Hg(II) concentrations, MeHg concentrations in surface waters and largemouth bass at F1 also showed a predicted peak in the range of 20-30 μg L^{-1} (Figure 6-11 and Figure 6-12) All scenarios resulted in higher predicted MeHg concentrations at F1 with respect to current conditions. The largest increase under base flow conditions was on the order of a 75% increase in surface waters and a roughly 2-fold increase in largemouth bass. Note that largemouth bass don't exist at F1 currently due to poor habitat. Thus the F1 results for largemouth bass are strictly hypothetical, both for the management scenarios and estimates of what the concentrations might currently be if largemouth bass actually resided at F1.

Reduced flows were predicted to result in higher Hg(II) and MeHg concentrations at F1. In fact, reduced flows always resulted in higher Hg(II) and MeHg concentrations for all scenarios run for F1 or U3.

6.5.2 U3 Management Scenario Results

Figure 6-13 and Figure 6-14 suggest a slight trend towards lower surface water Hg(II) concentrations at U3 as phosphorus levels increase from 4 to 10 μg L^{-1}, although the magnitude of the predicted change was minor under base flow conditions, on the order of 10-20%. This would be very difficult to ascertain from field data given natural variability. Note that there are several points presented on these graphs for base flow conditions and a phosphorus concentration of 10 μg L^{-1}. This is because U3 results depend on conditions assumed upstream, and several simulations were run with different phosphorus levels assigned to F1 (10, 20, 30, 50, 75, 120 μg L^{-1}), while a concentration of 10 μg L^{-1} was held constant at U3. The effect was that higher phosphorus levels at F1 generally caused lower surface and porewater Hg(II) concentrations at that site, and contributed to lower concentrations at U3 as well, although the effect was not large (e.g., less than 10% change in predicted surface and porewater Hg(II) concentrations at U3 due to varying phosphorus at F1 from 10 to 120 μg L^{-1}).

In contrast to the predicted effects of TP on Hg(II) concentrations at U3, methylmercury concentrations in surface waters and fish were predicted to increase slightly as a function of phosphorus levels at U3 ranging from 4 to 10 μg L^{-1} (Figure 6-15 and Figure 6-16). The effects of different phosphorus levels at F1 cascading to U3 did not substantially affect predicted MeHg levels at U3 (<10%).

Figure 6-17 and Figure 6-18 show the predicted gross methylation rates at F1 and U3 for the management scenarios. At F1, simulations with total phosphorus at or above 120 μg L^{-1} had water column methylation, while runs with total phosphorus less than 120 μg L^{-1} had methylation

occurring in sediments. The predicted trends for gross methylation at these sites were similar to the trends for predicted methylmercury concentrations in fish.

Management scenario simulations indicated that the predicted relationships between fish mercury and total phosphorus levels were affected by the assumed relationship between total phosphorus and particle fluxes, particularly peat accretion. As a demonstration of this sensitivity, Figure 6-19 and Figure 6-20 show predicted effects of management scenarios on age 3-4 largemouth bass at F1 and U3 respectively, but for two different calibrations of particle budgets. In each figure, results are shown for (1) the base case particle budget, where peat accretion rates increase as phosphorus levels increase, and (2) the alternative particle budget shown in Figure 6-6, where peat accretion rates peaked in the range of 50 $\mu g\ L^{-1}$, decreasing at higher or lower TP concentrations. It is clear from these figures that very different results can emerge depending on the assumptions made relating to the effects of phosphorus on particle budgets.

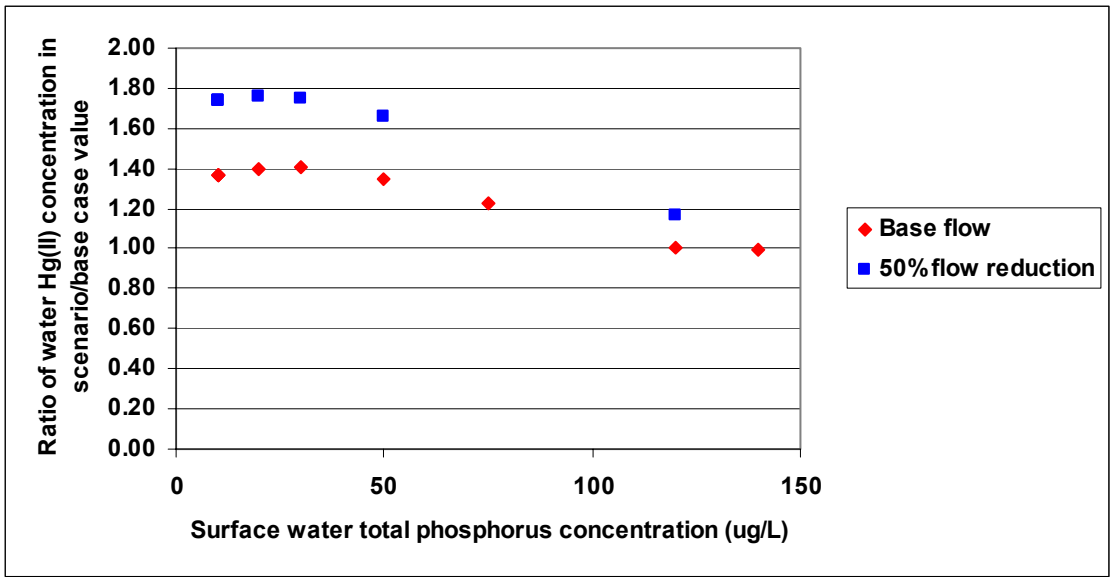

Figure 6-9. Predicted effects of management scenarios on surface water Hg(II) concentrations at F1.

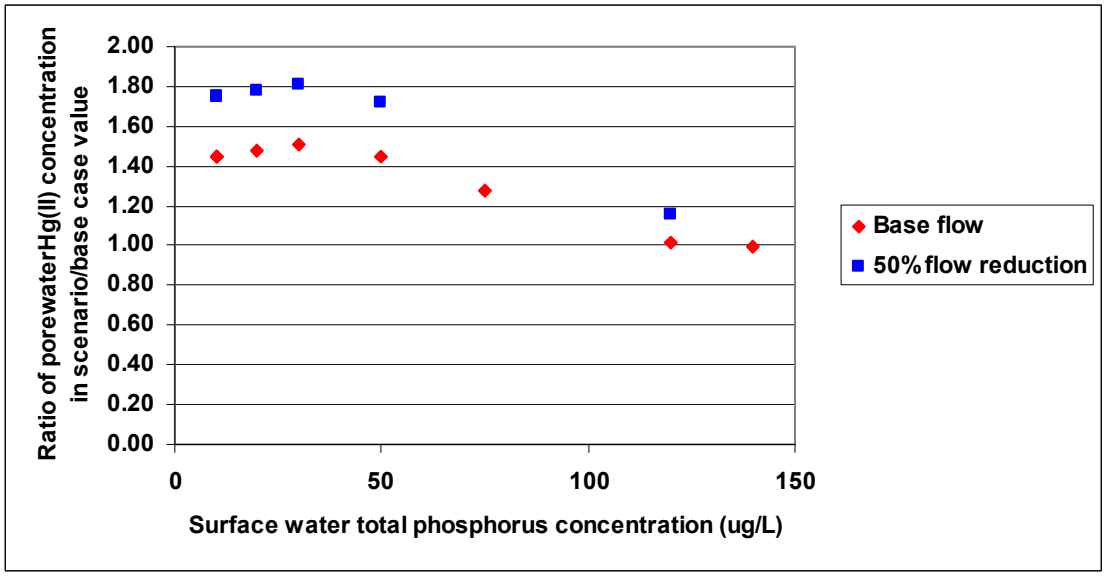

Figure 6-10. Predicted relationship between porewater Hg(II) concentrations and total phosphorus in surface waters at F1.

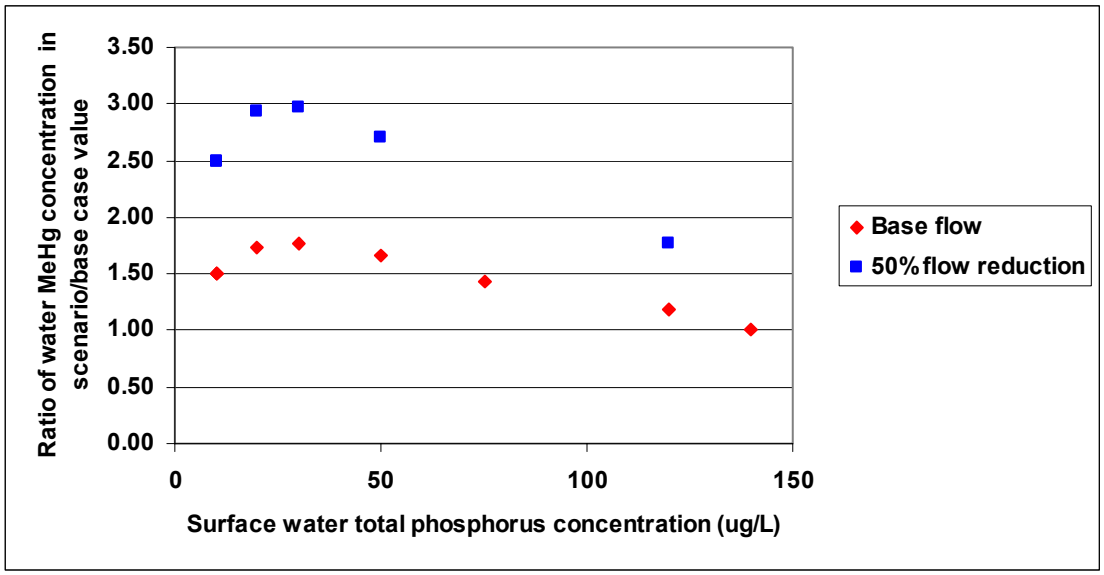

Figure 6-11. Predicted effects of total phosphorus concentrations on surface water methylmercury concentrations at F1.

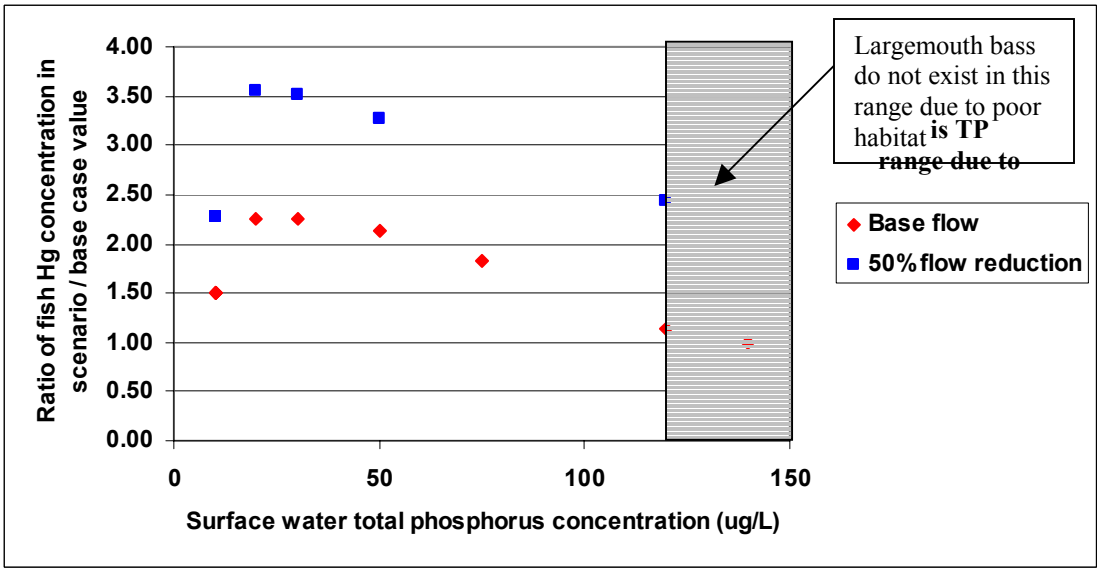

Figure 6-12. Predicted effects of surface water total phosphorus concentrations on largemouth bass Hg concentrations at F1

(Note: Due to poor habitat, largemouth bass are currently not present at F1. Thus these results are essentially hypothetical comparisons between a modeled "current" level of Hg that might exist in largemouth bass at F1, versus the effects of various nutrient and flow regimes.)

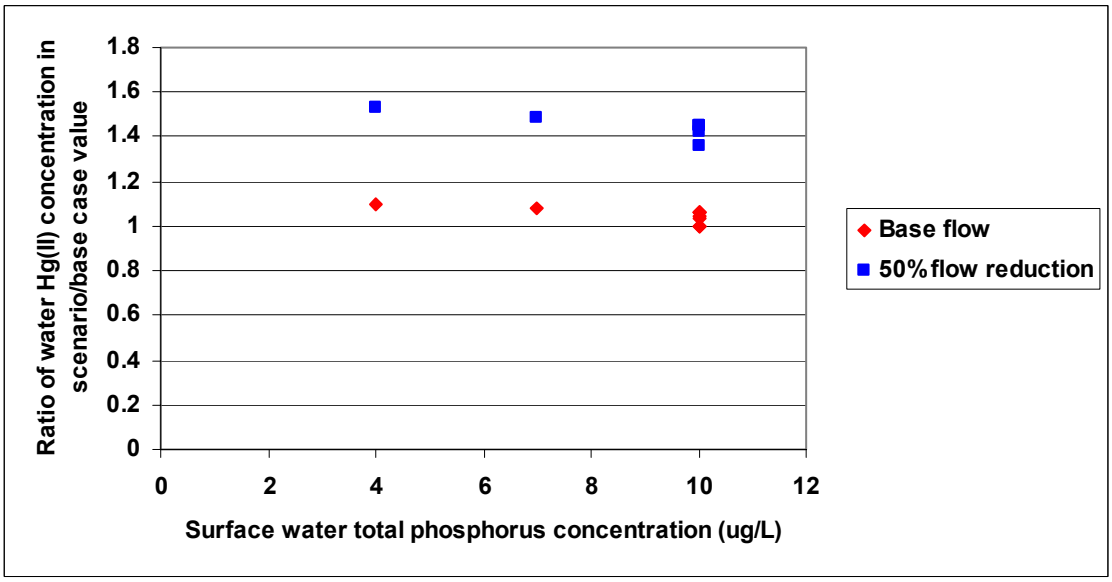

Figure 6-13. Predicted effects of management scenarios on surface water Hg(II) concentrations at U3

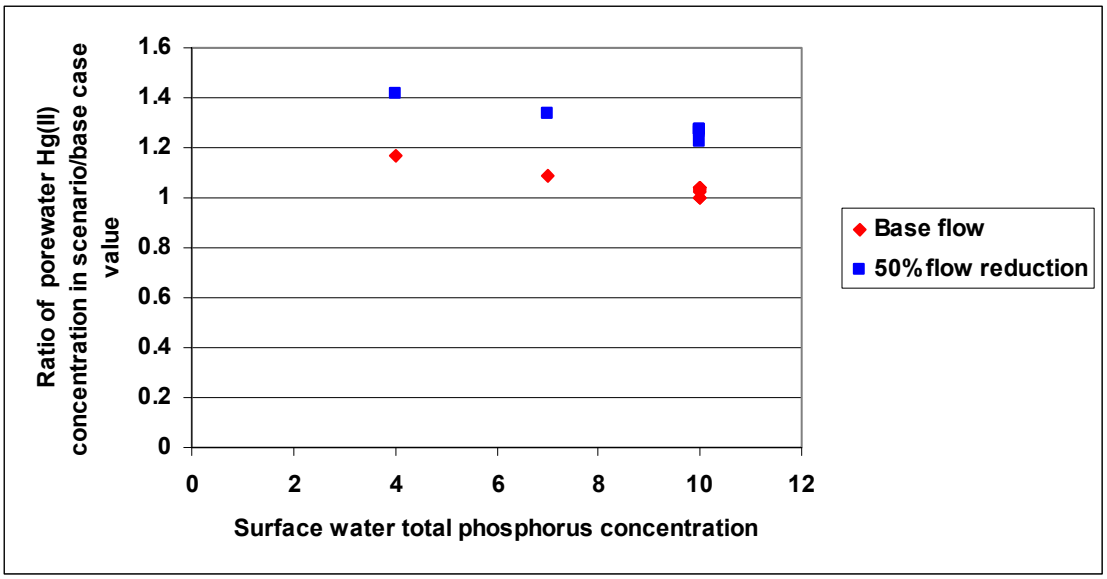

Figure 6-14. Predicted relationship between porewater Hg(II) concentration and surface water total phosphorus concentration at U3.

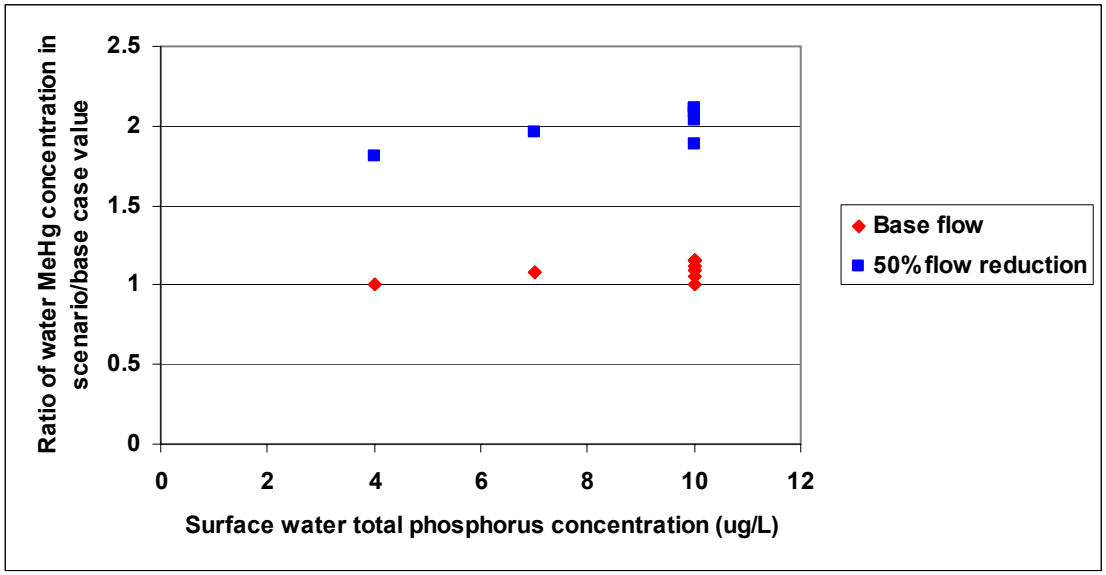

Figure 6-15. Predicted effects of surface water concentrations of total phosphorus on predicted concentrations of methylmercury in surface waters (ng/L unfiltered) at U3.

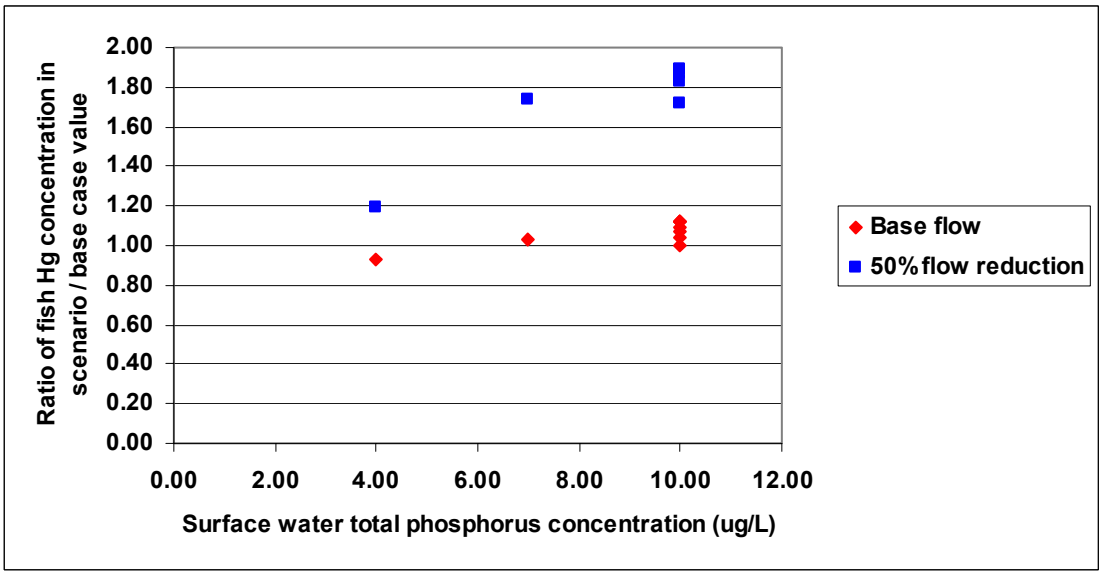

Figure 6-16. Predicted effects of total phosphorus concentrations in surface waters on mercury concentrations in largemouth bass at U3.

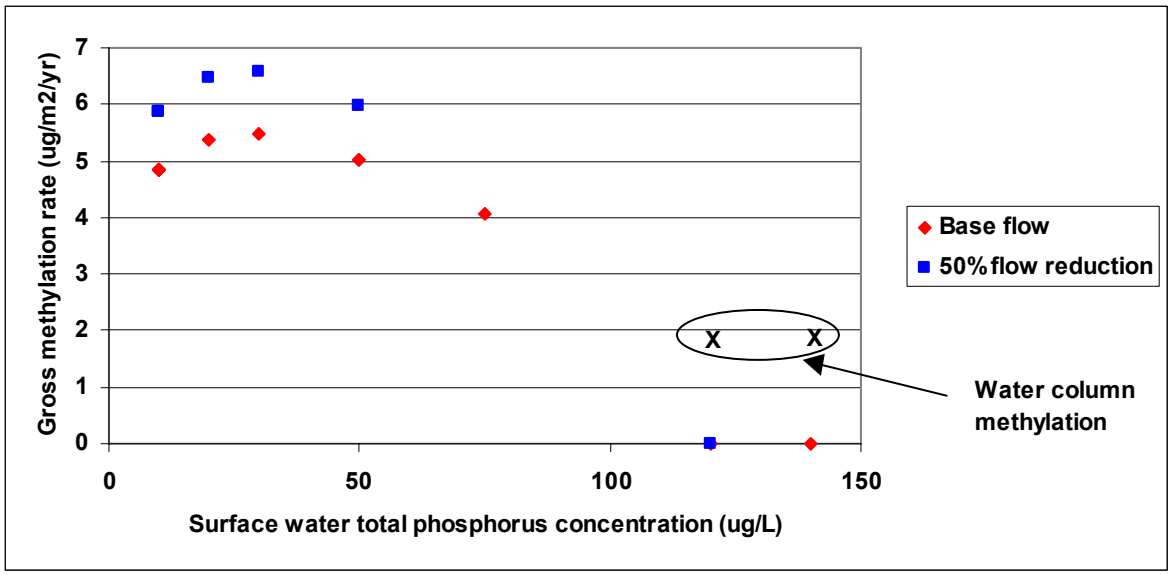

Figure 6-17. Predicted rates of gross methylation in sediments vs surface water total phosphorus concentrations at F1.

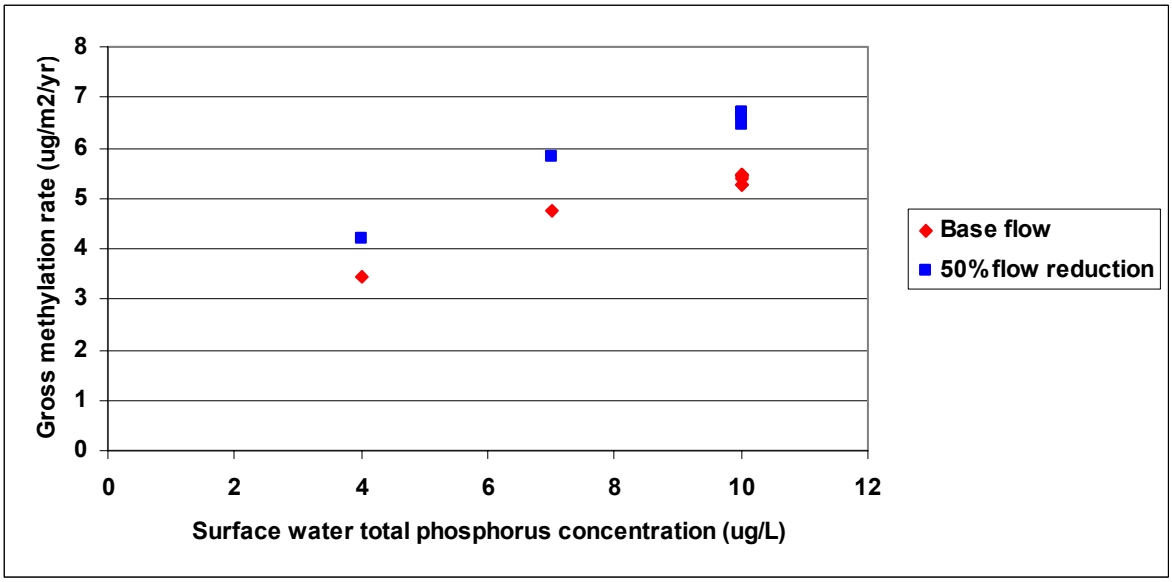

Figure 6-18. Predicted gross methylation rates in sediments vs surface water total phosphorus concentrations at U3.

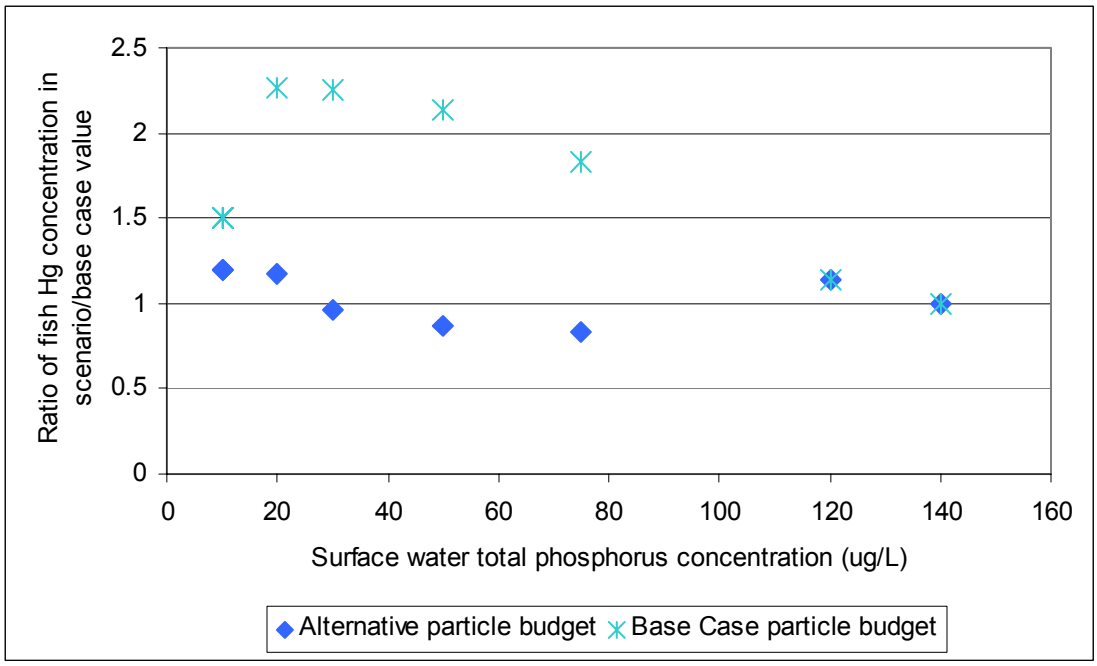

Figure 6-19. Comparison of effects of management scenarios on predicted Hg levels in age 3-4 largemouth bass at F1 for two different particle budgets.

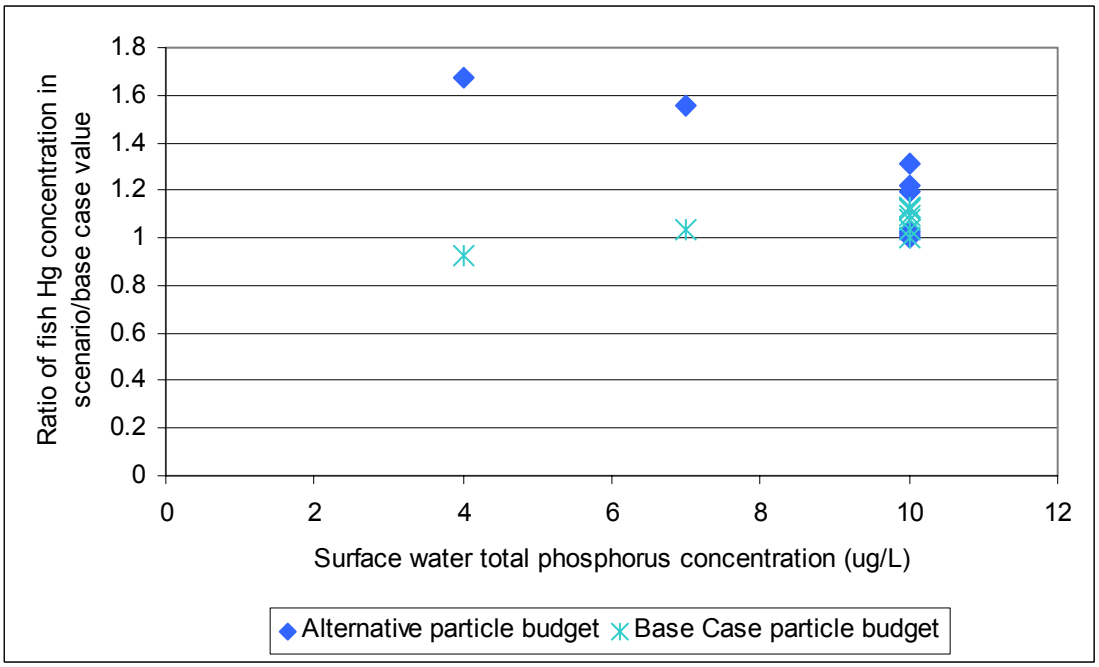

Figure 6-20. Comparison of effects of management scenarios on predicted Hg levels in age 3-4 largemouth bass at U3, for two different particle budgets.

6.6 Discussion of Management Scenario Simulations

Appropriate use of management scenario results

For reasons summarized below, **we interpret the management scenarios simulations in this report to represent some initial insights rather than any definitive answers.** It is critical in the authors view that this be recognized when reading the results of the management scenario simulations. Factors contributing to this opinion include:

- Significant scientific uncertainties remain regarding factors governing mercury cycling in aquatic systems (e.g., interactions with sulfur cycling). The predictive capability of the model is constrained by these gaps.
- The model simulations were sensitive to assumed changes in the particle budgets as a function of water column phosphorus concentrations, but the field information available on peat accretion rates, decomposition rates, and supply of litter was not robust.
- When examining the effects of system productivity on fish mercury concentrations, the relative importance of particle budgets versus other local factors influenced by system productivity remains to be fully determined.
- All management scenarios tested involved changes to total phosphorus levels in the system. A simplified approach had to be devised to determine which inputs to alter in response to a change in phosphorus levels, and what the new values should be. Relationships between phosphorus and particle budgets, and phosphorus and methylation rate constants were developed in the absence of either well-established field relationships or a soft-link to a calibrated and verified nutrient dynamics model. These relationships have considerable uncertainty
- The effects on Hg cycling of wetting/drying cycles associated with changing water levels is an ongoing important area of research. E-MCM does not yet mechanistically handle the effects of wet/dry cycles on methylation rates.

Examination of results of the management scenarios

Overall, the WCA-2A management scenarios in Phase III resulted in fish mercury concentrations varying by about 2-3 fold or less due to changes in nutrient levels, increasing to 3-4 fold or less when flow reductions were added. Some unexpected trends emerged, however, from the Phase III management scenarios. In particular, the prediction that MeHg levels in water and fish at F1 would peak with a total phosphorus concentration on the order of 20-30 $\mu g\ L^{-1}$ was not expected and may be an artifact of the assumptions that were required to conduct the analysis. Nor was the prediction expected that decreasing total phosphorus concentrations from 10 to 4 $\mu g\ L^{-1}$ at U3 would result in decreasing concentrations of Hg in largemouth bass (the opposite trend was expected). Furthermore, the dependency of these trends on the relationships assumed between phosphorus and particle budgets was significant, a less than optimal situation since the particle budgets themselves, and effects of phosphorus on them, are quite uncertain. Finally, in some situations involving very low dissolved oxygen concentrations (e.g. $\sim 2\ mg\ L^{-1}$) combined with significant methylmercury concentrations in surface waters, gill uptake appeared to be a modest but significant source of MeHg to the fish. This was unexpected since previous model simulations in lake environments with the related D-MCM model for lakes consistently predicted

gill uptake to be a secondary source of methylmercury to fish (e.g. usually less than 5 % of the overall exposure). This E-MCM result needs further exploration.

Our interpretation of the predicted peak fish Hg levels at F1 with total phosphorus concentrations in the range of 30 $\mu g\ L^{-1}$ is as follows: Methylation in E-MCM is dependent on three conditions: (1) the rate of decomposition, (2) the concentration of Hg(II) available to methylate, and (3) a rate constant. The estimated methylation rate constant is declining as TP increases in the range of 30 $\mu g\ L^{-1}$ (Figure 6-8). This would be expected to decrease methylation rates as TP increases. Working against this trend were the other two factors affecting methylation. Assumptions about the particle budgets resulted in decomposition rates increasing significantly in the range of TP = 30 $\mu g\ L^{-1}$ (Figure 6-4) and dissolved surface or porewater Hg(II) concentrations (the pools methylated) also were predicted to increase slightly as TP increased toward 30 $\mu g\ L^{-1}$ at F1 (Figure 6-10). The latter result was in itself unexpected, and was again influenced by assumptions regarding the particle budget. As decomposition rates increase in any given compartment, particulate matter is lost. Hg associated with these decomposing particles is simply released into the compartment in the model, increasing concentrations. Thus the overall combination of the rates of change of methylation rate constants, decomposition and porewater Hg(II) was predicted to generate a peak methylation rate in the vicinity of 30 $\mu g\ L^{-1}$ of total phosphorus at F1, declining at higher or lower levels.

It is critical to note that the trends between system productivity and fish mercury concentrations predicted by E-MCM in this report are tentative. Such model predictions are currently sensitive to the effects of system productivity on decomposition and sedimentation. These relationships are themselves not well documented however, resulting in uncertainty about the predicted effects of system productivity on fish mercury concentrations. Modeled methylation rates are directly linked to carbon turnover in the interfacial sediment layer. The quantititative relationship between productivity and decomposition/carbon turnover is not well established. Consequently, the predicted effects of system productivity on methylation rates and ultimately on fish mercury concentrations should be considered as provisional. Furthermore, it is quite possible that system productivity could affect the methylmercury levels in ways that have not been considered in the current implementation of E-MCM. Specifically, an important consideration in the model is the concentration of Hg(II) available to methylate. In the scenarios in this report, all dissolved Hg(II) was assigned as available to methylate. Particle budgets were assumed to affect this overall dissolved Hg(II) concentration in management scenarios, thus affecting methylation rates and methylmercury concentrations at the modeled site. It is quite possible however, that only a portion of the dissolved Hg(II) pool is available to methylate, and this pool could be strongly impacted by water chemistry (e.g. sulfide levels), as suggested by C. Gilmour and others. It is likely that system productivity directly affects water chemistry and bioavailable Hg(II) concentrations, but this is not fully represented in the model yet due to a lack of scientific knowledge about bioavailable Hg(II) for methylation, and difficulties implementing mercury complexation by sulfides in the model to date.

It is important to note that, simply because predicted methylation rates peaked at a phosphorus concentration of 30 $\mu g\ L^{-1}$, this ambient phosphorus concentration does not necessarily translate into higher MeHg concentrations in the Everglades. The effects of site conditions on the ability of the marsh to eliminate MeHg via burial, demethylation, etc. also need to be considered. For the range of peat accretion rates considered for WCA-2A (approximately 2 to 7.5 mm bulk sediment per year at a depth of 4 cm), burial was important as a loss mechanism for Hg(II), but was not as important for methylmercury removal. Thus the particular combination of site

conditions applied in these management scenarios led to MeHg concentrations being closely related to MeHg production. This is not necessarily true at all sites.

At U3, our interpretation of the results of the management scenarios is as follows. For total phosphorus concentrations ranging from 4 to 10 μg L^{-1} lower concentrations of Hg(II) were predicted as system productivity increased (Figure 6-13 and Figure 6-14). This was consistent with *a priori* notions. The reason that methylation rates and concentrations *increased* as TP increased from 4 to 10 μg L^{-1} (Figure 6-18, Figure 6-16) was related to the factors affecting the model trends at F1. Predicted decomposition rates were increasing fast enough as TP increased from 4 to 10 μg L^{-1} (Figure 6-4) to overwhelm the effects of predicted decreasing porewater Hg(II) concentrations Figure 6-14). With different assumptions and calibrations for particle budgets, very different trends could emerge at both F1 and U3 (Figure 6-19, Figure 6-20).

In all scenarios modeled, reduced flows led to higher predicted Hg(II) and MeHg concentrations at the sites. This was because the cells modeled in WCA-2A were predicted to be net sources of Hg(II) and MeHg through atmospheric deposition and *in situ* methylation respectively as water passed through them. In other words, the predicted amount of Hg(II) or MeHg added (or produced internally as is the case for MeHg) to a cell as water passes through is greater than the amount being removed by processes such as burial or reactions converting the Hg species to another form. In this type of situation, the longer the water resides in a cell (i.e. lower flows), the more time there is for *net* loading of Hg into the cell to increase. *Note that these simulations do not consider the effects of reduced flows on exposed sediments and dry/wet cycles.* These effects may well be important in their own right, as being investigated by researchers such as D. Krabbenhoft and L. Fink (Krabbenhoft *et al.* 2000).

7 Future Directions

During this study, the development of E-MCM progressed significantly. This progress reflects both advances in the state of Hg science, as well as fundamental enhancements in model features such as including Monte Carlo capabilities that improve our ability to approach and resolve management questions. Despite the improvements in our understanding of Hg cycling yielded by continued field research, there still remain a number of scientific gaps regarding the behavior of mercury (e.g., factors governing methylation and Hg partitioning). Because of some of these gaps in understanding, as well as field data constraints, E-MCM cannot yet be considered as predictively robust. E-MCM simulations suggest that additional knowledge/field information also is needed regarding particle and carbon cycling to better constrain model predictions for mercury. Furthermore, other mercury research in the Everglades (e.g., the research program undertaken by ACME researchers) is highlighting the need to better understand the effects of hydrology, particularly dry/wet cycles on mercury cycling in the Everglades, and the role of new versus. historical or legacy Hg in governing biotic cycling.

Extensive efforts have been made to extend the structure of E-MCM to better accommodate conditions affecting Hg cycling in the Everglades. The model now can handle cells linked in series, which is important when considering gradients across a region such as WCA-2A, and helps in an environment where discrete boundaries between "cells" do not exist. A sulfur module has been added, as well as a Monte Carlo capability and the option to use a bottom-up food web approach. With these model features in place, it is recommended that attention again be directed to an integrated modeling and field effort that investigates processes and how to best represent them in a model that should ultimately be able to make predictions with confidence
To move E-MCM towards a more predictive capability, the following future directions are recommended:

- Basic interpretation of changes in Hg cycling across the Everglades has been confounded by changes in multiple site conditions. Resolving the dose-response relationship between Hg cycling and variables such as Hg loading, DOC, sulfate, and phosphorus demands controlled experimentation. The mesocosm work currently conducted by D. Krabbenhoft, C. Gilmour *et al*. that focuses on the effect of changes of individual parameters on Hg cycling is extremely valuable, and its continuation is critically needed. Applying E-MCM at the spatial and temporal scale of the mesocosm experiments would undoubtedly benefit the representation of various processes in the model and should lead to a more robust model.

- Conduct a series of model simulations targeting specific trophic-related effects on fish mercury concentrations, including trophic structure effects on particle fluxes, water chemistry, methylation rates, fish diets and fish growth rates. Work in this area is currently being supported by FDEP, and includes updating the representation of trophic state dynamics in E-MCM.

- E-MCM model application to a given site currently involves manually tuning a number of model coefficients to yield a proper calibration. Ideally, the calibration of the model would be sufficiently robust so that application of the model to different sites would require only changing the boundary and site conditions, while model coefficients would not need to be readjusted. Model testing also should be done with simulations spanning a wide range of Everglades conditions, but using the same model calibration for Hg reaction and partitioning constants. Different representations of Hg reactions and

partitioning also could be tested to see if some provide better results than others across a range of conditions. Prior to this exercise however, the following steps are needed:

  - Update the existing datasets for site conditions (e.g. DOC gradients in surface and porewaters, trophic structure, fish diets and growth rates) and mercury concentrations.
  - Update and reactivate sulfide mercury complexation. This will likely require a modification of Hg parititioning on solid phases as well.
  - Review and perhaps modify how E-MCM handles mercury complexation by DOC, particularly in view of recent studies by G. Aiken that indicate that the nature of DOC (with respect to Hg-binding) changes across the Everglades.
  - Consider modeling other sites downstream of 3A-15, either as a linked model or as a unit wetland, where site conditions are comparably oligotrophic, but fish mercury concentrations are lower than at WCA 3A-15. This type of modeling exercise would seek to resolve the hydrological and biogeochemical forcing functions that would account for the spatial heterogeneity in Hg cycling and fish Hg concentrations in WCA-3A.

- Results emerging from the mesocosm studies conducted by the ACME team strongly indicate that the system responds extremely rapidly to additions of new mercury. If substantiated by continued experimentaton, these results indicate that how E-MCM represents the availability of pools of reactive or labile Hg for methylation will need to be revised. As a resultkey factors affecting the response dynamics in E-MCM should be critically examined, including:

  - Examine the effects of the assumed thickness of actively exchanging sediment layers;
  - Examine effects of slow vs fast exchanging Hg(II) on particles;
  - Model the diel Hg cycle in Everglades marshes further, including possible effects of daily vertical migration of zoobenthos;
  - Consider the need for creating distinct pools of new and old Hg in the model, as well as the transition between the two.

- Better field information is needed on particle and carbon budgets and how they change across nutrient gradients in the Everglades. Until the particle dynamics (e.g. sedimentation rates and decomposition) are better understood and *constrained*, calibrations of E-MCM will be *underconstrained*.

- Test the sulfur module component of the model across the Everglades. In addition, link organic S fluxes to primary production rates so that the effect of changing sulfate and phosphorus loads on the S and Hg cycles can be independently evaluated.

- Test the bottom-up food web component of the model.

- Improve the understanding of factors governing methylmercury production and accumulation in the lower food web.

- Add an E-MCM module that calculates and maintains a water mass balance. Currently, E-MCM requires that the user maintain and input an external hydrologic mass balance and, if the user is not careful, independent hydrologic inputs can generate artifacts in

results which might not occur if an internal hydrologic balance was maintained. For example, sudden spikes in concentration can occur due to implied evaporation via changing water levels).

- Continue efforts to explore novel approaches towards an analysis of the aggregated effects of multiple paramenter uncertainty. Although Monte Carlo methods are extremely useful for analyzing the effects of parameter estimation error on overall model uncertainty, Monte Carlo simulations can be misleading when interparameter dependencies are not properly considered. Alternative approaches include continued development of dependencies between inputs, and the tree-structured density parameter estimation (TSDE) technique of Grieb et al. (1999). This latter approach extends the ability of Monte Carlo-based analyses to explore parameter interactions and uncertainty in complex environmental models. Both types of approaches should be discussed and compared.

- Incorporate mechanisms in the model to accommodate the effects of wet/dry cycles for sediments that are periodically exposed.

- A continuing series of workshops is recommended between the E-MCM model team and several key Everglades mercury researchers, to exchange ideas and recent results so necessary to the advancement of the model. Ideally, access to either the model or the E-MCM modelling team should be formalized so that researchers can more readily use E-MCM for hypothesis testing and help guide continued research.

- Use E-MCM in conjunction with ongoing field studies to examine why such high methyl mercury concentrations are being produced in STA-2. Methyl Hg concentrations exported from Cell 1 are among the highest ever reported using reliable techniques, and the processes and antecedent conditions that are responsible need to be better understood as CERP moves forward, and other STAs' and water storage reservoirs are constructed and brought into use.

Ultimately, decision makers will want a model that can make reasonable predictions, given a reasonable level of input data. E-MCM is currently quite complex, partly because the "short list" of factors affecting Hg cycling and bioaccumulation is not yet clear. It is the hope of the E-MCM model development team that eventually E-MCM can be significantly simplified as the state of knowledge improves – still obtaining good model predictions by considering the most important factors affecting Hg cycling, yet ignoring less critical factors.

8 Conclusions

During this study, development of E-MCM progressed significantly. The structure of E-MCM has been enhanced so the model now can handle cells linked in series. A sulfur module has been added, as well as a Monte Carlo capability and the option to use a bottom-up food web approach.

It has been possible to calibrate E-MCM to a range of Everglades marsh conditions, ranging from eutrophic to oligotrophic. These model calibrations have been instructive, but have been tuned on a site-by-site basis. There is a need to move towards a single model calibration that performs reasonably over a range of Everglades conditions. A better mechanistic understanding of some processes and governing factors is needed to achieve this goal. This includes an improved understanding of methylation, demethylation, MeHg dynamics in the lower food web and mercury partitioning between solids and dissolved phases. Model assumptions about sediment compartment depths significantly affect the response dynamics in model simulations and should also be examined.

Due to the current limitations to the predictive strength of E-MCM, the results of the management scenarios simulated in this study must be considered as possible, rather than probable outcomes due to management actions. It is expected however that continued advances by mercury researchers in the Everglades will indeed lead to a stronger predictive capability for the model.

Acknowledgments

The authors of this report wish to thank the following people for their insights, efforts and support: Tom Atkeson and Don Axelrad of the Florida Department of Environmental Protection; Larry Fink and Pete Rawlik of the South Florida Water Management District, Ted Lange of the Florida Fish and Wildlife Conservation Commission; and the entire ACME research team, including Dave Krabbenhoft, Cynthia Gilmour, Jim Hurley and Lisa Cleckner.

9 References

Ambrose, R.B. Jr., K.J. Shell and I.Tsiros (1997) South Florida Mercury Screening Study Part 1 – Mercury in Everglades Marsh. US EPA Office of Research and Development, National Exposure Research Laboratory, Ecosystems Protection Division, Athens, GA. January 1997.

Bates, A.L., W.H. Orem, J.W. Harvey, and E.C. Spiker. In review. Sulfate contamination in the Florida Everglades: Sources and relation to methyl mercury production. Nature

Benoit, J.M., C.C. Gilmour, and R.P. Mason (2001) Aspects of bioavailability of mercury for methylation in pure cultures of *Desulfobulbus propionicus* (1pr3). Appl. Environ. Microbiol. 67: 51-58.

Benoit, J.M., C.C. Gilmour, R.P. Mason and A. Heyes (1999a). Sulfide controls on mercury speciation and bioavailability to methylating bacteria in sediment pore waters. *Envir. Sci. Technol*., 33(6):951-957.

Benoit, J.M., R.P. Mason and C.C. Gilmour (1999b) Estimation of mercury-sulfide speciation in sediment pore waters using octanol-water partitioning and its implications for availability to methylating bacteria. *J. Env. Toxicol. Chem*., 8(10):2138-2141.

Branfireun, B.A., N.T. Roulet, C.A. Kelly, and J.M.W. Rudd (1999) Global Biogeochem. Cycles 13: 743-750.

Cleckner, L.B., P.J. Garrison, J.P. Hurley, M.L. Olson and D.P. Krabbenhoft (1998) Trophic transfer of methyl mercury in the northern Florida Everglades. Biogeochemistry 40(2/3): 347-361.

Cook, R.B. and C.A. Kelly (1992) Sulphur cycling and fluxes in dimictic lakes, pp.145 – 188. *In* R.W. Howarth, J.W.B. Stewart and M.V. Ivanov [eds.], SCOPE 48: Sulphur cycling on the continents. J. Wiley and Sons, Chichester.

Christian R., Luczkovich J. (1999) Organizing and understanding a winter's seagrass foodweb network through effective trophic levels. Ecological Modelling, 117.

Delfino, J.J, T.L. Crisman, J.F. Gottgens, B.E. Rood, and C.D.A. Earle (1993) Spatial and temporal distribution of mercury in Everglades and Okefenokee wetland sediments. Final Project Report, April 1, 1991 – June 30, 1993. Volume I. Submitted to Florida Department of Environmental Protection, Tallahassee, FL. Department of Environmental Engineering Sciences, University of Florida, Gainesville, FL.

Delfino, J.J, B.E. Rood, J.M. Andes, and C.D.A. Earle (1994) Mercury spatial heterogeneity in Everglades soil cores and a comparison of mercury accumulation in wetlands and associated lakes. Final Project Report. Submitted to Florida Depatrment of Environmental Protection, Tallahassee, FL. Department of Environmental Engineering Sciences, University of Florida, Gainesville, FL.

FDEP (2002) Integrating Atmospheric Mercury Deposition and Aquatic Cycling in the Florida Everglades: An approach for conducting a Total Maximum Daily Load analysis for an atmospherically derived pollutant. Florida Department of Environmental Protection. October, 2002

Fink L. (2002a) Spreadsheet Biomass Production Model.001.xls.

Fink L. (2002b) Spreadsheet "New STA-2 Hg Budgets.xls

Fink L. (2002c) Spreadsheet "STA-2 Data Mass Budget All.001.xls"

Fink L. (2002d) Spreadsheet "STA-2 Mosquitofish Data Analysis Short.xls"

Fink L. (2002e) Spreadsheet "STA-2 Cell 1 Mass Budget All.0011.xls"

Fink, L.E. (2001) The effect of surface and pore water quality on mercury bioaccumulation. Appendix 7-11 in *2001 Everglades Consolidated Report*. South Florida Water Management District, West Palm Beach, FL. January.

Fink, L.E. and P. Rawlik (2000) Chapter 7: The Everglades Mercury Problem, in *2000 Everglades Consolidated Report*, The South Florida Water Management District, West Palm Beach, FL. January.

Fink, L.E. (2000a) ENR Project Mercury Studies: 1994-1999. Appendix 7-5 in *2000 Everglades Consolidated Report*. South Florida Water Management District, West Palm Beach, FL. January.

Fink (2000b) Spreadsheet "S6Rain.xls" received May 4, 2000

Fitz , H.C., E.B. DeBellevue, R. Costanza, R. Boumans, T. Maxwell, L. Wainger, and F.H. Sklar (1996) Development of a general ecosystem model for a range of scales and ecosystems. Ecological Modelling 88: 263-295.

Florida Fish and Wildlife Conservation Commission (2000) Spreadsheet "Raw Data ENR all Sites.xls" dated May 24, 2000, with ENR data (except mosquitofish) on fish size, age and Hg from T. Lange.

Gherini, S.A., L. Mok, R.J.M. Hudson, G.F. Davis, C.W. Chen, and R.A. Goldstein (1985) The ILWAS model: Formulation and application. Water Air Soil Poll. 26: 425-459.

Gilmour, C., A. Heyes, J. Benoit, G. Reidel, and J.T. Bell (1998a) Distribution and Biogeochemical Control of Mercury Methylation in the Florida Everglades, SFWMD contract #C-7690

Gilmour, C.C., G.S. Riedel, M.C. Ederington, J.T. Bell, J.M. Benoit, G.A. Gill, and M.C. Stordal. (1998b) Methylmercury concentrations and production rates across a trophic gradient in the northern Everglades. Biogeochemistry 40(2/3): 327-345.

Gilmour, C.C. and G.S. Riedel (1995) Measurement of Hg Methylation in Sediments Using High Specific-Acitivity ^{203}Hg and Ambient Incubations. Water Air Soil Poll. 80: 747-756.

Gilmour, C.C., E.A. Henry, and R. Mitchell (1991) Env. Sci. Technol. 26: 2281-2287.

Gill, G.A., W.M. Landing, and C.D. Pollman (1999) Florida Atmospheric Mercury Study (FAMS). Data Dictionary, Version 2.0. Submitted by Florida State University, Department of Oceanography to Florida Department of Environmental Protection, Tallahassee, FL and Electric Power Research Institute, Palo Alto, CA.

Grieb, T.M., R.J.M. Hudson, R.C. Spear, S.A. Gherini, and R.A. Goldstein (1999) Examination of model uncertainty and parameter interaction in a global carbon cycling model (GLOCO). Environment Internat. 25: 787-803.

Guentzel, J.L., W.M. Landing, G.A. Gill, and C.D. Pollman (2001) Processes influencing rainfall deposition of mercury in Florida. Environ. Sci. Technol. 2001: 863-873.

Guentzel, J.L., W.M. Landing, G.A. Gill, and C.D. Pollman (1995) Atmospheric deposition of mercury in Florida: The FAMS project (1992-1994). Water, Air, and Soil Pollution. 80: 393-402.

Harris, R.C. and W.J. Snodgrass (1993) Bioenergetics Simulations of Mercury Uptake and Retention in Walleye (*Stizostedion vitreum*) and Yellow Perch (*Perca flavescens*). Water Poll. Res. J. Canada. 28(1): 217-236

Hewett and Johnson (1992) Fish Bioenergetics Model 2. Published by the University of Wisconsin Sea Grant Institute (WIS-SG-91-250)

Hudson, R.J.M., S.A. Gherini, C.J. Watras, and D.B. Porcella (1994). Modeling the Biogeochemical Cycle of Mercury in Lakes: The Mercury Cycling Model (MCM) and its Application to the MTL Study Lakes. In " Mercury Pollution Integration and Synthesis ". Watras C.J. and J.W. Huckabee (Eds.). Lewis Publishers. p473-523.

Hurley, J.P., L.B. Cleckner and P. Gorski (1999) *Everglades Nutrient Removal Project Mosquitofish Bioaccumulation Study*. Draft Report. Prepared for the South Florida Water Management District, West Palm Beach, FL. Contract (PC C-8691-0300). University of Wisconsin Water Chemistry Program, Madison. May.

Hurley, J.P., D.P. Krabbenhoft, L.B. Cleckner, M.L. Olson, G.R. Aiken and P.S. Rawlik Jr.. (1998) System controls on the aqueous distribution of mercury in the northern Florida Everglades. Biogeochemistry 40(2/3): 293-310.

HydroQual, Inc. (1997) SFWMD Wetlands Model: Calibration of the Coupled Periphyton/Vegetation Model to WCA-2A. October 21, 1997

Jorgensen, S, Nielson (1991) Handbook of Ecological Parameters and Ecotoxicology. Elsevier Press.

Keeler, G.J., F. J. Marsik, K.I. Al-Wali and J. T. Dvonch (2000) Project Final Technical Report - Modeled Deposition of Speciated Mercury to the SFWMD Water Conservation Area 3A: 22 June 1995 to 21 June 1996. Project Description and Results. The University Of Michigan Air Quality Laboratory. Ann Arbor, Michigan 48109

Knuth D. (1990) The Art of Computer Programming vol. 2, sec 3.2.2

Krabbenhoft, D.P., L.E. Fink, M.L. Olson and P.S. Rawlik (2000) *The effect of drydown and natural fires on mercury methylation in the Florida Everglades*. Conf. proc., International Conference on Heavy Metals in the Environment. University of Michigan, Ann Arbor. August.

Krabbenhoft D.P., J.P Hurley, ML. Olson & L.B. Cleckner (1998) Diel variability of mercury phase and species distributions in the Florida Everglades. Biogeochemistry 40: 311-325.

Lange, T. (2001) "Task Through 2000.xls", April 17, 2001

Lange, T. (2000) "Temp Food.DOC" sent to R. Harris October 30, 2000.

Lange, T.R., D.A. Richard and H.E. Royals (1998) Trophic Relationships of Mercury Bioaccumulation in Fish From the Florida Everglades. Annual Report. August 1998. Prepared for the Florida Department of Environmental Protection. Tom Atkeson, PhD, Project Officer. Prepared by Florida Game and Fresh Water Fish Commission, Fisheries Research Laboratory, Eustis

Lindberg, S.E., W. Dong and T. Meyers (2002) Transpiration of gaseous elemental mercury through vegetation in a subtropical wetland in Florida. *Atmos. Environ*. 36:5207-5219.

Lindberg, S.E. and H. Zhang (2000) Air/water exchange of mercury in the Everglades II: measuring and modeling evasion of mercury from surface waters in the Everglades Nutrient Removal Project. *Sci. of Total Envir*., 259:135-143.

Lindberg, S.E., H. Zhang and Meyers, T.P. (1999) *Application of field methods and models to quantify mercury emissions from wetlands at the Everglades Nutrient Removal Project (ENR)*. Prepared by Environmental Sciences Division, Oak Ridge National Laboratory, Oak Ridge, TN, and National Oceanic and Atmospheric Administration, ATDD, Oak Ridge, TN. Second Final Report. *Everglades Mercury Air/Surface Exchange Study (E-MASE)*. Prepared for the South Florida Water Management District, West Palm Beach, FL (C-6660). January.

Miles, C.J. and L.E. Fink (1998) Monitoring and mass budget for mercury in the Everglades Nutrient Removal Project. *Archives of Envir. Contam. and Toxicol*., 35(4):549-557.

Pollman, C.D., T.M. Lee, W.V. Andrews, L.A. Sacks, S.A. Gherini, and R.K. Munson (1991) Preliminary Analysis of the Hydrologic and Geochemical Controls on Acid Neutralizing Capacity in Two Acidic Seepage Lakes in Florida. Water Resources Research 27: 2321-2335.

Rawlik, P. (2000) Mercury Dynamics in the Everglades. Draft SFWMD letter and attached report from P. Rawlik to R. Harris Aug 25, 2000.

Reeder, P.B. and S.M. Davis (1983) Decomposition, Nutrient Uptake and Microbial Colonization of Sawgrass and Cattail Leaves in Water Conservation Area 2A. SFWMD Tech. Pub #83-4

Rumbold D. and L. Fink (2001) Attachment 1. Report on Expanded Mercury Monitoring at Stormwater Treatment Area – 2.

Rutchey, K, and L. Vilchek. 1999. Air photointerpretation and satellite imagery analysis tehniques for mapping cattail coverage in a northern Everglades impoundment. Photogrammetric Engineering and Remote Sensing. 65: 185-191

SAS Institute (1998) JMP Statistics and Graphics Guide, Version 3. SAS Institute, Inc. Cary, NC.

SFWMD (2000a) Spreadsheet "Dec99ENRMassBudget.xls" received from P. Rawlik, South Florida Water Management District, West Palm Beach, FL.

SFWMD (2000b) Spreadsheet "ENRCoverage.xls" with ENR vegetation coverage received from Peter Rawlick, South Florida Water Management District.

SFWMD (2000c) Spreadsheet "ENR PW data.xls" received from L. Fink, South Florida Water Management District.

SFWMD (2000d) Spreadsheet "ENR_Feldspar Markers.xls" received from L.Fink, South Florida Water Management District

SFWMD (2000e) Spreadsheet "If_Pro_ENR_1.002.xls" received from L.Fink, South Florida Water Management District, West Palm Beach, FL.

SFWMD (2000f) Spreadsheet "S10Flows.xls" received from L.Fink, South Florida Water Management District, West Palm Beach, FL.

SFWMD (2000g) Spreadsheet "Research Water Quality database Merged.001.xls" received from L.Fink, South Florida Water Management District, West Palm Beach, FL.

SFWMD (2000h) Everglades Consolidated Report. South Florida Water Management District, West Palm Beach, FL.

SFWMD (2000i) Spreadsheet "STA-2 Collateral Data.xls" received from L.Fink, South Florida Water Management District, West Palm Beach, FL.

SFWMD (2000j) Spreadsheet "STA-10 Mercury Concentrations" received from L.Fink, South Florida Water Management District, West Palm Beach, FL.

SFWMD (1999a) *Everglades Nutrient Removal Project: 1998 Monitoring Report*. South Florida Water Management District, West Palm Beach, FL. March.

SFWMD (1999b) *Final Report on the Effect of Best Management Practices on the Loading of Mercury Species to/from the Everglades Nutrient Removal Project: Monitoring Program (Project C-1)*. Submitted by the South Florida Water Management District, West Palm Beach, Florida, to the Floirda Department of Environmental Protection, Tallahassee, Florida, to fulfill the requirements of a Section 319 Grant (SP335/C-6663/4) from U.S. Environmental Protection Agency Region 4, Atlanta.

SFWMD (1998) *Everglades Nutrient Removal Project: 1999 Monitoring Report*. South Florida Water Management District, West Palm Beach, FL. March.

SFWMD (1997) *Everglades Nutrient Removal Project: 1996 Monitoring Report*. South Florida Water Management District, West Palm Beach, FL. March.

SFWMD (1996) *Everglades Nutrient Removal Project: 1995 Monitoring Report*. South Florida Water Management, Prepared for the Florida Department of Environmental Protection, Tallahassee, FL.

SFWMD (1995) *Everglades Nutrient Removal Project: 1994 Monitoring Report*. South Florida Water Management, Prepared for the Florida Department of Environmental Protection, Tallahassee, FL.

Smith R. and A.E. Martell (1976a) Critical Stability Constants, Volume 3, Plenum Press

Smith R. and A.E. Martell (1976b) Critical Stability Constants: Volume 4: Inorganic Complexes, Plenum Press

Smith R. and A.E. Martell (1976c) Critical Stability Constants: Volume 5: First Supplement, 1976c, Plenum Press

Stober, Q.J., K. Thornton, R. Jones, J. Richards, C. Ivey, R. Welch, M. Madden, J. Trexler, E. Gaiser, D. Scheidt, and S. Rathbun (2001) South Florida Ecosystem Assessment: Phase I/II – Everglades Stressor Interactions: Hydropatterns, Eutrophication, Habitat Alteration, and Mercury Contamination (Summary). USEPA 904-R-01-002. USEPA, Region 4 Science & Ecosystem Support Division, Water Management Division, and Office of Research and Development.

Tetra Tech Inc. (2003) Revised Trophic State Relationships and Hg Cycling in the Florida Everglades. In preparation.

Tetra Tech, Inc. (2002) Mercury Cycling and Bioaccumulation in Everglades Marshes Phase I and II Interim Report. Final Draft. Report prepared for Florida Department of Environmental Protection and South Florida Water Management District. Tetra Tech, Lafayette, CA.

Tetra Tech, Inc. (2001) Florida Pilot Mercury Total Maximum Daily Load (TMDL) Study: Application of the Everglades Mercury Cycling Model (E-MCM) to Site WCA 3A-15. Final report submitted to United States Environmental Protection Agency and Florida Department of Environmental Protection. Tetra Tech, Inc., Lafayette, CA.

Tetra Tech Inc. (1999a) Dynamic Mercury Cycling Model for Windows 95/NT. A Model for Mercury Cycling in lakes – D-MCM Version 1.0 – User's Guide and Technical Reference. Prepared for EPRI. April 1999. Tetra Tech, Inc., Lafayette, CA.

Tetra Tech Inc. (1999b) Everglades Mercury Cycling Model for Windows 95/NT. A Model for Mercury Cycling in Everglades Marsh Areas – Draft User's Guide and Technical Reference. Version 1.0 Beta. Prepared for the United States Environmental Protection Agency. June 1999. Tetra Tech, Inc., Lafayette, CA.

Tsiros, I.X. and R.B. Ambrose. 1998. Environmental screening modeling in the upper Everglades of south Flroida. J. Environ. Sci. Health, A33(4):497-525.

USGS (2001) Spreadsheet "Final Glades data.xls" dated March 19, 2001 from D. Krabbenhoft, USGS

USGS (2000) Spreadsheet "Burn Study Data.xls" dated 2000 from D. Krabbenhoft, USGS

USGS (1999) Spreadsheet "gladesplants.xls" dated June 3, 1999, received from D. Krabbenhoft, USGS

Vaithiyanathan, P., C. Richardson, R.G.Kavanaugh, C.B. Craft, and T. Barkay (1996) Relationships of Eutrophication to the Distribution of Mercury and to the Potential for Methylmercury Production in the Peat Soils of the Everglades. Env. Sci and Tech. 30(8):2591-2597.

Walker, W.W., Jr. and R.H. Kadlec (1996) A model for simulating phosphorus concentrations in waters and soils downstream of Everglades Stormwater Treatment Areas. Prepared for U.S. Department of theInterior, Draft (August 13, 1996). http://www.wwwalker.net/index.html.

Appendix A
Detailed list of data sources for ENR single cell deterministic simulation

Input	Units	Data Source
1) Physical Characteristics		
Surface water temperature	Celsius	Same as 3A 15: Hydroqual (1997). See Appendix F
Surface light exposure	$\mu E\ m^{-2}\ s^{-1}$	Same as 3A 15: Hydroqual (1997). See Appendex F
Light extinction coefficient	m^{-1}	Approximated as equal to the DOC value in mg L^{-1} (more DOC extinguishes light faster)
2) Hydrology		
Surface Inflow	$m^3\ day^{-1}$	Based on daily flows averaged over 2 week intervals (SFWMD 2000a)
Surface Outflow	$m^3\ day^{-1}$	Based on daily flows averaged over 2 week intervals (SFWMD 2000a)
Groundwater inflow	$m^3\ day^{-1}$	Seepage pump data used as Fracture Inflow to model (SFWMD 2000a)
Groundwater outflow	$m^3\ day^{-1}$	
Precipitation	m day^{-1}	SFWMD (2000a) used biweekly data
3) Elevations and Areas		
Cell area .	m^2	SFWMD (2000a)
Water surface elevation	m	SFWMD (2001)
4) Surface Water Quality (applies to both upper and lower water column compartments if applicable)		
DOC	mg L^{-1}	SFWMD (2000e)
Dissolved oxygen	mg L^{-1}	SFWMD (1999b)
pH		SFWMD (2000e)
Chloride	mg L^{-1}	USGS (2000)
Sulfate	$\mu eq\ L^{-1}$	Gilmour *et al*. (1998a) p.12 (400 to 1000uM) converted using midpoint to 1400 ueq/l
5) Water Column Solids		
Concentration of non-detrital suspended solids particles in water	mg L^{-1}	Estimated from SFWMD (2000e)
Concentration of detrital particles in water	mg L^{-1}	Derived using contributsion from turnover of macrophytes, based on L. Fink equations from Ambrose et al. (1997)
Settling velocity for non-detrital suspended solids	m day^{-1}	Calibrated 0.4 m day^{-1}
Settling velocity for detrital solids	m day^{-1}	Calibrated 0.4 m day^{-1}
Phytoplankton biomass	mg L^{-1} dry	Assumed equal to 20% of seston
Zooplankton biomass	mg L^{-1} dry	Assumed equal to 10% of seston

Input	Units	Data Source
6) General Biological		
Biomass of benthos	Kg wet ha^{-1}	Assumed value of 10
Biomass of shrimp	Kg wet ha^{-1}	Assumed value of 10
Biomass of Periphyton	Kg dry ha^{-1}	Calculated using TP = 50 ug L^{-1} using equations of L. Fink from Ambrose et al. (1997)
Fraction of area covered by periphyton (surface or mat on bottom)	fraction	SFWMD (2000b)
Fraction of periphyton on surface instead of bottom	Fraction	Assumed value of 0.5
Caloric density of shrimp	kcal g^{-1} wet	Assumed 0.85 kcal g^{-1} wet
Caloric density of benthos	kcal g^{-1} wet	Assumed 0.85 kcal g^{-1} wet
Caloric density of zooplankton	kcal g^{-1} wet	Assumed 0.75 kcal g^{-1} wet
Caloric density of phytoplankton	kcal g^{-1} wet	Assumed 0.65 kcal g^{-1} wet
Caloric density of periphyton	kcal g^{-1} wet	Assumed 0.25 kcal g^{-1} wet
Ratio of dry weight/wet weight for periphyton	fraction	Assumed 0.075
Ratio of dry weight/wet weight for phytoplankton	fraction	Assumed 0.10
Ratio of dry weight/wet weight for zooplankton	fraction	Assumed 0.15
7) Macrophytes		
Cattail biomass	g m^{-2}	Calculated using TP=50 ug L^{-1} using equations from Ambrose et al. (1997)
Sawgrass biomass	g m^{-2}	Calculated using TP=50 ug L^{-1} using equations from Ambrose et al. (1997)
Surface areal coverage by cattails	fraction	SFWMD (2000b)
Surface areal coverage by sawgrass	fraction	SFWMD (2000b)
Surface areal coverage by lilies	fraction	SFWMD (2000b)
Turnover rate for cattails	day^{-1}	Calculated using TP=50 ug L^{-1} using equations from Ambrose et al. (1997)
Turnover rate for sawgrass	day^{-1}	Calculated using TP=50 ug L^{-1} using equations from Ambrose et al. (1997)
Turnover rate for periphyton	day^{-1}	Calculated using TP=50 ug L^{-1} using equations from Ambrose et al. (1997)
Transpiration rate for cattails	g H_2O g^{-1} biomass day^{-1}	Assumed value of 10
Transpiration rate for sawgrass	g H_2O g^{-1} biomass day^{-1}	Assumed value of 10
Transpiration rate for lilly pads	g H_2O g^{-1} biomass day^{-1}	Assumed value of 10
Fish (for each of 3 species)		
Species		
Maximum Age	years	Assumed 8 years for piscivore, 6 years for omnivore, 2 years for non-piscivore
Maximum weight for growth equation	g	Tuned LMB growth curve with age weight data from Florida Fish And Wildlife Conservation Commission (2000). Used max weight of bluegill of

Input	Units	Data Source
		250g from Florida Fish And Wildlife Conservation Commission (2000) to get field max weight of 211g.
Fish diet (matrix of who wants to eat what)		Used data from phone conversation with Doug Richard (May 30, 2000) for LMB and bluegill. Also used Lange (2000) and Hurley et al. (1999)
Minimum prey length as a fraction of predator length (for fish eating other fish)	fraction	Largemouth bass value assumed = 0.15 Bluegill value assumed = 0.05 Not applicable to mosquitofish
Maximum prey length as a fraction of predator length (for fish eating other fish)	fraction	Largemouth bass value assumed = 0.40 Bluegill value assumed = 0.33 Not applicable to mosquitofish
Initial biomass	kg ha^{-1}	Same as 3A-15: Marshwide average = 40 kg/ha (wet) (Jordan, 1996 cited in Ambrose *et al.,* 1997)
λ (Term for length/weight relationship)		See Florida Fish And Wildlife Conservation Commission (2000) for bluegill and largemouth bass.
η (Term for length/weight relationship)		See Florida Fish And Wildlife Conservation Commission (2000) for bluegill and largemouth bass. No data for non-piscavore used 3A-15 values
Efficiency of MeHg uptake from food	fraction	Value of 0.7 used (Harris and Snodgrass 1993)
Efficiency of MeHg uptake from water	fraction	Based on applications of D-MCM lake model calibrated at various sites (range typically 0.12 to 0.36)
Bionergetics inputs to determine metabolic rates and food consumption		Hewlett and Johnson (1992)
<u>Sediment characteristics for each layer</u>		
Surface layer thickness	cm	3 cm assumed, consistent with previous E-MCM and D-MCM applications. This assumption is under review.
layer porosity	fraction	Gilmour et al. (1998a) -Appendix 1
Moisture content	fraction	Assumed saturated
Porewater DOC	mg L^{-1}	SFWMD (2000c)
Porewater pH		Used surface water mean value
Porewater chloride	mg L^{-1}	Used surface water value
Porewater sulfate	ueq L^{-1}	From Gilmour et al. (1998a) used single value
<u>Initial Mercury Concentrations</u>		
Initial MeHg concentration in water (unfiltered, includes all seston & plankton)	ng L^{-1}	From SFWMD (2000a) mean of all monitoring sites in ENR for Mar 20, 1995
Initial MeHg concentration on bulk sediment particles in each layer	ng g^{-1}	Gilmour et al. (1998a)
Initial Hg concentrations in fish (each age class, each species)	ug g^{-1} wet	From Florida Fish And Wildlife Conservation Commission (2000)

Input	Units	Data Source
Initial HgII concentration in water (unfiltered, includes all seston)	ng L^{-1}	From SFWMD (2000a) mean of all monitoring sites in ENR for Mar 20, 1995
Initial HgII concentration on bulk sediment particles for each layer	ng g^{-1}	Gilmour et al. (1998a) Appendix 1
Initial Elemental Hg concentration in water	ng L^{-1}	Assumed 0.015. The model is not sensitive to this input, and elemental Hg concentrations change rapidly.
Initial Elemental Hg concentration in porewater (for each layer)	ng L^{-1}	Assumed 0.03. The model is not sensitive to this input, and elemental Hg concentrations change rapidly.
Initial HgII concentration in sawgrass	ng g^{-1} dry	USGS (2000)
Initial HgII concentration in lilies	ng g^{-1} dry	USGS (2000)
Initial HgII concentration in cattails	ng g^{-1} dry	USGS (2000)
		USGS (2000)
Initial MeHg concentration in sawgrass	ng g^{-1} dry	USGS (2000)
Initial MeHg concentration in lilies	ng g^{-1} dry	USGS (2000)
Initial MeHg concentration in cattails	ng g^{-1} dry	USGS (2000)
<u>External Hg loads and Concentrations</u>		
Concentration of gaseous elemental mercury in air	ug m^{-3}	Same as 3A 15
Concentration of reactive gaseous HgII (RGM) in air	ug m^{-3}	Same value as derived for WCA 3A-15. Note that modeled dry deposition also accounts for different macrophyte coverage at each site.
Concentration of HgII in inflow (unfiltered)	ug m^{-3}	SFWMD (2000a)
Concentration of MeHg in inflow (unfiltered, not inert)	ug m^{-3}	SFWMD (2000a)
Concentration of HgII in groundwater inflow	ug m^{-3}	SFWMD (2000a)
Concentration of MeHg in groundwater inflow	ug m^{-3}	SFWMD (2000a)
Concentration of MeHg in wet deposition	ug m^{-3}	SFWMD(2002a)
Concentration of HgII in wet deposition	ug m^{-3}	SFWMD (2000a)
Particle HgII dry deposition rate	ng m^{-2} day	Derived from Keeler *et al.* (2000) data, adjusted for vegetative cover.
Point source load of MeHg	ug day^{-1}	Not applicable
Point source load of HgII	ug day^{-1}	Not applicable
Point source load of elemental Hg	ug day^{-1}	Not applicable
<u>Hg Rate Constants</u>		
Vertical thickness of sediment methylation zone	m	Assumed upper 3 cm
Methylating efficiency of microbes	ug MeHg per ug $Hg(II)_{avail}$ per g C decomposed per m^3	Set to 0 in final calibration
$Q10_{Meth}$	dimensionless	Value of 2.0 assumed
Half-saturation constant for sulfate effect on methylation	ueq L^{-1}	Value of 200 used , same as 3A 15. This constant requires future attention

Input	Units	Data Source
		when sulfide complexation is revisited
Factor to relate efficiency with which microbes methylate in the absence or presence of sulfate	dimensionless	Value of 1.0 , same as 3A 15. This constant requires future attention when sulfide complexation is revisited
Fraction of biological demethylation going to elemental Hg	Fraction	Low value needed to avoid buildup of elemental Hg in porewater (not observed). Value of 0.05 assumed
Demethylating efficiency of microbes	ug HgII per ug $MeHg_{avail}$ per g C decomposed per m^3	Set to zero in final calibration
MeHg photodegradation rate constant at water surface	m^2 $uEinsteins^{-1}$	Same as 3A 15 calibration
Hg(II) photoreduction rate constant at water surface	m^2 $uEinsteins^{-1}$	Derived from application of D-MCM to four lakes as well as examined during ENR runs.
Elemental Hg oxidation rate constant at water surface	m^2 $uEinsteins^{-1}$	Set to zero. Thus the photoreduction rate represents net reduction.
Hg Mass transfer coefficient in air	m day^{-1}	100 m day^{-1} assigned
Hg Mass transfer coefficient at water surface	m day^{-1}	0.5 m day^{-1} assigned
Hg Mass transfer coefficient across sediment/water interface	m day^{-1}	0.03 m day, same as value calibrated at WCA 3A-15.
RGM deposition velocity	m day^{-1}	Value of 864 m day^{-1} assumed (1 cm s^{-1})
<u>Hg Partitioning: non-living particles</u>		
Partitioning constant between MeHg on non-living solids and a fraction of dissolved pool in surface water	m^3 g^{-1}	Calibrated to ENR site data for final 2 cell simulation
Partitioning constant between HgII on non-living solids and a fraction of dissolved pool in surface water	m^3 g^{-1}	Calibrated to ENR site data for final 2 cell simulation
Partitioning constant between MeHg on detritus and a fraction of dissolved pool in surface water	m^3 g^{-1}	Calibrated to ENR site data for final 2 cell simulation
Partitioning constant between HgII on detritus and a fraction of dissolved pool in surface water	m^3 g^{-1}	Calibrated to ENR site data for final 2 cell simulation
Partitioning constant between MeHg on sediment solids and a fraction of dissolved pool in porewater (for each layer)	m^3 g^{-1}	Calibrated to ENR site data for final 2 cell simulation
Partitioning constant between HgII on sediment solids and a fraction of dissolved pool in porewater (for each layer)	m^3 g^{-1}	Calibrated to ENR site data for final 2 cell simulation
<u>Hg Partitioning in Lower Food Web</u>		
Ratio between MeHg concentration in zooplankton and phytoplankton	dimensionless	Value of 2.0 used (Same value as previous applications of E-MCM and D-MCM)
Ratio of MeHg concentrations in	(ug MeHg/g wet shrimp) /	Value of 12 used (Same value as

Input	Units	Data Source
shrimp and detritus	(ug MeHg /g detritus)	previous applications of E-MCM at WCA 3A-15
Ratio of MeHg concentrations in benthos and sediments.	(ug MeHg/g wet benthos) / (ug MeHg /g sed)	Value of 25 used (within range used for previous applications of E-MCM and D-MCM)
MeHg partitioning between periphyton and dissolved inorganic MeHg complexes	[ug MeHg /g dry part]/[ug dissolved inorganic MeHg/m3].	Value of 0.35 used (Same value as previous applications of E-MCM at WCA 3A-15
Switch to determine MeHg species taken up by phytoplankton (options will exist)	-	Assumed non-DOC bound MeHg taken up by phytoplankton. This was based on previous applications of D-MCM and E-MCM (R. Harris unpublished).
MeHg facilitated uptake rate constant for phytoplankton	L cell^{-1} day^{-1}	Based on Hudson et al. (1994)
Protonation constant for facilitated MeHg uptake by phytoplankton	L mole^{-1}	Based on Hudson et al. (1994)
Phytoplankton cell permeability of MeHg	dm d^{-1}	Based on Hudson et al. (1994)
Phytoplankton cell density	kg dry L^{-1} cell	Based on Hudson et al. (1994)
Phytoplankton cell radius	dm	Based on Hudson et al. (1994)
Phytoplankton MeHg clearance rate constant	d^{-1}	Assumed to be negligible
Phytoplankton turnover rate	Day^{-1}	Based on Hudson et al. (1994)
Coefficient for diffusion limited uptake of MeHg by phytoplankton	dm^2 day^{-1}	Based on Hudson et al. (1994)
Thermodynamic Equilibrium		
Thermodynamic constants for all relevant MeHg and HgII complexes. Complexing agents include chloride, sulfide, OH, and the thiol component of DOC	L Mole^{-1}	Smith and Martell (1976c, 1976b, 1976c), Hudson *et al.* (1994)

Appendix B
Probabalistic input distributions assigned for sample ENR Monte Carlo simulation

Input category	Input Description	Units	Distribution Type	Mean value	Standard Deviation	Minimum	Maximum
Physical	Te is the Epilimnion Temperature. Thisis a time series input. You can enter data with different time intervals between values.	Degrees C	Normal	1	0.05	0.85	1.5
Hydrology	Daily precipitation equivalent in meters of rainfall per day. No Hg loading to the lake via atmospheric deposition will occur during periods of ice cover, even if precipitation is indicated with this input.	m/d	Normal	1	0.1	0.7	1.3
Hydrology	Flowrate for surface inflow. This time-series input enters the epilimnion directly.	m3/day	Rectangular	1	0.8	0.2	1.8
Water Quality	Concentration of chloride in the epilimnion. This parameter is used in thermodynamic speciation calculations	mg/L	Rectangular	166.16	33	133.16	199.16
Water Quality	Dissolved organic carbon in the epilimnion. This parameter is used in calculations of mercury complexation and bioavailability for methylation and demethylation in the epilimnion.	mg/L	Rectangular	1	0.2	0.8	1.2
Water Quality	Dissolved oxygen concentration in epilimnetic waters. This time series is used to determine whether or not methylation occurs in the epilimnion, and in calculations of gill uptake of MeHg by fish. Methylation in the epilimnion occurs if DO(epi) = 0, w	mg/L	Rectangular	4	1	3	5

Input category	Input Description	Units	Distribution Type	Mean value	Standard Deviation	Minimum	Maximum
Water Quality	Phosphorous concentration in water	ug/l	Rectangular	1	0.33	0.67	1.33
Water Quality	Sulfate concentration in epilimnetic waters . This can affect methylation in epilimnetic waters if you wish, depending on the value of KSO4 you choose. KSO4 is the half saturation constant for the effect of sulfate on methylation. Set KSO4 to zero to	ueq/L	Rectangular	1400	200	1200	1600
Water Column Solids	Non-living settling seston concentration in epilimnion. This is a time series input. It does not include living phytoplankton and zooplankton in the water column.	mg/L	Rectangular	1	0.2	0.8	1.2
Biological (General)	Caloric density of benthos on a wet weight basis, usually around 0.6 to 0.85	KCal/g wet Benthos	Rectangular	0.725	0.15	0.575	0.875
Biological (General)	Caloric density of periphyton	kcal/g wet	Rectangular	0.25	0.05	0.2	0.3
Biological (General)	Caloric density of phytoplankton per wet weight, usually around 0.5 to 0.65	Kcal/g wet Phyto	Rectangular	0.45	0.1	0.35	0.55
Biological (General)	Caloric density of shrimp	kcal/g wet	Rectangular	0.725	0.15	0.575	0.875
Biological (General)	Caloric density of zooplankton on a wet weight, usually around 0.5 to 0.65.	Kcal/g wet Zoo	Rectangular	0.55	0.1	0.45	0.65
Biological (General)	Ratio of dry to wet weight for periphyton. For example, if periphyton were 90% water on a weight basis, the value of DryWetFacPhyto would be 0.1.	dimensionless	Rectangular	0.075	0.025	0.05	0.1

Input category	Input Description	Units	Distribution Type	Mean value	Standard Deviation	Minimum	Maximum
Biological (General)	Ratio of dry to wet weight for phytoplankton. For example, if phytoplankton were 90% water on a weight basis, the value of DryWetFacPhyto would be 0.1.	dimensionless	Rectangular	0.075	0.025	0.05	0.1
Biological (General)	Ratio of dry to wet weight for zooplankton. For example, if the zooplankton were 80% water by weight, value of DryWetFacZoo would be 0.2	dimensionless	Rectangular	0.1	0.03	0.07	0.13
Macrophytes	Biomass density of macrophyte species #2 (g/m2 of area covered)	g/m2	Rectangular	450	40	410	490
Carbon	The factor by which carbon turnoverincreases due to a 10 degree C rise above the base temperature (eg. 2x). This applies to the sediments.	degrees C	Rectangular	2	0.1	1.9	2.1
Carbon	Degradation rate of carbon (DOC) in epilimnetic waters at temperature TbaseCT. (eg. 0.0001 per day turnover rate for this carbon fraction). This input is used in calculations of methylation and demethylation rates. Methylation and demethylation are	1/day	Rectangular	0.0001	0.00001	0.00009	0.00011
Carbon	Base temperature at which carbon turnover rate is measured. Temperature effects are included through a Q10 factor. This base temperature applies to the sediments.	degrees C	Rectangular	15	2	13	17
Sediments - general	Fraction of detriatal particles that decompose upon settling without being incorporated into the sediments	fraction	Rectangular	0.1	0.05	0.05	0.15

Input category	Input Description	Units	Distribution Type	Mean value	Standard Deviation	Minimum	Maximum
Sediments - general	Fraction of particles that decompose upon settling without being incorporated into the sediments	fraction	Rectangular	0.1	0.05	0.05	0.15
Sediments - general	Resuspension rate from top sediment layer (g/m2 sed/yr)	g/m2 sed/d	Rectangular	0.4	0.1	0.3	0.5
External Hg Loads & Conc'ns	Inflow elemental Hg concentration. This time-series input is treated as a step function.	ng/L unfilt	Rectangular	0.03	0.003	0.027	0.033
External Hg Loads & Conc'ns	Elemental Hg concentration in air. eg. 0.001 to 0.003 ug/m3. This time series is a boundary condition and is not altered by the model calculations.	ug Hg/m3	Rectangular	0.0016	0.00016	0.00144	0.00176
External Hg Loads & Conc'ns	Groundwater inflow concentration for elemental Hg.	ng/L	Rectangular	0.05	0.005	0.045	0.055
External Hg Loads & Conc'ns	Inflow Hg(II) concentration. This includes dissolved, SS, and planktonic Hg(II), and andy solid HgS in the inflow. (ie. all Hg(II) in the water column of the inflow).	ng/L unfilt	Rectangular	1	0.3	0.7	1.3
External Hg Loads & Conc'ns	Groundwater inflow concentration of Hg(II).	ng/L	Rectangular	0.45	0.0045	0.4455	0.4545
External Hg Loads & Conc'ns	Inflow MeHg concentration. This includes dissolved, SS, and planktonic MeHg (ie. all MeHg in the water column of the inflow). This time-series input is treated as a step function.	ng/L unfilt	Rectangular	0.6	0.3	0.3	0.9
External Hg Loads & Conc'ns	CH3HgCl concentration in air. This time series is a boundary condition and is not altered by the model calculations.	ug Hg/m3	Rectangular	0.000001	1E-07	9E-07	1.1E-06

Input category	Input Description	Units	Distribution Type	Mean value	Standard Deviation	Minimum	Maximum
External Hg Loads & Conc'ns	Groundwater inflow concentration of MeHg.	ng/L	Rectangular	0.05	0.005	0.045	0.055
External Hg Loads & Conc'ns	Dry deposition of Hg(II). This value represents deposition of HgII onto the waterbody via dry deposition. During periods of ice cover, no dry (or wet) deposition of Hg occurs, regardless of the numbers input for this time series input.	ug Hg/d/m2	Rectangular	1	0.1	0.9	1.1
External Hg Loads & Conc'ns	Concentration off Hg(II) in precipitation. Dry deposition of MeHg. During periods of ice cover, no wet (or dry) deposition of Hg occurs, regardless of the numbers input for this time series input.	ng/L	Rectangular	1	0.074	0.926	1.074
External Hg Loads & Conc'ns	Dry deposition of MeHg. This value represents deposition of MeHg onto the waterbody via dry deposition. During periods of ice cover, no dry (or wet) deposition of Hg occurs, regardless of the numbers input for this time series input.	ug Hg/d/m2	Rectangular	0.00001	0.000001	9E-06	0.000011
External Hg Loads & Conc'ns	Concentration of MeHg in precipitation. Dry deposition of MeHg. During periods of ice cover, nowet (or dry) deposition of Hg occurs, regardless of the numbers input for this time series input.	ng/L	Rectangular	0.05	0.005	0.045	0.055
External Hg Loads & Conc'ns	RGM (reactive gaseous mercury) in the atmosphere. (pg Hg/m3)	pg Hg/m3	Rectangular	1	0.074	0.926	1.074
Hg Rate Constants	The factor by which methylation increases due to a 10 degree C rise above the base temperature (eg. 2x). This applies to the water column, interface and sediments.	degrees C	Rectangular	2	0.1	1.9	2.1

Input category	Input Description	Units	Distribution Type	Mean value	Standard Deviation	Minimum	Maximum
Hg Rate Constants	Demethylating efficiency of microbes, per unit of carbon flux and unit available MeHg concentration . If you wish to calibrate the demethylation rate, use this input. Demethylation does not depend on temperature in this version of the model.	g ElemHg/g TOC lab	Lognormal	0.0004	3.5	9.33E-06	0.01715
Hg Rate Constants	Methylating efficiency of microbes, per unit of carbon flux and unit available HgII concentration . If you wish to calibrate the methylation rate, use this input. To adjust the tempeature sensitivity of methylation, see Q10meth.	g MeHg/g TOC labile	Lognormal	0.0004	3.5	9.33E-06	0.01715
Hg Rate Constants	MeHg photodegradation) rate constant at waterbody surface per unit of surface light intensity. There is ongoing research into the wavelengths associated with this process. See also Ke (light extinction) in the physical input category.	ng/m3/day	Lognormal	0.0006	0.464	0.00006	0.006
Hg Rate Constants	HgII photor4eduction rate constant at waterbody surface per unit of surface light intensity. There is ongoing research into the wavelengths associated with this process. See also Ke (light extinction) in the physical input category.	ng/m3/day	Lognormal	0.004	0.464	0.0004	0.04
Hg Rate Constants	Mass transfer coefficient for gaseous CH3HgCl in air (eg. 100 m/day). This is used in calculations of an overall MTC for air/water in estimates of volatilization.	m/day	Rectangular	100	10	90	110
Hg Rate Constants	Mass transfer coefficient for CH3HgCl in water (eg.5 m/day). This is used in calculations of an overall MTC for air/water in estimates of volatilization.	m/day	Rectangular	0.5	0.05	0.45	0.55

Input category	Input Description	Units	Distribution Type	Mean value	Standard Deviation	Minimum	Maximum
Hg Rate Constants	Epilimnion/sediment MTC (Mass transfer coefficient). (eg. 0.01-0.1 m/day). This is used to calculate diffusion across the sediment/water column boundary in the epilimnion. Assumed to be the same for HgII and MeHg.	m/day	Lognormal	0.03	0.7565	0.015	0.08
Hg Rate Constants	Fraction of HgII taken up by roots of macrophyte species 1 that is reduced to Hg0	fraction	Rectangular	0.05	0.005	0.045	0.055
Hg Rate Constants	Fraction of HgII taken up by roots of macrophyte species 2 that is reduced to Hg0	fraction	Rectangular	0.05	0.005	0.045	0.055
Hg Rate Constants	Fraction of HgII taken up by roots of macrophyte species 2 that is reduced to Hg0	fraction	Rectangular	0.05	0.005	0.045	0.055
Hg Rate Constants	Base temperature at which methylation rate is measured. Temperature effects are included through a Q10 factor. This base temperature applies to the water column, interface and sediments.	degrees C	Rectangular	15	1.5	13.5	16.5
Hg Rate Constants	RGM deposition velocity (m/d)	m/d	Rectangular	864	86.4	777.6	950.4
Hg Partitioning - Non Living Particles	log 10 Protonation constant for adsorption of Hg++ on detritus.	L/mole	Rectangular	10	1	9	11
Hg Partitioning - Non Living Particles	log 10 protonation constant for adsorption/desorption of HgII on non-living particles in water column or sediments.	L/mole	Rectangular	10	1	9	11

Input category	Input Description	Units	Distribution Type	Mean value	Standard Deviation	Minimum	Maximum
Hg Partitioning - Non Living Particles	log 10 Protonation constant for adsorption of CH3Hg on detritus.	L/mole	Rectangular	4.5	0.45	4.05	4.95
Hg Partitioning - Non Living Particles	log 10 Protonation constant for adsorption of CH3Hg on non-living particles in water or sediments.	L/mole	Rectangular	4.5	0.45	4.05	4.95
Hg Partitioning - biotic particles	Bioconcentration factor for CH3Hg in zooplankton. The model uses this to estimate zooplankton MeHg on the basis of phytoplankton MeHg.	dimensionless	Lognormal	4	1.44	2	12
Hg Partitioning - biotic particles	log 10 protonation constant for uptake of MeHg in Periphyton	L/mole	Rectangular	4.5	2.25	2.25	6.75
Hg Partitioning - biotic particles	Ratio of MeHg concentrations in benthos and sediments. = (ug MeHg/g wet benthos) / (ug MeHg /g sed)	g dry/g wet	Lognormal	50	1.44	25	150
Hg Partitioning - biotic particles	MeHg partitioning between periphyton and dissolved inorganic MeHg complexes = [ug MeHg /g dry part]/[ug dissolved inorganic MeHg/m3]. m3/g dry part	m3/g dry periphyton	Lognormal	0.7	1.44	0.35	2.1
Hg Partitioning - biotic particles	Ratio of MeHg concentrations in shrimp and detritus. = (ug MeHg/g wet shrimp) / (ug MeHg /g detritus)	g dry/g wet	Lognormal	24	1.6	6	96
Carbon	Carbon fraction of mineralizing particulates in surface sed	fraction	Rectangular	0.55	0.055	0.495	0.605

Input category	Input Description	Units	Distribution Type	Mean value	Standard Deviation	Minimum	Maximum
Carbon	Carbon fraction of mineralizing particulates in 2nd sed layer	fraction	Rectangular	0.52	0.052	0.468	0.572
Carbon	Carbon fraction of mineralizing particulates in 3rd sed layer	fraction	Rectangular	0.5	0.05	0.45	0.55
Carbon	Carbon fraction of mineralizing particulates in fourth sed layer	fraction	Rectangular	0.48	0.048	0.432	0.528
Carbon	Carbon fraction of detritus in epilimnion	fraction	Rectangular	0.55	0.055	0.495	0.605
Carbon	Carbon fractgion of detritus in hypolimnion	fraction	Rectangular	0.55	0.055	0.495	0.605
Carbon	Carbon fraction of decomposing non-detrital particles in epilimnion	fraction	Rectangular	0.55	0.055	0.495	0.605
Carbon	Carbon fraction of decomposing non-detrital particles in hypolimnion	fraction	Rectangular	0.55	0.055	0.495	0.605
Fish bioenergetics	Digestive tract uptake efficiency for methylmercury for mosquitofish .	fraction	Rectangular	0.7	0.1	0.6	0.8
Fish bioenergetics	Digestive tract uptake efficiency for methylmercury for omnivore	fraction	Rectangular	0.7	0.1	0.6	0.8
Fish bioenergetics	Digestive tract uptake efficiency for methylmercury for piscivore	fraction	Rectangular	0.7	0.1	0.6	0.8
Fish bioenergetics	Proportion of consumption lost to egestion for mosquitofish	fraction	Rectangular	0.158	0.0158	0.1422	0.1738
Fish bioenergetics	Proportion of consumption lost to egestion for omnivore	fraction	Rectangular	0.158	0.0158	0.1422	0.1738
Fish bioenergetics	Proportion of consumption lost to egestion for piscivore	fraction	Rectangular	0.104	0.01	0.094	0.114
Hg partitioning	HgII partitioning between detritus particles and dissolved inorganic HgII in epilimnion	m3/g	Rectangular	5.15E+10	5.15E+09	4.64E+10	5.67E+10
Hg partitioning	HgII partitioning between non-living seston and dissolved inorganic HgII in epilimnion	m3/g	Rectangular	1.04E+10	1.04E+09	9.32E+09	1.14E+10
Hg partitioning	HgII partitioning between non-living seston and dissolved inorganic HgII in hypolimnion	m3/g	Rectangular	1E+10	1E+09	9E+09	1.1E+10

Input category	Input Description	Units	Distribution Type	Mean value	Standard Deviation	Minimum	Maximum
Hg partitioning	HgII partitioning between sediment particles and porewater inorganic HgII in surface sed	m3/g	Rectangular	5.15E+10	5.15E+09	4.64E+10	5.67E+10
Hg partitioning	MeHg partitioning between detritus particles and dissolved inorganic HgII in epilimnion	m3/g	Rectangular	0.07	0.007	0.063	0.077
Hg partitioning	MeHg partitioning between non-living seston and dissolved inorganic MeHg complexes in epilimnion	m3/g	Rectangular	0.77	0.077	0.693	0.847
Hg partitioning	MeHg partitioning between sediment particles and porewater inorganic MeHg complexes in surface sed	m3/g	Rectangular	0.07	0.007	0.063	0.077
Hg partitioning	Rate constant for adsortion onto non-detrital particles during adsorption in epilimnion		Rectangular	7819000	780900	7038100	8599900
Hg partitioning	Rate constant for adsortion onto non-detrital particles during adsorption in surface sediments		Rectangular	2000000	200000	1800000	2200000
Hg partitioning	Rate constant for adsortion onto detritus during adsorption in epilimnion		Rectangular	13030000	1300000	11730000	14330000
Hg partitioning	Rate constant for desorption from non-detrital particles (during adsorption) in epilmnion		Rectangular	0.3	0.03	0.27	0.33
Hg partitioning	Rate constant for desorption from detritus during adsorption in epilimnion		Rectangular	0.5	0.05	0.45	0.55
Hg partitioning	Rate constant for desorption from non-detrital particles (during desorption) in epilimnion		Rectangular	0.000001	1E-07	9E-07	1.1E-06
Hg partitioning	Rate constant for adsortion onto sediment particles during desorption in surface sed		Rectangular	0.000001	1E-07	9E-07	1.1E-06
Hg partitioning	Rate constant for desorption from detritus during (during desorption) in epilimnion		Rectangular	0.000001	1E-07	9E-07	1.1E-06

Input category	Input Description	Units	Distribution Type	Mean value	Standard Deviation	Minimum	Maximum
Hg partitioning	Solid phase concentration (ug/g) for inert Hg++ on non-detrital particles at saturation, in epilimnion	ug/g	Rectangular	10	1	9	11
Hg partitioning	Solid phase concentration (ug/g) for inert Hg++ on detritus at saturation in epilimnion	ug/g	Rectangular	10	1	9	11
Hg partitioning	Solid phase concentration (ug/g) for inert Hg++ at saturation in surface sediments	ug/g	Rectangular	71.9	7.19	64.71	79.09
Fish bioenergetics	RA from Wisconsin Respiration equation for mosquitofish		Rectangular	0.0108	0.00108	0.00972	0.01188
Fish bioenergetics	RA from Wisconsin Respiration equation for omnivore		Rectangular	0.0154	0.00154	0.01386	0.01694
Fish bioenergetics	RA from Wisconsin Respiration equation for piscivore		Rectangular	0.00279	0.000279	0.002511	0.003069
Carbon	carbon turnover rate for surface sediment dissolved organic carbon	1/day	Rectangular	0.00005	0.000005	0.000045	0.000055
Carbon	carbon turnover rate for 2nd sed layer dissolved organic carbon	1/day	Rectangular	0.00005	0.000005	0.000045	0.000055
Carbon	carbon turnover rate for 3rd sediment layer dissolved organic carbon	1/day	Rectangular	0.00005	0.000005	0.000045	0.000055
Carbon	carbon turnover rate for 4th sediment layer dissolved organic carbon	1/day	Rectangular	0.00005	0.000005	0.000045	0.000055
Carbon	carbon turnover rate for sediment particulate organic carbon in surface sediments	1/day	Rectangular	0.000225	2.25E-05	0.000203	0.000248
Carbon	carbon turnover rate for sediment particulate organic carbon in 2nd sed layer	1/day	Rectangular	3.75E-05	3.75E-06	3.38E-05	4.13E-05
Carbon	carbon turnover rate for sediment particulate organic carbon in 3rd sed layer	1/day	Rectangular	1.3E-06	1.3E-07	1.17E-06	1.43E-06

Input category	Input Description	Units	Distribution Type	Mean value	Standard Deviation	Minimum	Maximum
Carbon	carbon turnover rate for sediment particulate organic carbon in 4th sed layer	1/day	Rectangular	7.8E-08	7.8E-09	7.02E-08	8.58E-08

Appendix C
Dependencies used for ENR Monte Carlo simulations

Dependent Variable	Independent Variable	Equation applied	Rationale
Surface_outflow -	Surface_inflow -	Surface_outflow = 0.746993 x Surface_Inflow + 92253	Used regression relationship derived from ENR inflow and outflow data (SFWMD 2000a)
BiomassDensity (m1) - Biomass density of macrophyte species #1 (g/m2 of area covered)	Total phosphorus concentration in water	BiomassDensity (m1) = 355 x Phosphorus $^{0.176}$	Fink 2002a
Periphyton - Biomass density of periphyton.	Total phosphorus concentration in water	Periphyton = 10 x 661 x Phosphorus $^{-0.225}$	Fink 2002a
BiomassDensity (m3) - Biomass density of macrophyte species #3 (g/m2 of area covered)	Total phosphorus concentration in water	BiomassDensity (m3) = 454 x Phosphorus $^{0.16}$	Fink 2002a
Turnover (m1) - turnover rate for macrophyte species #1	Total phosphorus concentration in water	turnover (m1) = (1.53 x Phosphorus ^ $^{0.114}$) / 365	Fink 2002a
Turnover (m3) - Turnover rate for macrophyte species #1	Total phosphorus concentration in water	DependentValue = (2.74 x Phosphorus $^{0.137}$) / 365	Fink 2002a
Light extinction coefficient (ke). Used for photochemical reactions	DOC_epi - Dissolved organic carbon in the epilimnion.	ke = DOC_epi x 0.9) + (0.5 x SettlingSolids_epi	
	SettlingSolids_Epi - Non-living settling seston concentration in epilimnion.		
Detritus - Bulk concentration of detritus in water.	Turnover (m1) - Turnover rate for macrophyte species #1	Detritus = f(macrophyte biomass, macrophyte turnover rate, settling velocity)	Detrital load is the predominantly the sum of litter supplied by macrophytes and periphyton
	BiomassDensity (m1) - Biomass density of macrophyte species #1 (g/m2 of area covered)		
	BiomassDensity (m21) - Biomass density of macrophyte species #2 (g/m2 of area covered)		

Dependent Variable	Independent Variable	Equation applied	Rationale
	turnover (m3) - turnover rate for macrophyte species #2		
	BiomassDensity (m3) - Biomass density of macrophyte species #2 (g/m2 of area covered)		
Phytoplankton - biomass, expressed on a dry weight basis	Total Phosphorus concentration in water	Phytoplankton = Phosphorus x 0.01	Assumed relationship due to lack of field information
Benthos_sed1 - Biomass density of benthos in sediment zone 1	Phytoplankton - Concentration, expressed on a dry weight basis	Benthos_sed1 = Phytoplankton x 12 / 10 Divide by 10 to convert to dry weight	Assumed relationship due to lack of field information
Shrimp - Biomass density based on the total surface area.	Phytoplankton - Concentration, expressed on a dry weight basis, of phytoplankton in epilimnion. This is a time series input.	Shrimp = Phytoplankton x 12 / 10 Divide by 10 to convert to dry weight	Assumed relationship due to lack of field information
Zooplankton - Concentration, expressed on a dry weight basis	Phytoplankton concentration, expressed on a dry weight basis	Zooplankton = Phytoplankton x 0.5	Assumed relationship due to lack of field information

Appendix D
Detailed list of data sources for WCA 2A (F1 and U3) simulations

Input	Units	Data In-house
1) Physical Characteristics		
Surface water temperature (upper compartment)	Celsius	Same as 3A 15 Hydroqual (1997) See Appendix F
Surface light exposure	$\mu E\ m^{-2}\ s^{-1}$	Same as 3A 15 Hydroqual (1997) see Appendex F
Light extinction coefficient	m^{-1}	Approximated as equal to the DOC value (more DOC extinguishes light faster)
2) Hydrology		
Surface Inflow	$m^3\ day^{-1}$	Combined Fink (2002a) control structures flow plus rain input, see Fink (2002a) and SFWMD (2000g)
Surface Outflow	$m^3\ day^{-1}$	SFWMD (2000g)
Precipitation	$m\ day^{-1}$	Fink (2000b)
3) Elevations and Areas		
Cell area .	m^2	See Section 5.2.2 for description of derivation of cell areas.
Water surface elevation	m	SFWMD (2000g)
4) Surface Water Quality (applies to both upper and lower water column compartments if applicable)		SFWMD (2000g)
DOC	$mg\ L^{-1}$	SFWMD (2000g)
Dissolved oxygen	$mg\ L^{-1}$	SFWMD (2000g)
pH		SFWMD (2000g)
Chloride	$mg\ L^{-1}$	SFWMD (2000g)
Sulfate	$\mu eq\ L^{-1}$	SFWMD (2000g)
5) Water Column Solids		
Concentration of non-detrital suspended solids particles in water	$mg\ L^{-1}$	SFWMD (2000g)
Settling velocity for non-detrital suspended solids	$m\ day^{-1}$	Value of 0.4 assigned
Settling velocity for detrital solids	$m\ day^{-1}$	Value of 0.4 assigned
Phytoplankton biomass	$mg\ L^{-1}$	Assumed 20% of seston (dry wt.)
Zooplankton biomass	$mg\ L^{-1}$	Assumed 10% of seston (dry wt.)
Detritus biomass	$mg\ L^{-1}$	Calculated using TP = 50 $ug\ L^{-1}$ using equations of L. Fink from Ambrose et al. (1997)
6) General Biological		
Biomass of benthos	$Kg\ wet\ ha^{-1}$	Rawlik (2000)
Biomass of shrimp	$Kg\ wet\ ha^{-1}$	Assumed value of 10

Input	Units	Data In-house
Biomass of Periphyton	Kg dry ha^{-1}	Calculated using TP = 50 ug L^{-1} using equations of L. Fink from Ambrose et al. (1997)
Fraction of area covered by periphyton (surface or mat on bottom)	fraction	Estimated – see Section 6.3
Fraction of periphyton on surface instead of bottom	Fraction	Assumed value of 0.5
Ratio of dry weight/wet weight for periphyton	fraction	Assumed 0.075
Ratio of dry weight/wet weight for phytoplankton	fraction	Assumed 0.10
Ratio of dry weight/wet weight for zooplankton	fraction	Assumed 0.15
7) Macrophytes		
Cattail biomass	g m^{-2}	Calculated using TP=50 ug L^{-1} using equations from Ambrose et al. (1997)
Sawgrass biomass	g m^{-2}	Calculated using TP=50 ug L^{-1} using equations from Ambrose et al. (1997)
Surface areal coverage by cattails	fraction	Estimated – see Section 6.3
Surface areal coverage by sawgrass	fraction	Estimated – see Section 6.3
Surface areal coverage by lilies	fraction	Estimated – see Section 6.3
Turnover rate for cattails	day^{-1}	Calculated using TP=50 ug L^{-1} using equations from Ambrose et al. (1997)
Turnover rate for sawgrass	day^{-1}	Calculated using TP=50 ug L^{-1} using equations from Ambrose et al. (1997)
Turnover rate for periphyton	day^{-1}	Calculated using TP=50 ug L^{-1} using equations from Ambrose et al. (1997)
Transpiration rate for cattails	g H_2O g^{-1} biomass day^{-1}	Assumed value of 10
Transpiration rate for sawgrass	g H_2O g^{-1} biomass day^{-1}	Assumed value of 10
Transpiration rate for lilly pads	g H_2O g^{-1} biomass day^{-1}	Assumed value of 10
Fish (for each of 3 species)		
Maximum Age	years	Assumed 8 years for piscivore, 6 years for omnivore, 1 year for non-piscivore
Maximum weight for growth equation	g	Assumed same as 3A-15
Fish diet (matrix of who wants to eat what)		For non-piscivore used data from Email from Paul Garrison Oct 5, 2000 Re Who eats what at F1 and U3
Minimum prey length as a fraction of predator length (for fish eating other fish)	fraction	Largemouth bass value assumed = 0.15 Bluegill value assumed = 0.05

Input	Units	Data In-house
		Not applicable to mosquitofish
Maximum prey length as a fraction of predator length (for fish eating other fish)	fraction	Largemouth bass value assumed = 0.40 Bluegill value assumed = 0.33 Not applicable to mosquitofish
Initial biomass	kg ha^{-1}	From Rawlik, 2000
Efficiency of MeHg uptake from food	fraction	Value of 0.7 used (Harris and Snodgrass 1993)
Efficiency of MeHg uptake from water	fraction	Based on applications of D-MCM lake model calibrated at various sites (range typically 0.12 to 0.36)
Bionergetics inputs to determine metabolic rates and food consumption		Hewlett and Johnson (1992)
Sediment characteristics for each layer		
layer thickness	cm	3 cm (assumed), consistent with previous E-MCM and D-MCM applications. This assumption is under review.
Moisture content	fraction	Assumed saturated
Porewater DOC	mg L^{-1}	Used ratio of ~ 3 times surface water DOC . Used SFWMD (2000g) to construct time series
Porewater chloride	mg L^{-1}	Set to surface water concentration
Porewater sulfate	ueq L^{-1}	Gilmour (1998a)
Initial Mercury Concentrations		
Initial MeHg concentration in water (unfiltered, includes all seston & plankton)	ng L^{-1}	From USGS (2001)
Initial MeHg concentration on bulk sediment particles in each layer	ng g^{-1}	From Gilmour *et al.* (1998a)
Initial Hg concentrations in fish (each age class, each species)	ug g^{-1} wet	Same as 3A 15
Initial HgII concentration in water (unfiltered, includes all seston)	ng L^{-1}	USGS (2001)
Initial HgII concentration in sawgrass	ng g^{-1} dry	USGS (1999)
Initial HgII concentration in lilies	ng g^{-1} dry	USGS (1999)
Initial HgII concentration in cattails	ng g^{-1} dry	USGS (1999)
Initial MeHg concentration in sawgrass	ng g^{-1} dry	USGS (1999)
Initial MeHg concentration in lilies	ng g^{-1} dry	USGS (1999)
Initial MeHg concentration in cattails	ng g^{-1} dry	USGS (1999)
External Hg loads and Concentrations		
Concentration of reactive gaseous HgII (RGM) in air	ug m^{-3}	Same as 3A 15
Concentration of HgII in inflow (unfiltered)	ug m^{-3}	Combined data from SFWMD (2000j) and USGS (2001) to get timeseries

Input	Units	Data In-house
Concentration of MeHg in inflow (unfiltered, not inert)	ug m^{-3}	Combined data from SFWMD (2000j) and USGS (2001) to get timeseries
Concentration of MeHg in wet deposition	ug m^{-3}	Same as 3A 15
Concentration of HgII in wet deposition	ug m^{-3}	Same as 3A 15
Particle HgII dry deposition rate	ng m^{-2} day	Derived from 3A 15, but adjusted for vegetative cover.
Hg Rate Constants		
Vertical thickness of sediment methylation zone	cm	Assumed 3 cm
Methylating efficiency of microbes	ug MeHg per ug $HgII_{avail}$ per g C decomposed per m^3	Calibrated to site
$Q10_{Meth}$	dimensionless	Assumed 2.0
Half-saturation constant for sulfate effect on methylation	ueq L^{-1}	Value of 200 used , same as 3A 15. This constant requires future attention when sulfide complexation is revisited
Factor to relate efficiency with which microbes methylate in the absence or presence of sulfate	dimensionless	Value of 1.0 , same as 3A 15. This constant requires future attention when sulfide complexation is revisited
Fraction of biological demethylation going to elemental Hg	Fraction	Low value needed to avoid buildup of elemental Hg in porewater (not observed). Value of 0.05 assumed
Demethylating efficiency of microbes	ug HgII per ug $MeHg_{avail}$ per g C decomposed per m^3	Calibrated to site
MeHg photodegradation rate constant at water surface	m^2 $uEinsteins^{-1}$	Same as 3A 15
Hg(II) photoreduction rate constant at water surface	m^2 $uEinsteins^{-1}$	Derived from application of D-MCM to four lakes as well as examined during ENR runs.
Elemental Hg oxidation rate constant at water surface	m^2 $uEinsteins^{-1}$	Set to zero. Thus the photoreduction rate represents net reduction.
Hg Mass transfer coefficient in air	m day^{-1}	Used value of 100
Hg Mass transfer coefficient at water surface	m day^{-1}	Used value of 0.5
Hg Mass transfer coefficient across sediment/water interface	m day^{-1}	0.03 m day, same as value calibrated at WCA 3A-15.
RGM deposition velocity	m day^{-1}	Value 864 used (1 cm s^{-1})
Hg Partitioning: non-living particles		
Partitioning constant between MeHg on non-living solids and a fraction of dissolved pool in surface water	m^3 g^{-1}	Same as 3A 15 calibration
Partitioning constant between HgII on non-living solids and a fraction of dissolved pool in surface water	m^3 g^{-1}	Same as 3A 15 calibration
Partitioning constant between MeHg on	m^3 g^{-1}	Same as 3A 15 calibration

Input	Units	Data In-house
detritus and a fraction of dissolved pool in surface water		
Partitioning constant between HgII on detritus and a fraction of dissolved pool in surface water	$m^3 g^{-1}$	Same as 3A 15 calibration
Partitioning constant between MeHg on sediment solids and a fraction of dissolved pool in porewater (for each layer)	$m^3 g^{-1}$	Same as 3A 15 calibration
Partitioning constant between HgII on sediment solids and a fraction of dissolved pool in porewater (for each layer)	$m^3 g^{-1}$	Same as 3A 15 calibration
Hg Partitioning in Lower Food Web		
Ratio between MeHg concentration in zooplankton and phytoplankton	dimensionless	Value of 2.0 used (Same value as previous applications of E-MCM and D-MCM)
Ratio between HgII concentration in zooplankton and phytoplankton	dimensionless	Value of 0.25 used (Same value as previous applications of E-MCM and D-MCM)
Ratio of MeHg concentrations in shrimp and detritus	(ug MeHg/g wet shrimp) / (ug MeHg /g detritus)	Value of 12 used (Same value as previous applications of E-MCM at WCA 3A-15
Ratio of MeHg concentrations in benthos and sediments.	(ug MeHg/g wet benthos) / (ug MeHg /g sed)	Value of 25 used (within range used for previous applications of E-MCM and D-MCM)
MeHg partitioning between periphyton and dissolved inorganic MeHg complexes =	[ug MeHg /g dry part]/[ug dissolved inorganic MeHg/m3].	Value of 0.35 used (Same value as previous applications of E-MCM at WCA 3A-15
Switch to determine MeHg species taken up by phytoplankton (options will exist)	-	Assumed non-DOC bound MeHg taken up by phytoplankton. This was based on previous applications of D-MCM and E-MCM (R. Harris unpublished).
MeHg facilitated uptake rate constant for phytoplankton	$L\ cell^{-1}\ day^{-1}$	Based on Hudson et al. (1994)
Protonation constant for facilitated MeHg uptake by phytoplankton	$L\ mole^{-1}$	Based on Hudson et al. (1994)
Phytoplankton cell permeability of MeHg	$dm\ d^{-1}$	Based on Hudson et al. (1994)
Phytoplankton cell permeability of HgII	$dm\ d^{-1}$	Based on Hudson et al. (1994)
Phytoplankton cell density	$kg\ dry\ L^{-1}\ cell$	Based on Hudson et al. (1994)
Phytoplankton cell radius	dm	Based on Hudson et al. (1994)
Phytoplankton MeHg clearance rate constant	d^{-1}	Assumed zero
Phytoplankton turnover rate	Day^{-1}	Based on Hudson et al. (1994)
Coefficient for diffusion limited uptake of MeHg by phytoplankton	$dm^2\ day^{-1}$	Based on Hudson et al. (1994)
Thermodynamic Equilibrium		
Thermodynamic constants for all relevant	$L\ Mole^{-1}$	Smith and Martell (1976c, 1976b,

Input	Units	Data In-house
MeHg and HgII complexes. Complexing agents include chloride, sulfide, OH, and the thiol component of DOC		1976c), Hudson *et al.* (1994)

Appendix E
Summary of Data Sources for STA-2 simulations

Data Type	Parameter Estimate and Source
Hydrologic Data	
Precipitation	Fink 2002b, 2002c
Surface water elevations	Rumbold and Fink 2001, Fink 2002b
Surface Flow	Fink 2002b, 2002c
Physical Data	
Temperature and incident light	From 3A-15 scenario
Soil moisture content	Assumed 100% saturation at all times
Mercury Loadings	
Wet Hg(II) deposition	Fink (2002c)
Dry Hg(II) deposition	Fink (2002c)
Leaf Area Index	3 (assumed)
Upstream Surface water concentrations – Hg(II)	Fink (2002b, 2002c)
Upstream Surface water concentrations – MeHg (unfiltered)	Fink (2002b, 2002c)
Surface Water Chemistry	
DOC	Fink (2002c)
pH and dissolved oxygen	Fink (2002c), SFWMD (2000i)
SO_4^{2-}	SFWMD (2000i)
Hg Concentrations in Marsh	
Surface water total mercury and MeHg (filtered and unfiltered)	Fink (2002b, 2002c)
Elemental Hg (DGM)	No data
Sediment Hg	Fink (2002e)
Sediment porewater chemistry	No data
Food Web and Vegetation	
Fish growth (largemouth bass) and Hg concentrations	From 3A-15 scenario
Mosquitofish Hg concentrations	Fink (2002d)
Fish diets	From 3A-15 scenario
Fish biomasses	From 3A-15 scenario
Macrophyte and periphyton biomasses and turnover rates	From 3A-15 scenario
Macrophyte total mercury concentrations	From 3A-15 scenario, calibrated
Shrimp and zooplankton MeHg concentrations	No data
Benthos MeHg and total mercury concentrations	No data

Periphyton MeHg and total mercury concentrations	No data
Particle Dynamics	
Hg(II) Sorption	From 3A-15 scenario
Sediment accumulation rates	From 3A-15 scenario
Sediment decomposition rates	Initially From 3A-15 scenario, then calibrated to generate spikes in methylation to match observed MeHg concentrations at site.

Appendix F
Model inputs for simulations of WCA 3A-15 from earlier studies

Input data types and sources for WCA 3A-15 simulations carried out in connection with the pilot TMDL for the same site are summarized in Table F1. This information is from Tetra Tech (2001).

Table F1
Summary of data input sources for WCA 3A-15 simulations
-Grouped by major data type

Data Type	Parameter Estimate and Source
Hydrologic Data	
Precipitation	Monthly means from FAMS sites AT, FS, and TT, 1992-1996 (Guentzel, 1997; Gill *et al.*, 1999)
Physical Data	
Temperature and incident light	Monthly means estimated from NOAA gauge data at West Palm Beach, 10/89 to 9/94 – Hydroqual (1997)
Soil moisture content	Assumed 100% saturation at all times
Mercury Loadings	
Wet Hg(II) deposition	Monthly means from FAMS sites AT, FS, and TT, 1992 –1996. Guentzel, 1997; Gill et al., 1999.
Dry Hg(II) deposition	Model mean monthly estimates from Keeler *et al.*, (2000)
Leaf Area Index	3.0 (assumed)
Upstream Surface water concentrations – Hg(II)	Based on average for 3A-33 = 2.14 ng/L (n=6) sampled by USGS
Upstream Surface water concentrations – MeHg (unfiltered)	Based on average for 3A-33 = 0.27 ng/L (n=6) sampled by USGS
Food Web and Vegetation	
Fish growth (largemouth bass) and Hg concentrations	T. Lange, Florida Fish and Wildlife Conservation Commission (unpublished data)
Mosquitofish Hg concentrations	D. Krabbenhoft (ACME unpublished data)
Fish diets	Cleckner and Gorski (ACME unpublished data)
Fish biomasses	Marshwide average = 40 kg/ha (wet) (Jordan, 1996 cited in Ambrose *et al.,* 1997)
Macrophyte and periphyton biomasses and turnover rates	Ambrose *et al.,* (1997)
Macrophyte total mercury concentrations	USGS collected samples, FDEP funded

Table F1 Summary of data input sources for WCA 3A-15 simulations -Grouped by major data type	
	analyses by Frontier Geosciences
Shrimp and zooplankton MeHg concentrations	100 - 200 ng/g (dry) (Cleckner, personal communication)
Benthos MeHg and total mercury concentrations	No data
Periphyton MeHg and total mercury concentrations	(Cleckner *et al.*, 1998)
Particle Dynamics	
Hg(II) Sorption	Calibrated
Sediment accumulation rates	Derived from Delfino *et al.,* (1993 and 1994)
Sediment decomposition rates	Derived from litter turnover rates and net mass sedimentation.

Additional information describing selected inputs used in simulations is provided below:

WCA 3A-15 Water Temperature and Incident Light

Water temperatures were assumed to be the same as air temperatures. Daily data for air temperature and incident light were available from NOAA data collected at West Palm Beach, from October 1989 to September 1994 Hydroqual (1997). From these data, mean monthly temperatures and incident light were estimated as shown in Figures F1 and F2.

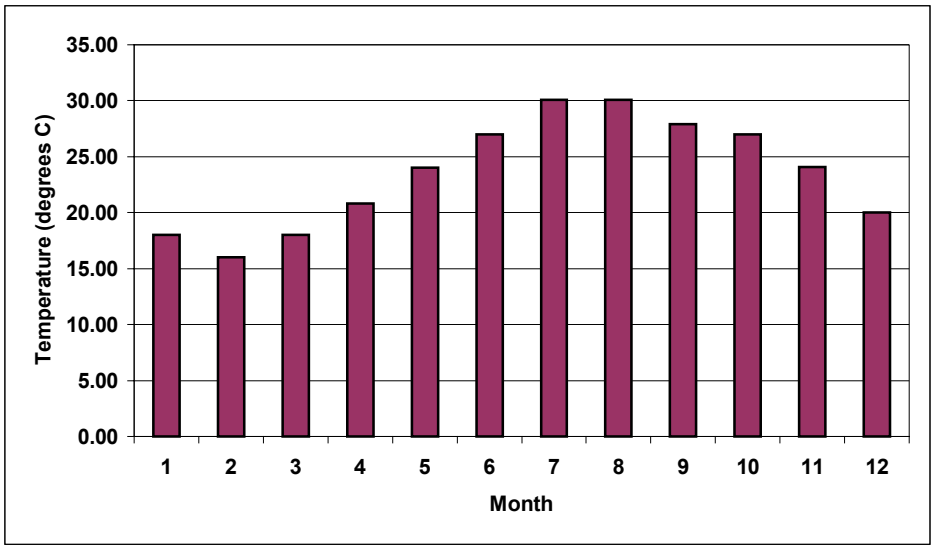

Figure F1. Estimated mean monthly water temperatures for WCA 3A-15. Estimated from Hydroqual (1997).

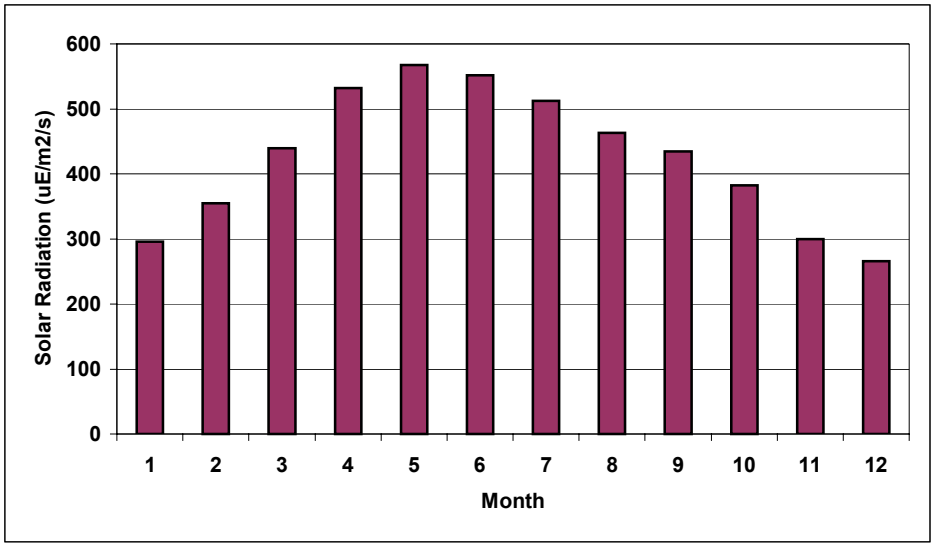

Figure F2. Estimated mean monthly incident light for WCA 3A-15. Source: Estimated from HydroQual (1997).

WCA 3A-15 precipitation

Precipitation data were averaged from three sites: FAMS data for Tamiami Trail (TT), Fakahatchee Strand (FS), and Andytown (AT) from 1992-96 (see Figure F3).

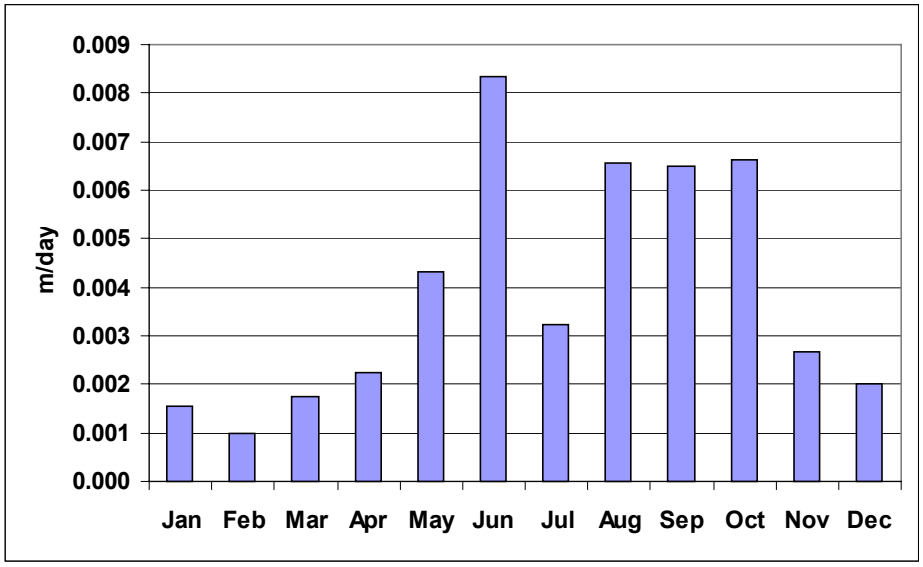

Figure F3. Estimated mean monthly precipitation for WCA 3A-15. Data from proximal Everglades FAMS sites, 1992-1996. Source: Guentzel, 1997; Gill *et al.*, (1999).

WCA 3A-15 external mercury loadings

Mean monthly wet Hg(II) deposition rates were estimated using precipitation and mercury concentration data from the FAMS study for three sites from 1992-96: Tamiami Trail (TT), Fakahatchee Strand (FS), and Andytown (AT). Direct empirical measurements of long-term dry deposition rates of RGM and Hg(II) associated with aerosols are not available. Estimates were obtained from local source-receptor modeling conducted as part of the TMDL pilot exercise (Keeler *et al*., 2000). The deposition rates used in the simulations with current atmospheric Hg(II) deposition are shown in Figures F4 and F5.

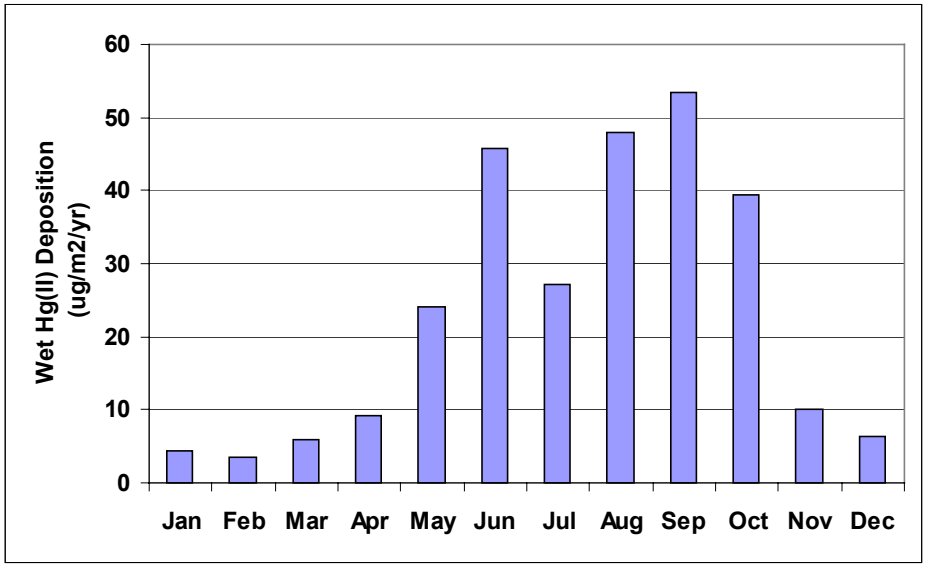

Figure F4. Monthly wet Hg(II) deposition rates used in long-term WCA 3A-15 calibration. Source: FAMS data (Guentzel, 1997) for Tamiami Trail (TT), Fakahatchee Strand (FS), and Andytown (AT) from 1992-96.

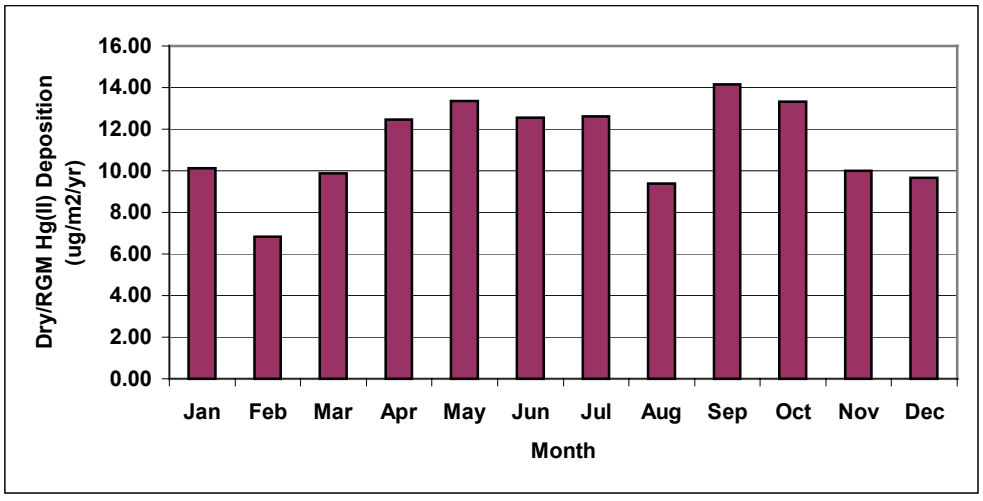

Figure F5. Monthly dry/RGM Hg(II) deposition rates used in long-term WCA 3A-15 calibration. Source: Model estimates from Keeler *et al.*, 2000)

Methylmercury concentrations in wet deposition were assumed to equal 0.02 ng/L. Limited data collected during FAMS at several Everglades sites showed that methylmercury concentrations in monthly integrated bulk deposition samples were equal to or below 0.020 ng/L (Guentzel *et al.*, 1995). Sensitivity analyses demonstrate that the model is insensitive to variations in concentrations at these comparatively low levels. Dry deposition rates for methylmercury were assumed to be negligible.

The USGS ACME study collected surface water concentrations of total and methylmercury at several sites, including 3A-33, a location upstream of 3A-15. The average concentrations of Hg(II) and methylmercury were 2.14 and 0.27 ng L^{-1} respectively for 8 sampling dates between December 1996 and November 1999. These concentrations were assumed to be the surface inflow concentrations for site 3A-15.

WCA 3A-15 Food Web Inputs

The food web in the Everglades is complex. For the purposes of this study, a simplified nine-compartment food web was selected as shown in Figure F6. These compartments are anticipated to be those most involved in the transfer of methylmercury through the food web to our endpoint, largemouth bass.

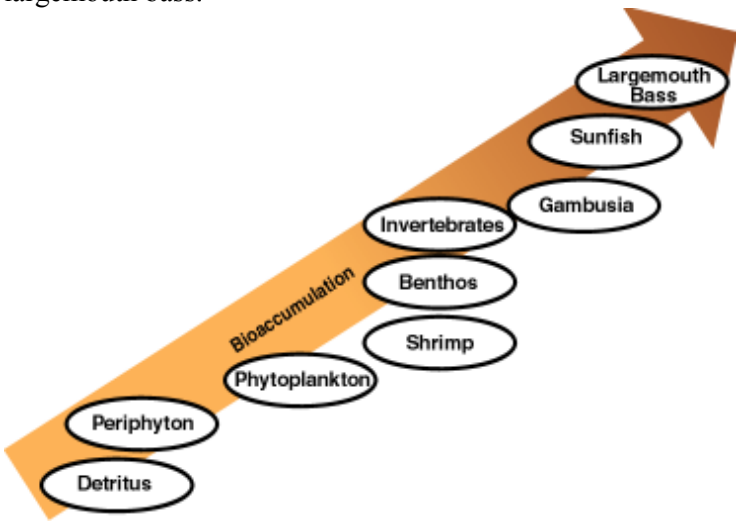

Figure F6. Food web compartments in E-MCM

In the above food web scheme, largemouth bass could eat any combination of food items desired from the other compartments. Bluegill and warmouth were combined as a single omnivorous fish category called sunfish, but could not eat largemouth bass. Mosquitofish (*Gambusia*) were assumed not to eat other fish, relying instead on plankton, periphyton and benthos. Tables F2 through F4 and Figure F7 show the diets used in the E-MCM calibration for each of the three fish populations at different ages. These diets were developed based on discussions with ACME researchers investigating the food web on-site (L. Cleckner, P. Garrison, pers. comm.).

Dietary Item	Fraction of diet by wet weight for largemouth bass at different ages (years)							
	1	2	3	4	5	6	7	8
Benthos (Crayfish)	0.26	0.64	0.15	0.015	0.015	0.015	0.015	0.015
Shrimp	0.37	0.24	0.05	0.005	0.005	0.005	0.005	0.005
Fish	0.37	0.12	0.80	0.98	0.98	0.98	0.98	0.98
Total	1	1	1	1	1	1	1	1

Table F2 Preferred dietary pattern of largemouth bass used for final WCA 3A-15 calibration

Figure F7. Fractions of largemouth bass diet (by weight) represented by *Gambusia* and Sunfish in final WCA 3A-15 calibration (Source: T. Lange unpublished data).

Dietary item	Fraction of diet by wet weight for sunfish at different ages (years)					
	1	2	3	4	5	6
Phytoplankton	0.05	0.05				
Periphyton	0.15	0.20	0.05	0.05	0.05	0.05
Invertebrates	0.30	0.15	0.20	0.05	0.05	0.05
Benthos	0.25	0.25	0.25	0.30	0.30	0.30
Shrimp	0.25	0.25	0.25	0.30	0.30	0.30
Gambusia		0.10	0.25	0.30	0.30	0.30
Total	1	1	1	1	1	1

Table F3. Dietary pattern of sunfish used for final WCA 3A-15 calibration.

Dietary Item	Fraction of diet on wet weight basis
Periphyton	0.25
Zooplankton	0.40
Benthos	0.25
Shrimp	0.10

Table F4. Dietary pattern of mosquitofish (Gambusia) used for final WCA 3A-15 calibration.

Fish growth rates can also significantly affect mercury concentrations. Growth data provided by the Florida Fish and Wildlife Conservation Commission (T. Lange, unpublished data) were used for largemouth bass as shown in Figure F8.

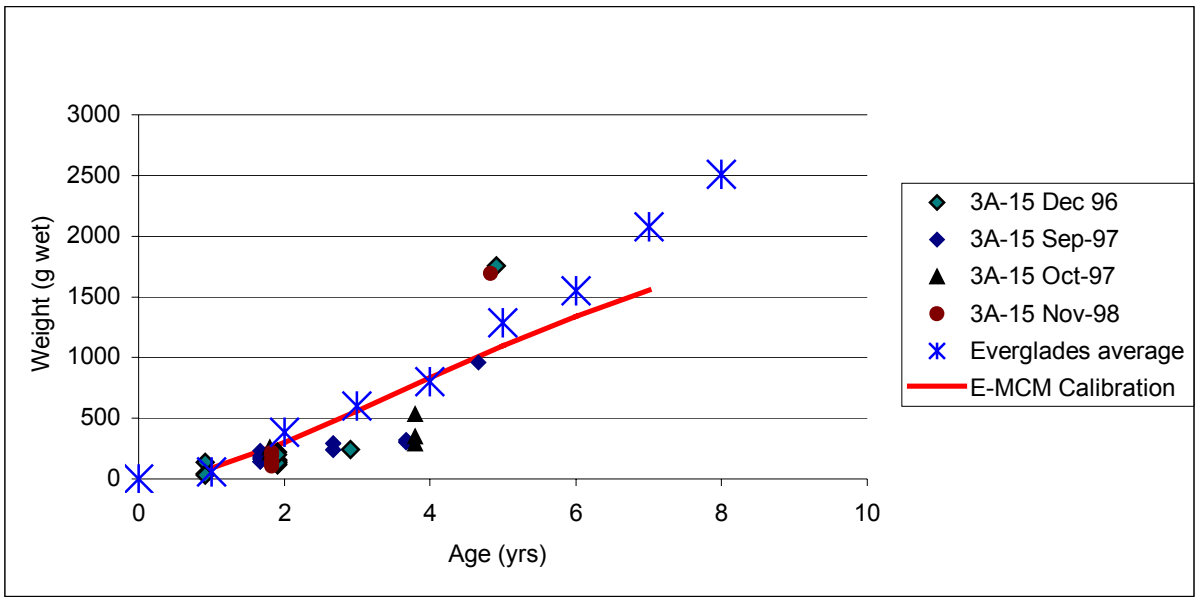

Figure F8. Observed and Calibrated Growth Rates for Largemouth Bass for WCA 3A-15. Source for observations: T. Lange, unpublished data

The relationship between fish length and weight is also important in E-MCM since there is a preferred prey size range for piscivory, based on fish lengths. Data provided by the Florida Fish and Wildlife Conservation Commission (T. Lange, unpublished data) were used for largemouth bass as shown in Figure F9. Largemouth bass were assumed to prefer prey ranging from 15 to 40% of their own length. On occasions where sunfish were piscivorous, they were assumed to prefer fish ranging from 5 to 33% of their own length. These preferences resulted in largemouth bass and sunfish fish consumption patterns shown earlier in Tables F3 and F4.

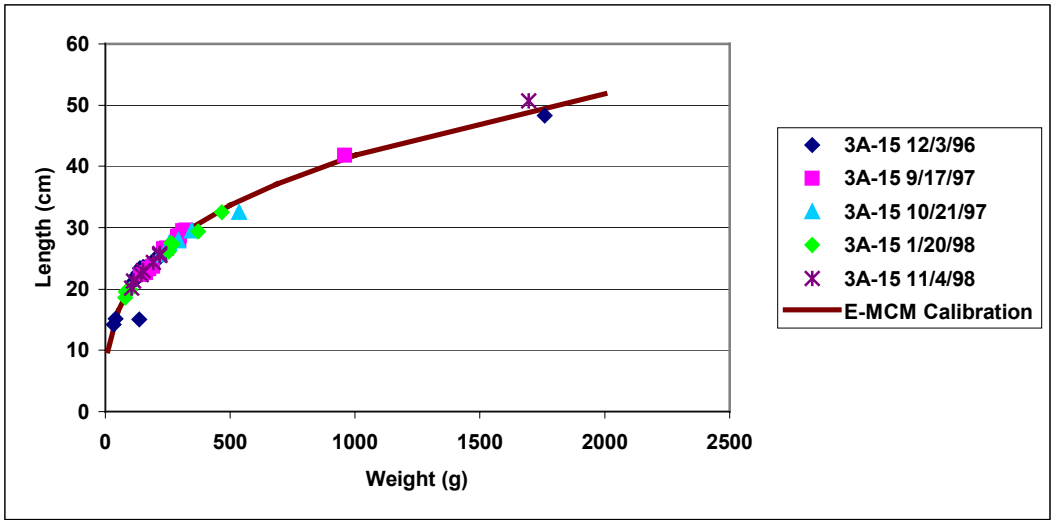

Figure F9. Length versus Weight relationship for Largemouth Bass at WCA 3A-15.